[Trupti Kathrotia, Patrick Oßwald, Clemens Naumann, Sandra Richter, Markus Köhler, Combustion Kinetics of Alternative Jet Fuels, Part-II: Reaction Model for Fuel Surrogate, 302 (2021) 120736]

The original publication is available at www.elsevier.com

https://doi.org/10.1016/j.fuel.2021.120736

Combustion Kinetics of Alternative Jet Fuels, Part-II: Reaction Model for Fuel Surrogate

Authors: Trupti Kathrotia*, Patrick Oßwald, Clemens Naumann, Sandra Richter, Markus Köhler

Institute of Combustion Technology, German Aerospace Center (DLR), 70569 Stuttgart, Germany

*Corresponding Author: Trupti Kathrotia

German Aerospace Center, Pfaffenwaldring 38-40, 70569 Stuttgart, Germany

phone: +49-711-6862-558; email: trupti.kathrotia@dlr.de

Abstract

Conventional transportation fuels used in aviation (jet fuel) or in ground transportation (gasoline, diesel) contain multitude of hydrocarbon components and are difficult to be modeled, if one has to consider each of the component present. A typical approach is the definition of a fuel surrogate with a limited number of fuel components. In this context, a single semi-detailed high temperature reaction kinetic mechanism is presented in this work, which contains all the important molecular classes required for the detailed surrogate modeling of a hydrocarbon fuel. The appeal of the mechanism is the suitability for a broad range of technical fuels covering gasoline, diesel and jet fuels. The reaction mechanism for hydrocarbon combustion is consisted of 238 species and 1814 reactions and is rigorously validated for 70 neat hydrocarbon components over a wide range of experimental conditions including combustion setups such as shock-tubes, laminar flames, jet-stirred and flow reactors.

The purpose of this study is to provide a single reaction model that (1) includes variety of hydrocarbon molecules of varying degree of complexity and carbon numbers, (2) has capability to model a spectrum of different fuels, initially aviation fuels, and (3) is compact to apply both in simple (fundamental kinetic investigations) and complex geometries (CFD studies) of combustion system enabled through customized mechanism reductions. The ultimate goal is to resolve the fuel differences using the model predictions obtained from the reaction mechanism that will supply parameters for fuel design and optimization of fuels. Extensive supporting information is available in this work.

Keywords: Reaction mechanism, aviation fuels, validation, hydrocarbons, oxygenates, soot precursors

1. Introduction

Conventional fuels in common technical applications, often derived from fossil sources, are a complex mixture of multitude of hydrocarbons ranging from single molecule to several hundreds of components of varying molecular complexity and carbon number. Modeling a technical fuel considering all hydrocarbon components present is quite impossible due to the limitation on computational resources required even for the simplest geometry. In order to overcome this issue, a model fuel (also known as surrogate fuel) is often used taking into account the selected carbon number of main molecular class as representative of certain physical or chemical property thereby restricting the number of components [1]. Usually, fuel surrogates used in literature are restricted mainly to 1 to 4 components that are found to be sufficient to represent the global combustion characteristics [1-13].

The selection of hydrocarbons for fuel components is bound to the physical and chemical properties of the fuel. On the molecular level the molar mass (i.e. molecular size) and complexity of the molecule (molecular structure) can have different influence on the combustion characteristics as commonly observed in literature. For example, the liquid properties of hydrocarbon such as viscosity, surface tension or boiling point influence the vaporization and mixing properties of a fuel in the combustor. From the molecular structural point of view, stable molecules such as cyclic structures will tend to resist break down and thereby have slower ignition characteristics. Longer chain molecules are easy to break down and faster to ignite. In addition, stable molecules, e.g. through molecular growth, can lead to particle formation increasing the tendency to form soot. For a combined effect, one requires different molecules (and molecular class) to represent different fuels. Recently, more detailed fuel models have been discussed including up to 5-12 components [14-17] to account for more detailing of fuel properties e.g. required for information of soot precursors. This in return requires more validated hydrocarbon components in the reaction model.

Since a variety of hydrocarbons is present in real fuels, not many reaction kinetic models available in literature are capable of representing multiple surrogate fuel components or large number of different hydrocarbons in a single mechanism. In addition, the studies related to fuels are also indirectly connected to the prediction of pollutants, which requires additional sub-mechanisms to predict aromatics and soot precursor species. Thereby, reactions mechanisms available in literature with various hydrocarbons including soot precursor chemistry are scarce. Among the few well-known reactions models that include multiple hydrocarbons are the mechanisms by POLIMI [18], LLNL [19], JetSurf2.0 [20] and RWTH [21]. The JetSurf2.0 model is specifically designed for Jet fuel surrogate, but provides a limited section of hydrocarbons. The reaction mechanisms for gasoline surrogate and limited components of jet fuel, oxygenates along with aromatics are available from the RWTH group [7, 22, 23]. In general, combinations of reactions from different mechanisms must be treated with care and may require revalidation. Compared to them LLNL model [19] is detailed

including low temperature chemistry, however the model size, species usually above 10^3 species, is severe limitation for complex model simulations. Last to our knowledge, but definitely not the least, the Ranzi group POLIMI-Mech [18] contains more diverse hydrocarbons. Compared to the mechanism presented in this work, the POLIMI reaction mechanism is the only model with semi-detailed species and contains variety of hydrocarbons with reasonably detailed aromatics chemistry. Compared to the POLIMI-Mech, closest to present work, our mechanism additionally includes hydrocarbons with three different degrees of branching namely iso-octane (quaternary carbon), farnesane (tertiary carbon) as well as 2,7-dimethyloctane and 2-methyldecane (secondary carbon). Thus, the mechanism of this work provides additional range of hydrocarbons to be considered for understanding real fuels from different production technologies and feedstocks. None of the other mechanisms are capable to model broad range of fuels and include components to the extent of mechanism described in this work. In contrast to detailed kinetic model, a hybrid chemistry approach has been recently proposed by Hai Wang group [24]. This innovative approach by Wang et al. to model real liquid fuels takes advantage of the key physics underlying the high-temperature combustion of large hydrocarbons fuels. Here, the fuel pyrolysis and pyrolysis products oxidation are expressed as two separate sub-models. The fuel molecule pyrolysis is described by seven lumped reaction steps forming C_0-C_4 cracked products whose oxidation chemistry can be described by validated foundational fuel chemistry models.

The DLR reaction mechanism presented in this work is a single reaction mechanism that include reactions for the detailed description of most n-paraffins in the range of C_1-C_{16}, iso-paraffins with varying degree of branching, cyclo-paraffins such as single-ring cyclohexane, n-propylcyclohexane, bicyclic decalin, cyclo-aromatics such as indane, tetralin, and number of aromatics. All these hydrocarbons are validated against the experiments from the literature and from in-house data (listed in Table 1). A summary of validation experiments and their sources are presented in next section. In addition to the common molecular families present in alternative and conventional jet fuels, some higher polycyclic aromatic hydrocarbons (PAH) up to C_{20} (e.g. phenanthrene, pyrene, chrysene), and polyynes up to C_{10} are implemented. Additionally, some oxygenated species such as C_1-C_4 alcohols, and oxymethylene ethers (OME_n, n = 0-5) are implemented in the model as well. Oxygenated fuel compounds are an own topic to be explored in greater detail and beyond the scope of the present work. A brief section is included in this work for a full picture.

The following sections present the features of the DLR reaction mechanism with a detailed validation of all the components present in the mechanism. An overview of the applicability of the reaction model to predict a Jet A-1 surrogate is given and discussion on difference in reactivity of individual hydrocarbons, significance of degree of branching of iso-paraffins and influence of molecular structure on soot precursors is presented.

The purpose of this work is to provide a single reaction model (1) with as many possible hydrocarbon molecules of varying degree of complexity as well as carbon number, (2) with capability to cover spectrum of different fuels ranging from road transportation to aviation, and (3) to provide a compact model for its further application both in simple (for fundamental studies) and complex geometry (for computational fluid dynamics (CFD) studies) of combustion system. The goal is to resolve compositional differences among the fuel using the reaction model that will supply parameters for fuel design and optimization of fuels. The initial focus is resolving differences in various aviation fuels [25] which are examined in part III of this paper series [26].

2. Validation experiments

The model validation is obtained by simulating the measurements obtained in five different experimental setups. The ignition delay times in high temperature regime and atmospheric to high pressure conditions obtained in shock-tube facilities (I). The laminar flame speeds are modeled using the conditions measured in laminar flame burners (II). These global combustion characteristics are available both in-house and in literature for most hydrocarbons. In addition, detailed speciation data are available for laminar flames (III) and flow reactors (IV), which supplies valuable intermediates data for the model validation. In-house measurements obtained in an atmospheric high temperature DLR flow reactor [27] are modeled. Additionally, jet stirred reactors (JSR) measurements (V) that provide speciation data are modeled, their validation data available for atmospheric and at high pressures, are provided in supplemental material. In variety of literature, burner stabilized low-pressure premixed flames are investigated at low to atmospheric pressures that are modeled. A summary of measurement data and window of combustion conditions covered for validation are presented in Table 1. The details of modeled conditions of each experiment are tabulated in the supplemental material.

Table 1: Summary of validation data and conditions covered in the reaction mechanism validation.

Type of Experiments	No. of expts modeled	Conditions covered	References of experiments
Shock-tube	89	ϕ = 0.063 - 2.5 p = 1 - 60 atm T = high T regime Dilution: Ar, N_2	In-house [28-33] Literature studies [34-67]
Laminar flame speed	91	T = 298 K - 473 K p = 1 - 10 atm ϕ = 0.4 - 2.0	In-house [29, 31-33, 68, 69] Literature studies [57, 70-133]
Burner stabilized premixed flames	40	ϕ = 0.67 - 3.06 p = 0.02 - 1 atm	In-house [134] Literature studies [131, 135-157]
DLR flow reactor	31	ϕ = 0.5 - 2.0 p = 1 atm	In-house [158-160]

		T = 700 - 1800 K Dilution: ~99% Ar	
Jet stirred reactor	70	ϕ = 0.1 - 2.0 p = 1 - 10 atm T = 600 - 1400 K τ = 0.07 - 2 s	Literature studies [63, 161-174]

3. Kinetic model – Features of reaction mechanism

The DLR reaction mechanism contains hydrocarbons of different types to help model reaction kinetics of different liquid hydrocarbon fuels for aviation to road transportation fuels such as diesel and gasoline. A single reaction mechanism is extensively validated against a large experimental data set employing a broad range of combustion applications. It includes recently renewed core mechanism consisting reaction kinetics of H_2-O_2 and hydrocarbons ranging from carbon number C_1 to C_5 upon which the larger hydrocarbon chemistry is built. A complete description of larger molecules includes n-paraffins (with carbon number C_6, C_7, C_9, C_{10}, C_{12}, and C_{16}) as well as iso-paraffins of varying degree of branching such as iC_8H_{18} (2,2,4-trimethyl-pentane), $iC_{10}H_{22}$ (2,7 dimethyl-octane), $iC_{11}H_{24}$ (2-methyl decane), and $iC_{15}H_{32}$ (2,6,10-trimethyl-dodecane). Among the cyclic hydrocarbons, cyclo-paraffins such as cyclohexane, n-propylcyclohexane, decalin, and variety of aromatics such as benzene, toluene, propylbenzene, styrene, as well as multi-cyclic-aromatics such as indane, indene, tetralin, naphthalene, methyl-naphthalene, biphenyl, phenanthrene, pyrene as well as larger aromatics up to C_{20}, polyynes up to C_{10} (useful for soot modeling), and oxygenated species such as C_1-C_4 alcohols, aldehydes such as acetaldehyde, butanal and oxymethylene ethers (OME_n, n = 0-5, iOME2) are implemented in the model as well.

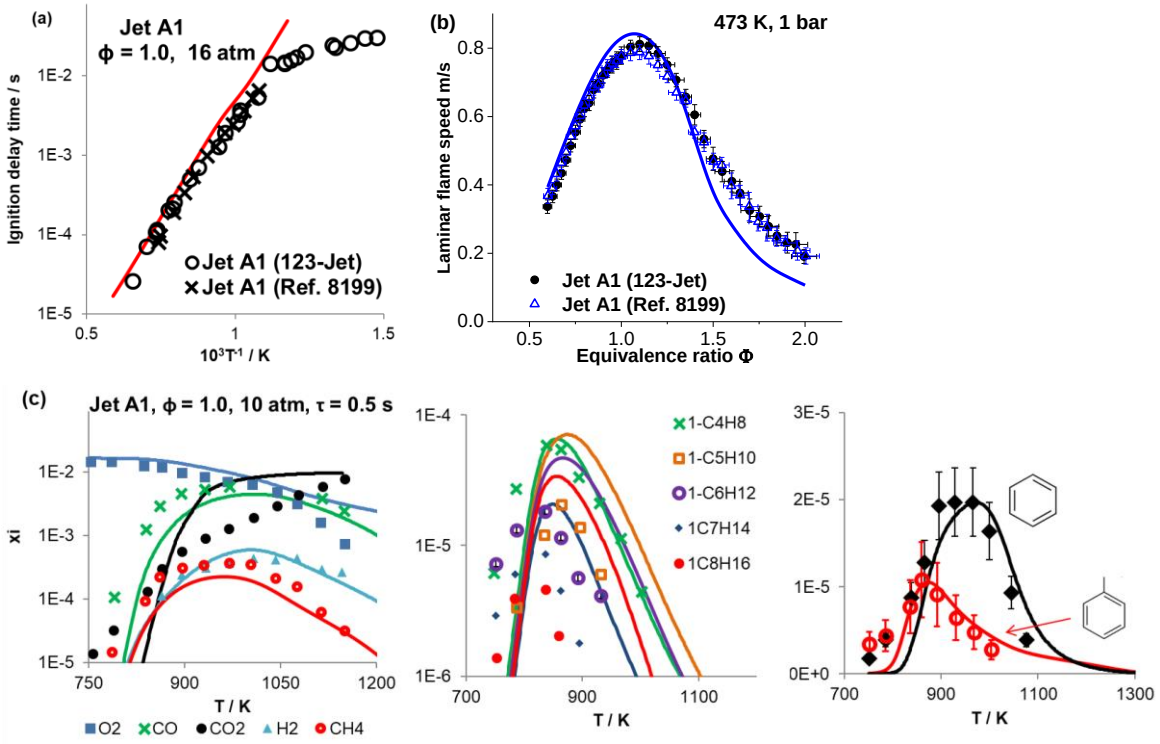

Fig. 1: Comparison of measured Jet A1 and predicted Jet A1 surrogate (a) ignition delay times [175, 32], (b) flame speeds [175, 32], (c) speciation in a jet stirred reactor [162].

In terms of jet fuels, the mechanism is aimed to model various aviation fuels to understand fuels' compositional variations on combustion intermediates and products. To illustrate this (Fig. 1), a fuel surrogate of Jet A1, consisting of 41.1 (mol)% n-decane, 24.1% 2-methyldecane, 13.6% n-propylcyclohexane, 18.4% n-propylbenzene, and 2.7% decalin, is selected based on the composition of Jet A1. For the modeling of this fuel surrogate, presence of all major molecular classes in the reaction mechanism is essential. Additionally, for the prediction of soot precursors, detailed description of single to multi-ring aromatics is needed in the model.

Although our semi-detailed model is small, it still accounts for minimal level of detailing required for the complete description of the hydrocarbon in question. The recommended reaction rates for all the reactions were evaluated step by step, considering their estimated temperature and pressure range. In a first step, the reaction rates predicted for wide *T*-, *p*-range suitable for combustion applications were selected and their influence were tested on predictions of various combustion setup experiments. For reactions where a detailed evaluation of reaction rates from comprehensive reaction mechanism are available, those reaction rates were also considered. Among different possible selection of reaction rates, those that best possibly recreate the intermediates' distribution obtained in various experimental setups such as burner stabilized flames, flow reactor or jet-stirred reactors were selected.

A simple schematic shown in Fig. 2 depicts the above-mentioned hydrocarbon components containing the complete description of their oxidation and thermal decomposition reactions in the reaction mechanism. The reaction model of present work includes 70 validated hydrocarbon components. The complete reaction mechanism is consisted of 238 (307) species, 1814 (2116) reactions excluding (including) oxygenated species (larger alcohols, OMEs) outside the core mechanism. Some part of present mechanism is loosely based on our earlier kerosene model [176], which has been largely reworked to expand the mechanism beyond kerosene focusing first to the chemistry of smaller hydrocarbons which has strong influence on the intermediate chemistry of larger molecules. This has also been essential in order to reduce the stiffness of the earlier mechanism due to certain reaction rates and few incorrectly implemented species which made even the 1-D flame calculation difficult to accomplish. Additionally, the reaction mechanism is expanded to include new molecules such as indane, decalin, tetralin, and oxygenates such as C_1-C_4 alcohols and OMEs.

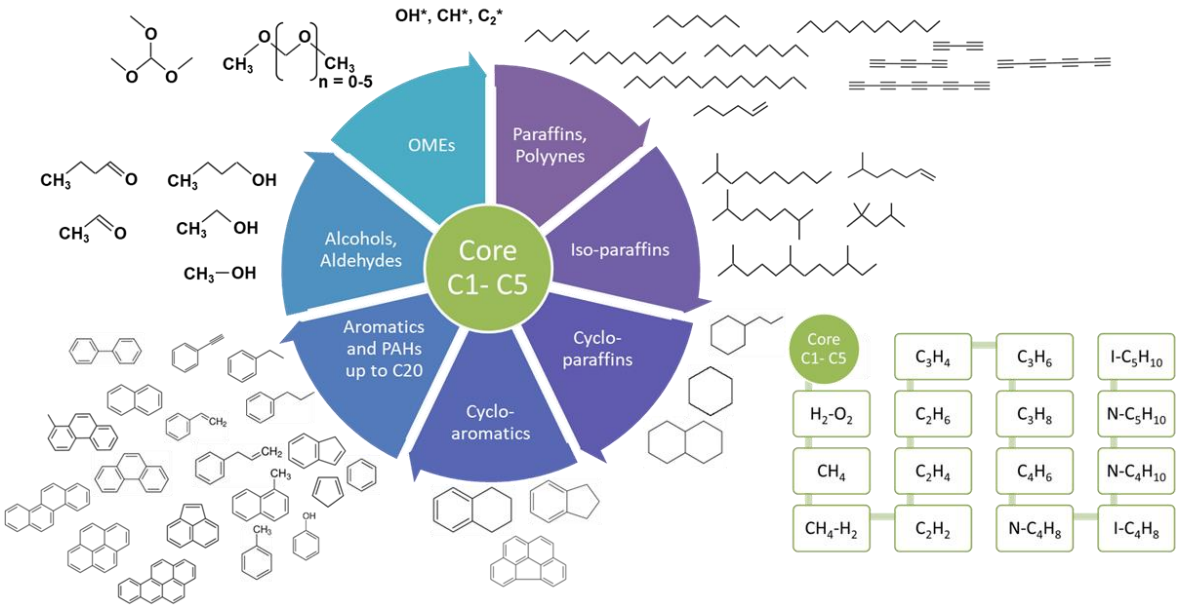

Fig. 2: Overview of validated 70 fuel components of the high temperature DLR reaction mechanism

The approach to the mechanism development is as follows: (1) Core mechanism C_1-C_5 with increasing C-number build upon H_2-O_2 system. (2) Addition of larger hydrocarbons decomposition up to the species present in the core mechanism. (3) Inclusion of only necessary species (and reactions) of a given hydrocarbon for complete description, in order to keep the reaction mechanism compact. (4) The number of isomers is restricted maximum up to 3 depending on the size and complexity of the molecule. (5) Implementation of low temperature peroxy chemistry possible, but not included at the moment.

The major part of the thermodynamic species properties in our model is obtained from the Burcat-Goos database (in-house) [177]. For species with no available thermodynamic data in the literature, data were obtained using RMG (Reaction Mechanism Generator, open source tool from W. Green

group, MIT) [178] that considers group additivity estimations for the evaluation of the thermodynamic data and transport parameters. In our previous model some of the reactions were identified to be stiff for the numerical solver leading to no solution or extremely long computing time. These has been linked to the reverse rate coefficients calculated through the thermodynamic data. In such cases, the thermodynamic data from various sources were tested and its influence on the mechanism were checked. The transport properties are collected over time for the core mechanism and for isomers and larger molecules analogies are made to similar molecules.

The sensitivity of the thermodynamic and transport data is of importance, which can supply the uncertainty limits of the mechanism. This is a separate topic in itself and at the given point not tested to the full extent. Especially for larger hydrocarbons (C>5) the uncertainty related to the rate coefficient is expected to be still higher for most reactions as no direct experimental or numerical rate data are available. Most studies focused on the sensitivities related to the kinetic parameters, thermodynamics and transport data are restricted to smaller molecules, mainly hydrogen, and methane where the influences are high. G. Smith [179] has showed in his diagnostics of methane flame, that the uncertainty in kinetics dominates. Compared to kinetics, thermodynamics and transport properties in the mechanism contributed relatively little to the modeling uncertainties. A detailed study on the molecular level of transport data has found large sensitivities with respect to the collision diameters, whereas no significant sensitivity for all other transport parameters such as well depths, collision number, dipole moment, rotational relaxation and molecular polarizability [180]. This topic has been of increased importance also for the automatic generated mechanisms where input uncertainties are correlated through kinetic rate rules and thermodynamic group values [181] suggesting the modelers to carefully prioritize optimizing thermochemical parameters before refining the rate coefficients. Studies have also demonstrated that thermodynamic data can have a high sensitivity on combustion characteristics under certain conditions; high impacts on the NTC of ignition delay times by updates of thermodynamic data in [182]. This study also revealed that the high temperature regime of the ignition delay times is not impacted by the update of the thermodynamic data. In our study we focus on the high temperature chemistry relevant for gas turbine conditions. For this reason, we have chosen the most convincing dataset of thermodynamic and transport data. Within this work we simultaneously prove the validity of this approach by simulations over a wide range of conditions. Further developments starting from this basis will estimate the uncertainty limit of various parameters including transport properties, thermodynamics data and kinetic rate constants.

This section presents the description of the reaction mechanism: first the core C_1-C_5 mechanism and then hydrocarbons separated by their molecular classes. The validation for each molecular class is presented for their global combustion characteristics such as ignition delay times or flame speeds as well as conversion of fuel and oxidizer leading to major combustion products in flames or at flow

reactor conditions. Finally, the intermediate species pool predicted by the model in the flame or flow reactor is elaborated in the end of this section. The validation of each species present in mechanism is performed for maximum possible experiments available in the literature. Due to the large number of experimental data involved, only limited data are presented here. The details of the references and experimental conditions presented in the figures as well as additional validation data are available as supplemental material.

3.1 Core C_1-C_5 chemistry

A well-validated core reaction mechanism is the very essential basis of this approach as the performance of larger hydrocarbons is strongly dependent on it. The core is defined on the C_1 to C_5 chemistry of these smaller hydrocarbons. A detailed validation of this core mechanism is performed in greater detail before further extension to the larger hydrocarbons. This is an important aspect for a correct implementation of oxygenate chemistry as well.

The base H_2-O_2 chemistry is considered from the recent works of Burke et al. [183]. They presented the hydrogen reaction mechanism with improvements made to resolve remaining discrepancies between experimental data and predictions especially at high pressures important for engine and gas turbine applications. Considering this as a starting point, the hydrocarbons mechanism is built up upon it. Generally, the larger hydrocarbon chemistry is highly sensitive to the smaller hydrocarbons. Additionally, the inclusion of oxygenated chemistry has large influence on the formation or consumption of formaldehyde CH_2O and related species, which subsequently influences the hydrocarbon chemistry. In general, for combined hydrocarbon and oxygenates chemistry, a careful consideration of reaction rates of C_1-C_2 system is highly required. The reaction rates of C_1-C_5 species is obtained from literature compilations and no estimations are made in this work therefore no detailed description is given here. Their references are supplied in the reaction mechanism as supplemental material.

The validation of ignition delay times and flame speeds of species in the core mechanism is presented in Fig. 3 and Fig. 4 respectively. Note, that only selected comparisons are shown here and the complete set of data are included in supplemental material. The comparison of model prediction to the measurements is obtained as a function of temperature, pressure and fuel stoichiometry to cover maximum range of validation. The ignition delay times are presented for the temperatures higher than 1000 K and pressures up to 60 bar. All the modeled small hydrocarbons successfully predict the measured temperature dependence of the ignition, in addition to pressure and fuel stoichiometry dependence.

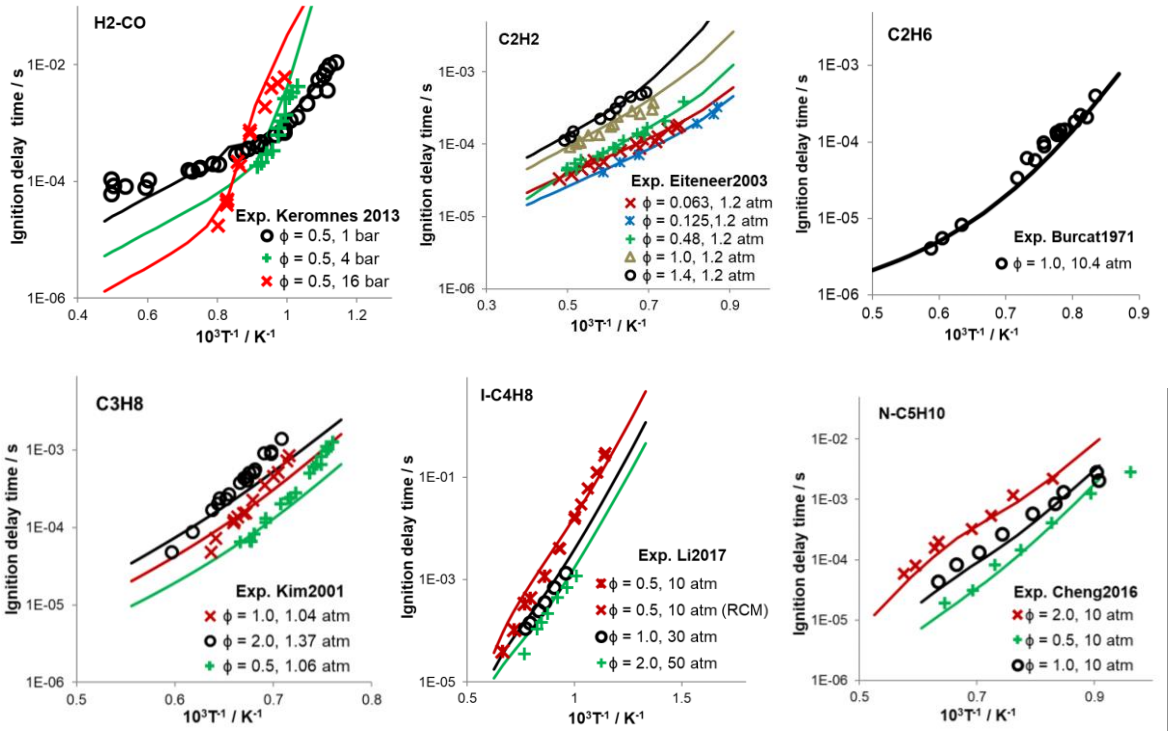

Fig. 3: Validation of ignition delay times of C_1 to C_5 hydrocarbons available in the core mechanism. A complete validation data and the input conditions is available in the supplemental material. References: Keromnes2013 [28], Eitenner2003 [36], Burcat1971 [38], Kim2001 [41], Li2017 [43], Cheng2016 [46].

The flame speed measurements are available for fuel stoichiometry ϕ = 0.4 – 2.0 and pressures up to 6 atm. In general, both the modeled ignition delay times and flame velocities show very good comparison with the measurements for the above specified parameter range for all core species in the mechanism. Only the modeled pentene flame speeds are higher than the uncertainty limits of their measured values (in supplemental material). This will not influence the mechanism as usually pentene is important as an intermediate rather than as fuel component.

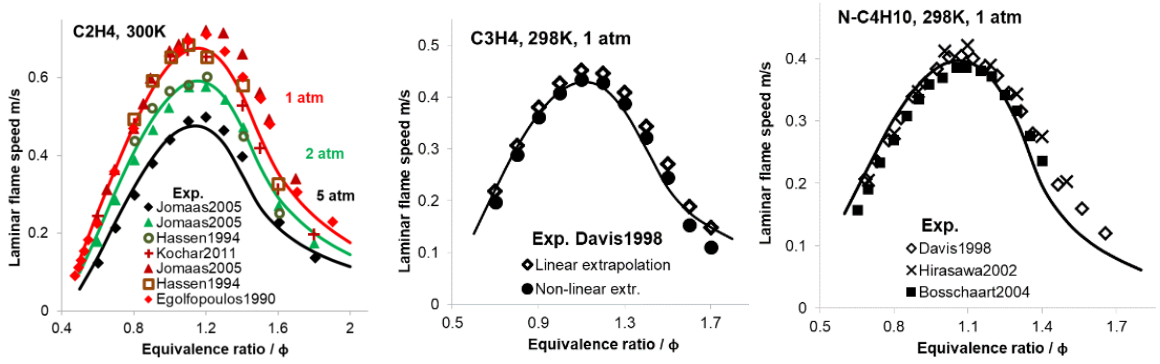

Fig. 4: Validation of laminar flame speed of C_1 to C_5 hydrocarbons present in the core mechanism. A complete validation data and the input conditions is available in the supplemental material. References: Jomaas2005 [83], Hassen1994 [85], Kochar2011 [74], Egolfopoulos1990 [79], Davis1998 [75], Hirasawa2002 [105], Bosschaart2004 [89].

This concludes the global characteristics. In addition, speciation in flame and flow reactor is also investigated for the stricter check of the model. Fortunately, for most of the core species, flame speciation is available in literature. Shown in Fig. 5 is the comparison of fuel and O_2 along with major species CO, CO_2, H_2O, and H_2 for various hydrocarbons in atmospheric or low-pressure burner-stabilized laminar flames. The major products are well reproduced by the mechanism. In these flames the measured temperature uncertainty, closer to the burner surface (used as model input) usually reflected in the fuel and oxidizer consumption, is very high.

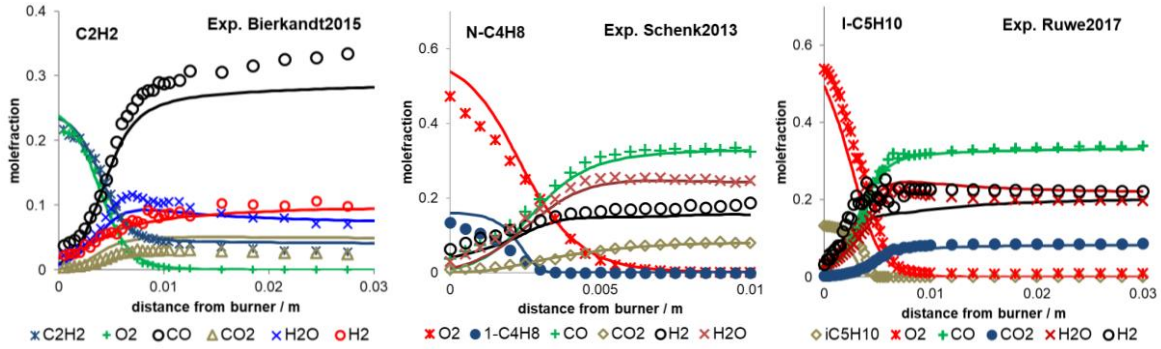

Fig. 5: Validation of speciation data in laminar flame of various hydrocarbons from C_1 to C_5 present in the core mechanism. A complete validation data and the input conditions is available in the supplemental material. References: Bierkandt2015 [136], Schenk2013 [141], Ruwe2017 [143].

Mixture of CH_4 doped with C_2H_2 is measured at fuel-rich condition in the DLR flow reactor. This earlier reported data [158] is presented in Fig. 6. The major species, C_2 species as well as benzene in the intermediate to high temperature regime, are well predicted by the model.

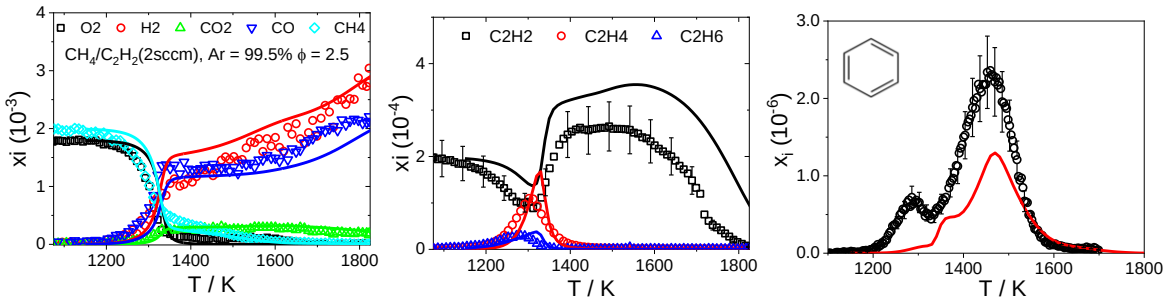

Fig. 6: Predictions of species obtained in a high temperature DLR flow reactor [158].

3.2 n-Paraffins

Outside the core (C>5), the mechanism includes n-paraffin components such as n-hexane, n-heptane, n-nonane, n-decane, n-dodecane, n-hexadecane and additionally n-hexene (mainly considered as intermediate however validated due to availability of experiments). It is known that the combustion characteristics of n-paraffins are similar [75, 184, 185]. However, the spectrum of different n-paraffins (small and larger) can be important in a fuel surrogate to represent their difference in

physical properties. A detailed description of three paraffins C_6, C_9, and C_{12} is recently published in [159]. In general, keeping the compactness in consideration, the reactions of n-paraffins (n-C_nH_{2n+2}) includes two fuel radicals (primary, and secondary C_nH_{2n+1} radical) for larger molecules (C>7), and one for smaller n-paraffins. It includes one species as lumped olefin (C_nH_{2n}) and reactions of olefins decomposing to smaller species is mainly part of core or other paraffins. The H-abstraction reactions of fuel converting to fuel radicals are included mainly for RH = H, O, OH, HO_2, O_2, CH_3, their rates are obtained from various literature sources, where rates of larger hydrocarbons are considered from the analogy of smaller molecules. Their references are supplied in the reaction mechanism as supplemental material. The reaction rates of the larger molecules are based on the analogy of smaller hydrocarbons. Among n-alkane reaction mechanisms in literature are, a comprehensive low- to high-temperature LLNL model containing nC_8-nC_{16} n-paraffins [19] and a lumped POLIMI-Mech for nC_7, nC_{10}, nC_{12}, and nC_{16} [18] and high temperature JetSurf2.0 model for nC_6-nC_{12} paraffins [20]. In general, the chemistry of n-paraffins is quite well studied.

The global validation of ignition delay times is shown in Fig. 7. The high temperature ignition delay times for n-hexene as well as n-hexane to n-dodecane are in good agreement with the measurements. In case of n-hexadecane, the ignition delay times are predicted slightly lower than the measurements. In this case, the ignition delay time was found highly sensitivity to the presence of reaction of C_2H_3 with O_2 which is puzzling due to no direct link to the fuel decomposition. Due to limited experimental data available for n-hexadecane in the literature, verification is not possible yet.

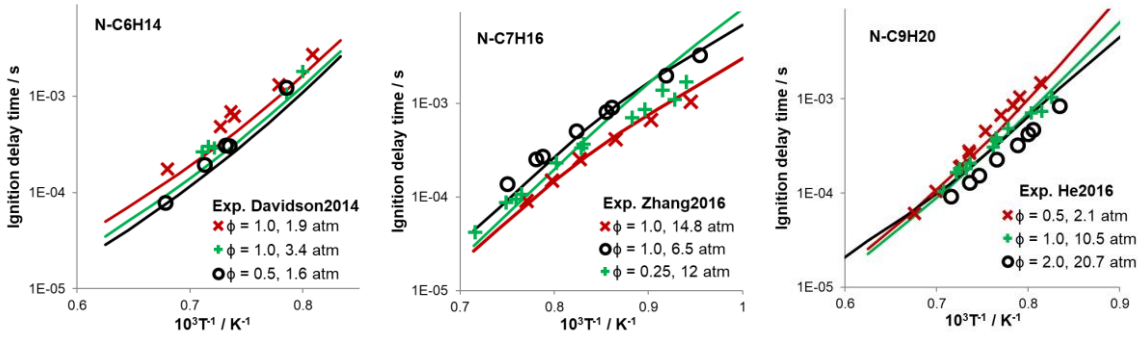

Fig. 7: Validation of ignition delay times of various hydrocarbons from nC_6-nC_{16}-paraffins available in the mechanism. A complete validation data and the input conditions is available in the supplemental material. References: Davidson2014 [49], Zhang2016 [50], He2016 [51].

The flame velocities of n-paraffins are available in literature for all n-paraffins studied in this work. As shown in Fig. 8, the flame speed of n-hexene is over predicted at lower pressure but agrees with measurement at higher pressures. For all other species, the modeled flame speeds are within the measurement uncertainty limits. In general, in the fuel-rich regime, the comparison of measured flame speed with model need careful consideration as the measurement uncertainties are high due to flame instabilities.

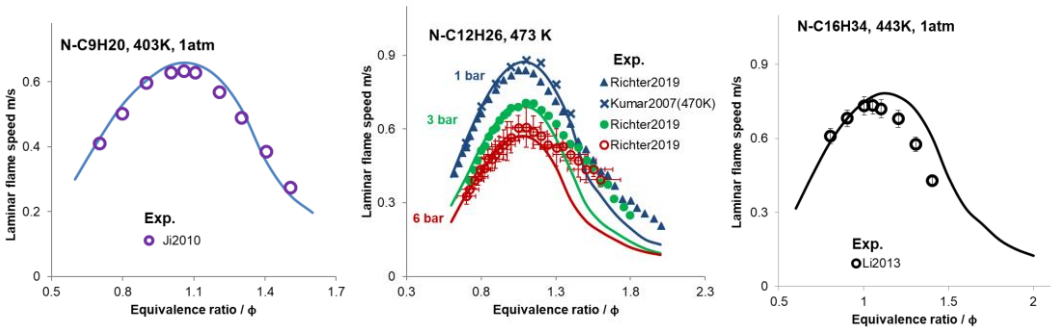

Fig. 8: Model validation of laminar flame speed as function of fuel stoichiometry for n-paraffins with carbon number C_6 to C_{16}. A complete validation data and the input conditions is available in the supplemental material. References: Ji2010 [109], Richter2019 [29], Kumar2007 [112], Li2013 [117].

The speciation data obtained at flame conditions are available for n-hexene, n-heptane and n-decane in literature. As shown in Fig. 9, the n-paraffin fuel decomposition and major species formation of all the three flames are excellently reproduced by the model.

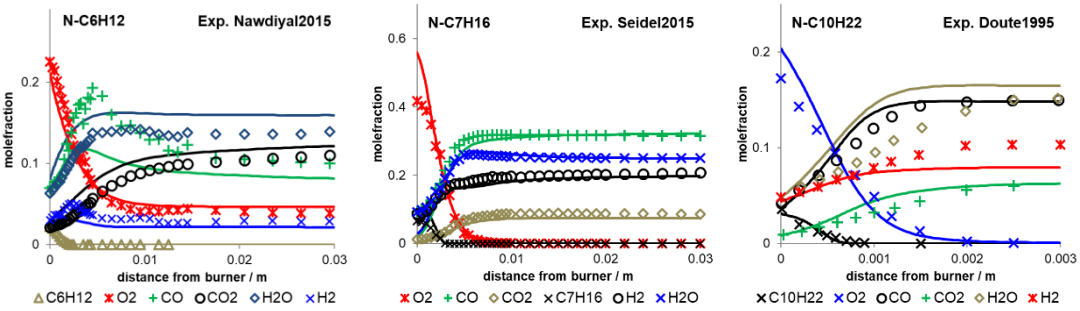

Fig. 9: Validation of speciation data in laminar flame of n-hexene, n-heptane, and n-decane present in the reaction mechanism A complete validation data and the input conditions is available in the supplemental material. References: Nawdiyal2015 [144], Seidel2015 [145], Doute1995 [146].

We recently reported species measurement in the DLR high temperature flow reactor for three n-paraffins [159]. They are presented with additional data of n-decane in Fig. 10. In general, the fuel and oxidizer conversion and major product formation are in good agreement with the measurements in the temperature range of 750 to 1200 K.

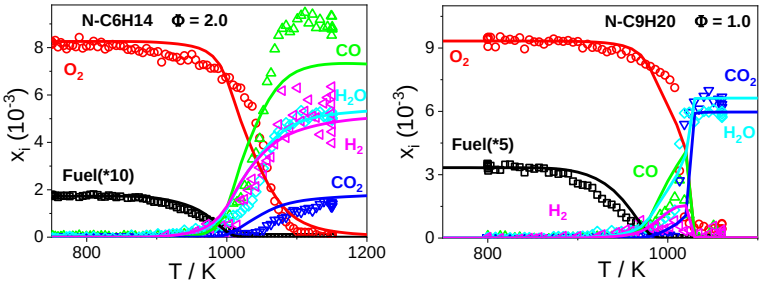

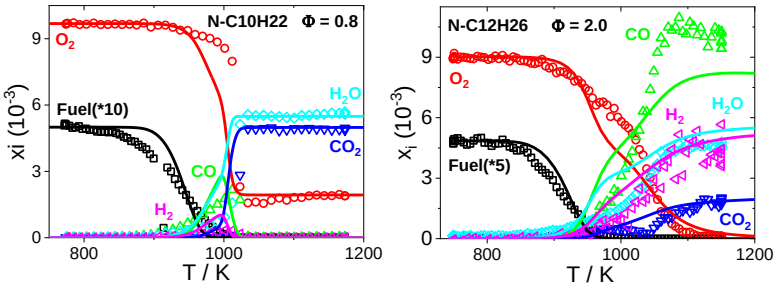

Fig. 10: Speciation in DLR high temperature flow reactor for n-paraffins with carbon number C_6, C_9, C_{12} [159] and C_{10}.

The oxidation of n-hexadecane is measured by Ristori et al. [161] in a jet stirred reactor for fuel-rich and atmospheric pressure condition. As shown in Fig. 11, the major species as well as various C_2 species and larger olefins ranging from C_4 to C_8, considering the measurement uncertainty, are very well reproduced by the model.

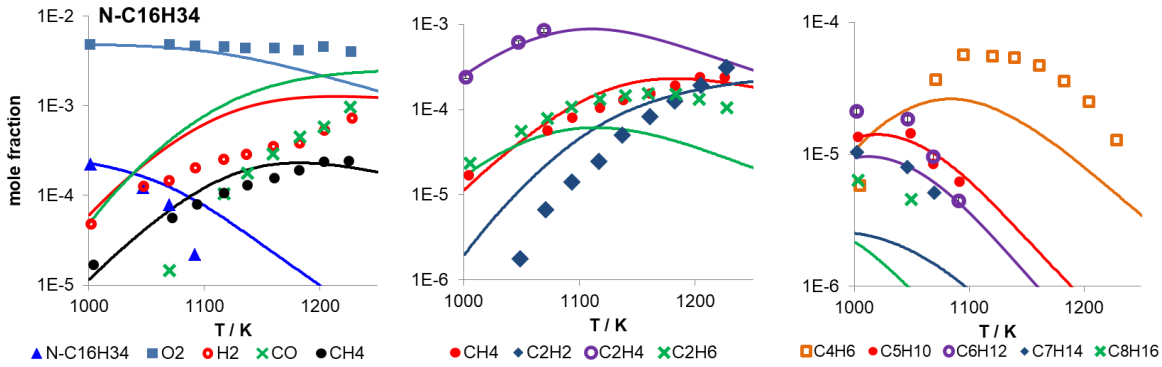

Fig. 11: Fuel oxidation of n-$C_{16}H_{34}$ obtained in a jet stirred reactor at fuel-rich condition Φ = 1.5 and 1 atm at residence time of 0.07s [161].

3.3 Iso-paraffins

Various iso-paraffins are included in the mechanism to cover broader palette of degree of branching as shown in Fig. 12. Conventional fuel contains less branched paraffins and the degree of branching is limited to lightly branched molecules. With the increased investigation of new alternative fuels this has changed significantly. A striking example are alcohol-to-jet fuels, which are designed to include heavily branched iso-paraffins in the first place due to the synthesis method.

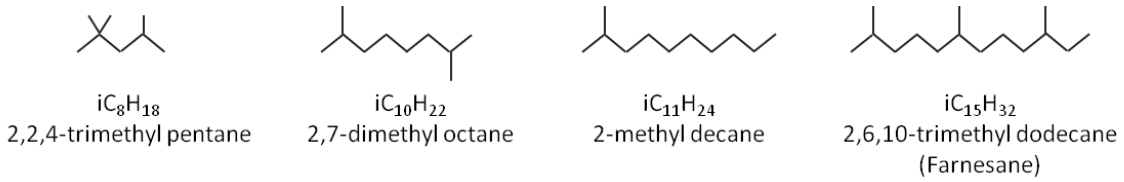

Fig. 12: Structure of iso-paraffins present in the reaction mechanism.

The reaction model for iso-paraffins includes one-methyl branched i-$C_{11}H_{24}$ (2-methyl decane), two-methyl branched i-$C_{10}H_{22}$ (2,7 dimethyl-octane), three-methyl branched with tertiary and quaternary carbon containing farnesane (2,6,10-trimethyl-dodecane) and iso-octane (2,2,4-trimethyl-pentane) respectively. In addition, iso-octene is also validated which is one of the olefins formed during the larger iso-paraffins formation. This is not intentionally present as fuel molecule however due to availability of the experiments its validation is carried out.

The importance of iso-butene in high temperature iso-octane combustion is widely accepted [186]. Important reactions to the global combustion of iso-octane are the decomposition reaction leading to C_4 and C_7 radicals i.e. $iC_8H_{18} = tC_4H_9 + iC_4H_9$, due to which also the C_4 subsystem is also important e.g. $H + iC_4H_7 = C_4H_6 + H_2$ is important for both ignition delay times and flame speeds. In addition to small extent the reaction and $iC_8H_{18} = iC_7H_{15} + CH_3$ and subsystem of iC_7 also becomes important. The reaction rates of iC_{11} sub-model are taken from the analogy of iC_8 and iC_{10} model and their reaction system subsequently breaks down from larger to smaller n-/iso-paraffins. The intermediate species formed from the iso-paraffin decomposition are dependent on the position of methyl branch on the parent molecule. A further discussion on the effect with the degree of branching is presented later.

The model validation is done with in-house experiments as well as from literature. Except for i-$C_{11}H_{24}$, the ignition delay times and flame speeds are available, whereas for i-$C_{11}H_{24}$, alcohol-to-jet (ATJ) is used for comparison. As shown Fig. 13, the ignition delay time of i-C_8H_{18} and i-$C_{10}H_{22}$ are excellently reproduced by the mechanism. For i-$C_{10}H_{22}$, the ignition delay times are available for two isomers (2,2,4 methyl heptane and 2,7 methyl octane), which are nearly similar. The modeled ignition delay times of i-$C_{11}H_{24}$ is compared with ATJ-synthetic paraffinic kerosene (ATJ-SPK) data where for $\Phi = 1.0$ and 2.0, they are well reproduced by the model at high temperatures. The deviation below 1000 K can be due to absence of low temperature chemistry in the present model. Additionally, iso-octene ignition delay times are well reproduced as function of fuel stoichiometry and pressure at all temperatures studied.

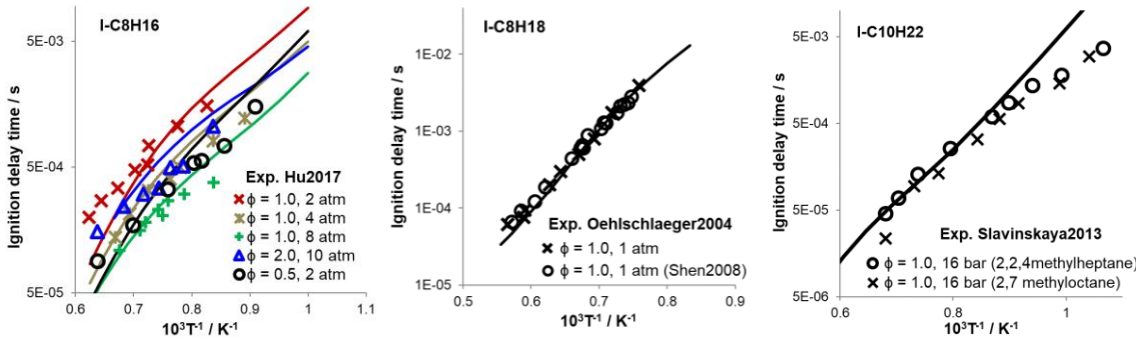

Fig. 13: Validation of ignition delay times of various iso-paraffins present in the mechanism. A complete validation data and the input conditions is available in the supplemental material. References: Hu2017 [53], Oehlschlaeger2004 [55], Shen2008 [54], Slavinskaya2013 [30].

The model prediction of laminar flame speeds of all four iso-paraffins and olefin iso-octene are compared with measurements at three different pressures in Fig. 14. The modeled data are reproduced within the experimental uncertainty as function of pressure and fuel stoichiometry. As mentioned earlier, in absence of any measured data the flame speeds for i-$C_{11}H_{24}$ are compared with ATJ. Additionally, the modeled i-C_8H_{16} also shows very good reproduction of flame speed for the three measured pressures.

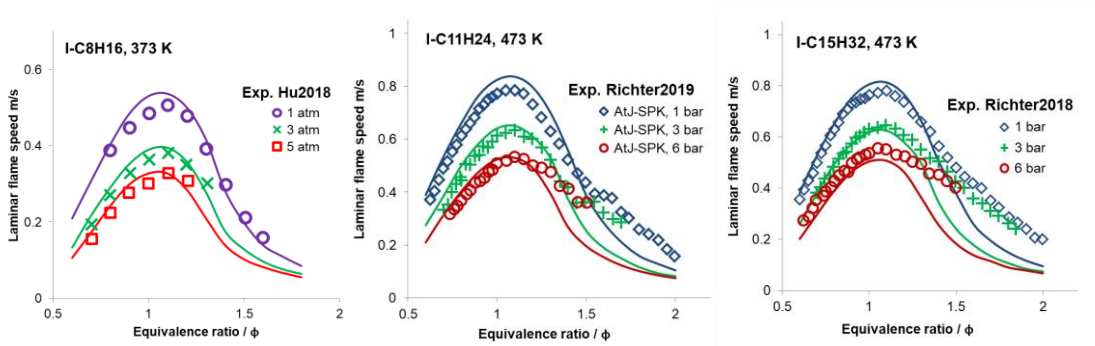

Fig. 14: Model validation of laminar flame speed as function of fuel stoichiometry for various iso-paraffins. A complete validation data and the input conditions is available in the supplemental material. References: Hu2018 [118], Richter2019 [31], Richter2018 [32].

The species profiles in the burner stabilized laminar flames are available only for iso-octane and 1-methylnonane isomer of i-$C_{10}H_{22}$. In absence of any other data the 2,7-dimethyl-octane as i-$C_{10}H_{22}$ isomer is compared to 1-methylnonane. The major species as well as fuel and oxidizer conversion of i-C_8H_{18} are excellently reproduced by the mechanism as shown in Fig. 15. As seen earlier, the ignition delay times of two i-$C_{10}H_{22}$ isomer were quite similar and therefore, the global prediction could be expected to be similar for both these isomers too. The fuel decomposition and major product formation of modeled 2,7-dimethyl-octane are quite similar to the measured 1-methylnonane. The main variation among these isomers is expected among the intermediates formed due to different positioning of methyl branch on the fuel molecule.

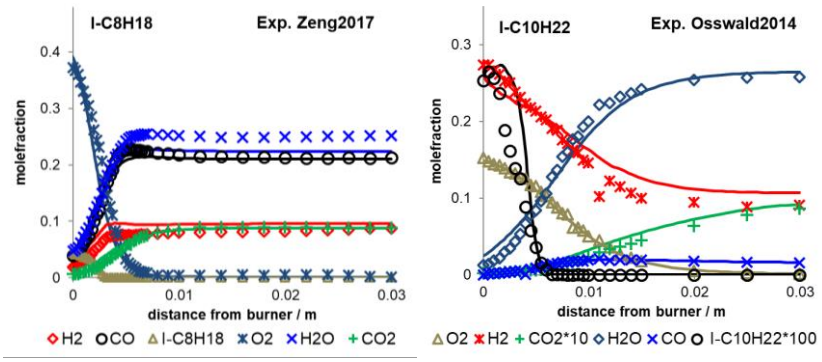

Fig. 15: Validation of speciation data in laminar flame of i-C_8H_{18} (iso-octane) and i-$C_{10}H_{22}$ (exp.:1-methyl nonane, model: 2,7 dimethyl-octane) present in the mechanism. References: Zeng2017 [147], Osswald2014 [134].

In addition, we have measured the speciation data of iso-octane and farnesane in our high temperature flow reactor [160]. In the temperature range of 750 to 1200 K for stoichiometric and fuel rich stoichiometry, the conversion of fuel and oxidizer as well as formation of major products are shown in Fig. 16. The conversion of iso-octane is well predicted by the model whereas the oxygen conversion in modeled farnesane is faster at temperatures above 900 K compared to the experiments.

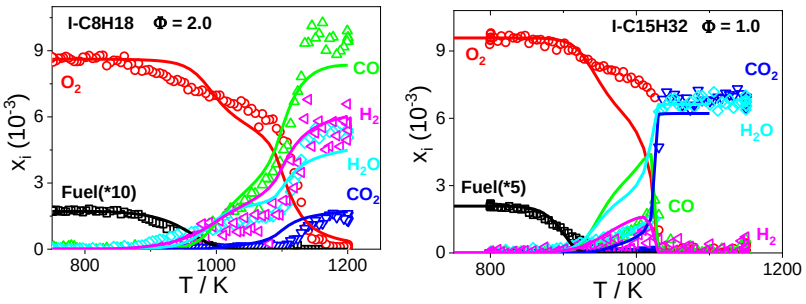

Fig. 16: Fuel, O_2, and major species obtained in DLR high temperature flow reactor for i-C_8H_{18} and i-$C_{15}H_{32}$ [160].

3.4 Cyclo-paraffins

The cyclo-paraffins are important component of various fuels and are present in varying composition. Typically, they account for roughly 10, 20, to 35% in gasoline, jet and diesel fuel respectively [187]. Their presence in the fuel mixture is important for various physical/chemical properties. It provides higher density, boiling points compared to other paraffins and supplies lower freezing point to enable safe operation of aviation fuels at higher altitude [188]. The present mechanism includes three different cyclo-paraffins, namely one-ring cyclohexane, one-ring alkylated n-propylcyclohexane as well as two-ring decahydronaphthalene widely known as decalin (Fig. 17). The reaction mechanism for decalin has been lately added to the model.

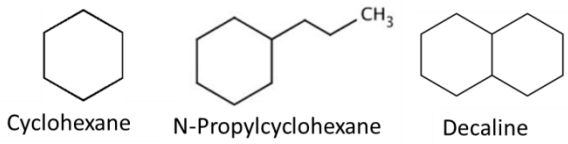

Fig. 17: Nomenclature of cy-paraffins present in the model.

The decomposition of cyclohexane follows two paths where either chemical cascading of cyclohexane via dehydrogenation leads to cyclohexyl radical followed by channel cyC_6H_{10} → cyC_6H_9 → cyC_6H_8 → cyC_6H_7 → C_6H_6 leading to benzene [187, 189, 190, 191]. More discussion on role of cyclo-paraffin to the PAH formation will follow in Part III of this series [26]. The second channel is the ring opening that leads to the straight chain isomers, which further breaks down to form smaller hydrocarbons. The importance of both these channels are dependent on the combustion environment. The C_6 intermediates such as cyclohexene, cyclohexa-1,3-diene, benzene of chemical cascading dehydrogenation channel is detected in the low temperature oxidation investigated in rapid compression machine [192]. Measurements in jet stirred reactor [193] and in stoichiometric premixed flame [194] showed dominance of dehydrogenation route leading to benzene. Compared to this, the importance of the second channel, i.e. ring opening reactions, is shown by McEnally and Pfefferle [195] in fuel-rich high temperature regime of non-premixed cyclohexane flames. The dehydrogenation path is typically observed at low temperature and near stoichiometric condition. The consumption route of n-propylcyclohexane and decalin involves H-abstraction leading to either benzene or cyclopentadiene formation. Due to symmetric structure, cyclohexane is highly stable compared to decalin [57]. The reactions of decalin sub-system are added from POLIMI-mech [18].

The model validation with respect to ignition delay times of cyclo-paraffins present in the reaction mechanism is shown Fig. 18. For all the three components, the measured ignition delay times are excellently reproduced by the model for given high pressure data. For n-propylcyclohexane and decalin, the variation of fuel stoichiometry is also reproduced along with the temperature dependence.

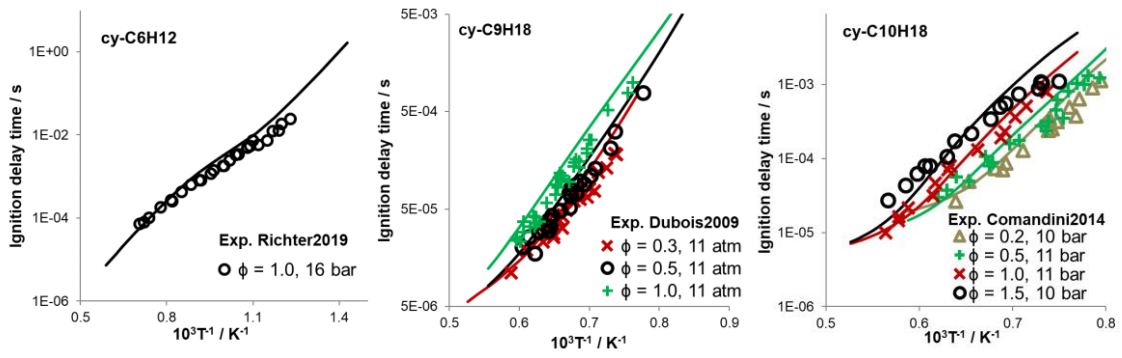

Fig. 18: Validation of ignition delay times of various cyclo-paraffins available in the mechanism. References: Richter2019 [29], Dubois2009 [56], Comandini2014 [57].

The laminar flame speed measurements are available for comparison with the model prediction. Both the cyclohexane and n-propylcyclohexane are excellently reproduced by the model at three pressures as shown in Fig. 19. The predictions of decalin flame speed are slightly higher in the fuel rich side of the model where one should also consider high measurement uncertainties.

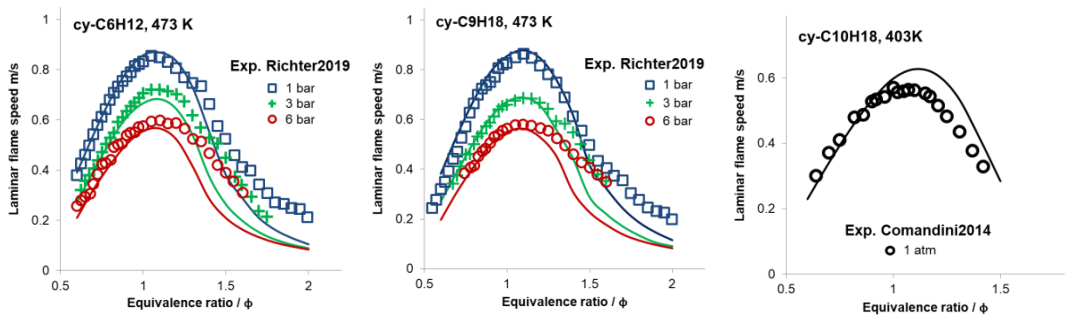

Fig. 19: Model validation of laminar flame speed as function of fuel stoichiometry for various cyclo-paraffins. References: Richter2019 [29], Comandini2014 [57].

The species profiles obtained in laminar premixed flames for these three cyclo-paraffins are available in literature. Comparisons of model predictions with measurements are shown in Fig. 20. The major predicted product concentrations are in very good agreement with the measurements.

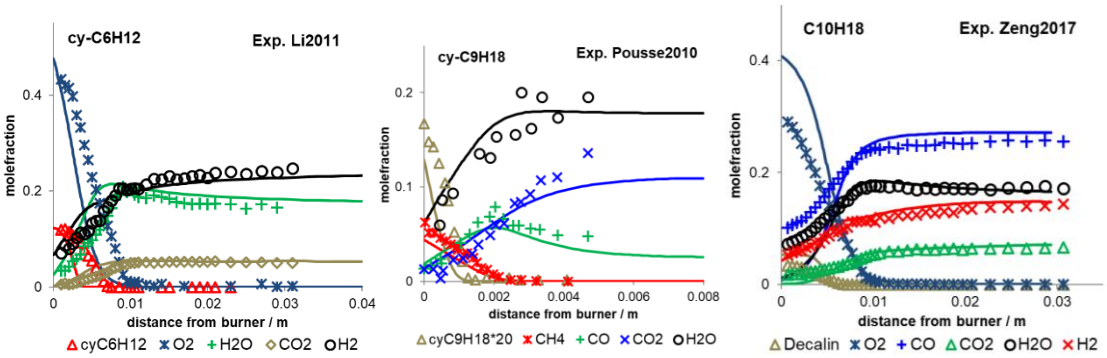

Fig. 20: Validation of speciation data in laminar flame of cyclohexane, n-propylcyclohexane, and decalin present in the mechanism. References: Li2011 [148], Pousse2010 [149], Zeng2017 [147].

The prediction of major species and fuel and oxidizer conversion of both cyclohexanes and decalin obtained in the DLR flow reactor are presented in Fig. 21. Overall, the oxygen and fuel conversion are slightly different than the measurements however the general temperature dependence is well reproduced.

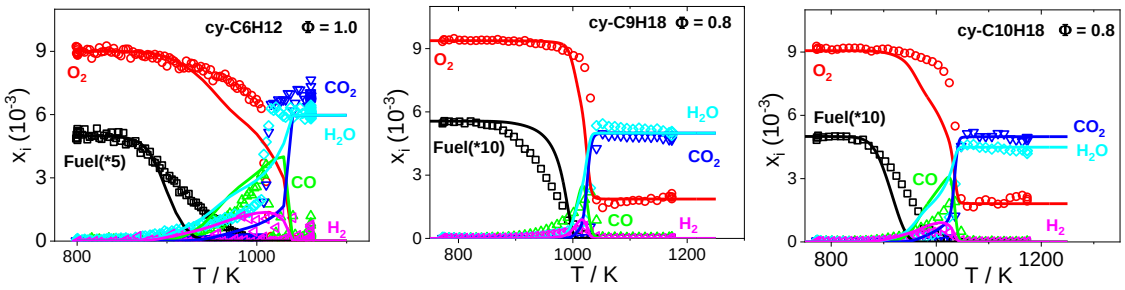

Fig. 21: Comparison of modeled major species with measured data in the DLR high temperature flow reactor for cyC_6H_{12}, cyC_9H_{18}, and decalin.

3.5 Aromatics and PAH up to C_{20} (including cyclo-aromatics)

The reaction model for aromatic species is important for their description as fuel component and as precursors leading to soot emission in complex fuels. In addition to single-ring benzene, toluene, styrene, n-propylbenzene, our reaction model also includes cyclo-aromatics such as indane, tetralin. Also, two-ring indene, naphthalene, methyl-naphthalene, and biphenyl are present in the reaction model. Larger PAHs included in the reaction mechanism are phenanthrene (A3, $C_{14}H_{10}$), methyl-phenanthrene ($A3CH_3$, $C_{15}H_{12}$), ethynyl-phenanthrene ($A3C_2H$, $C_{16}H_{10}$), pyrene (A4, $C_{16}H_{10}$), ethynyl-pyrene ($A4C_2H$, $C_{18}H_{10}$), benzo(ghi)fluoranthene ($C_{18}H_{10}$), chrysene (A4, $C_{18}H_{12}$), benzo(a)pyrene (A5, $C_{20}H_{12}$). Their molecular structures are presented in Fig. 22.

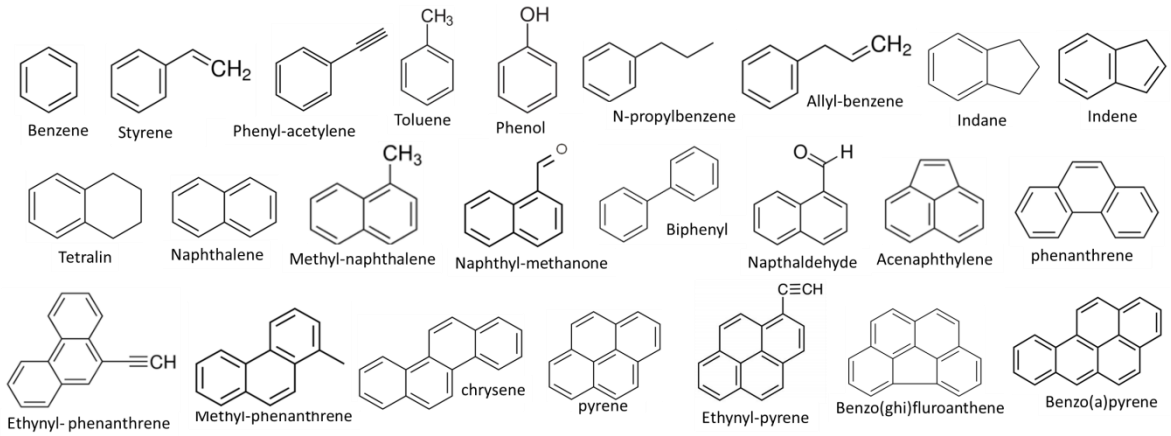

Fig. 22: Nomenclature of aromatics present in the model.

A detailed description of PAH mechanism is available in [196]. No major modifications are done to the aromatics description except modification of benzene pathways at intermediate temperature described in our earlier work [159]. The aromatics part of the mechanism is extended to include two new components indane and tetralin. The rates of indane related reactions, formation and consumption of indanyl radicals as well as important intermediates methyl-styrene are added from the study of Pousse et al. [149], whereas the reactions of sub-system of tetralin is added from POLIMI-mech [18].

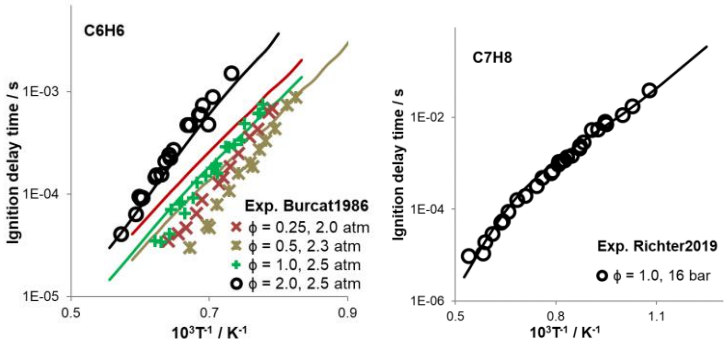

Fig. 23: Validation of ignition delay times of various aromatics available in the mechanism. A complete validation data and the input conditions is available in the supplemental material. References: Burcat1986 [58], Richter2019 [29].

The model prediction of ignition delay times of 1-ring benzene, toluene, styrene, n-propylbenzene as well as 2-ring methyl-naphthalene are shown and compared with measurements in

Fig. 23. All ignition delay times are well reproduced by the model when compared to measurements.

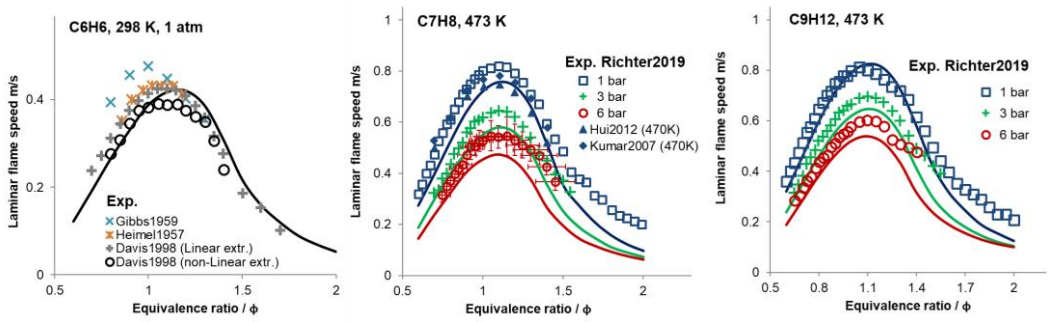

Fig. 24: Model validation of laminar flame speed of benzene, toluene and n-propylbenzene as a function of fuel stoichiometry. References: Gibbs1959 [101], Heimel1957 [132], Davis1998 [75], Richter2019 [29].

The measurements of flame velocities are only available for benzene, toluene and n-propylbenzene as shown in Fig. 24. All three fuels are reproduced by the mechanism within the available experimental uncertainty limit.

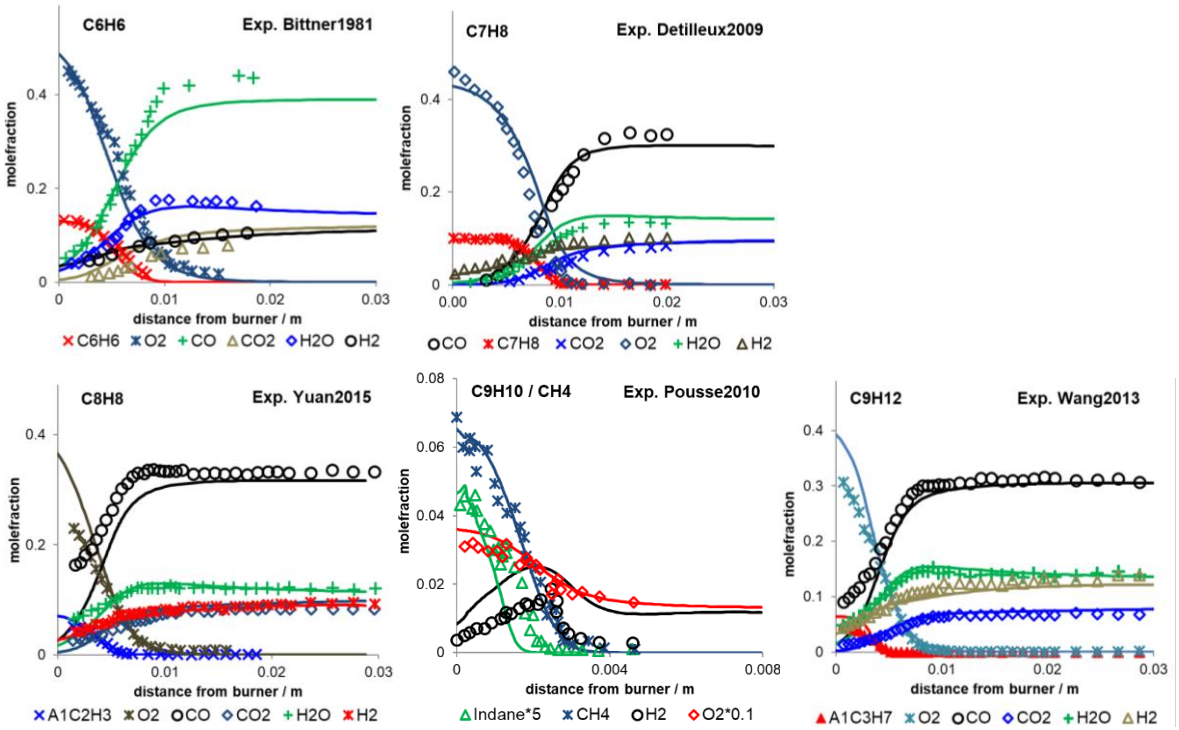

Fig. 25: Validation of speciation data in laminar premixed flame of benzene, toluene, styrene, indane-methane, and n-propylbenzene present in the mechanism. A complete validation data and the input conditions is available in the supplemental material. References: Bittner1981 [151], Detilleux2009 [152], Yuan2015 [153], Pousse2010 [154], Wang2013 [155].

Compared to global combustion predictions, speciation data are available in literature for five aromatics obtained in burner stabilized premixed flames. The fuel decomposition and major species formation as shown in Fig. 25, is excellently reproduced by the mechanism. The figure also compares the major species production. Additional data on speciation for toluene, n-propylbenzene, tetralin and methyl-naphthalene in the temperature range of 750 – 1350 K are obtained in DLR's atmospheric flow reactor as shown in Fig. 26. The model predictions of fuel and oxidizer conversion as well as major products formed are well in agreement with the measurements.

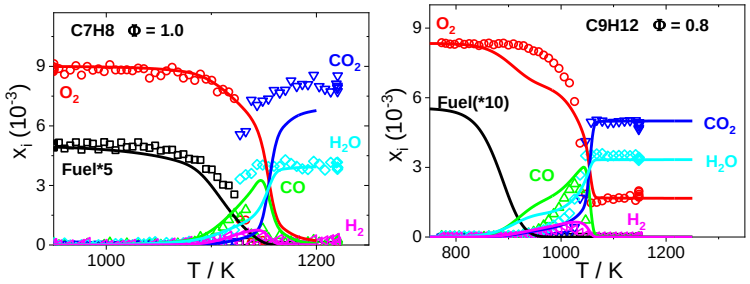

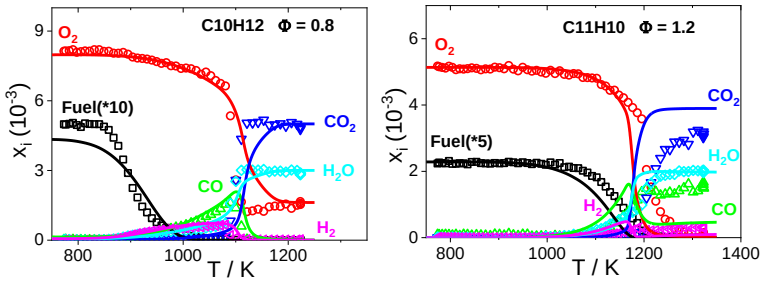

Fig. 26: Comparison of modeled major species with measured data in the DLR high temperature flow reactor for toluene, n-propylbenzene, tetralin and methyl-naphthalene.

3.6 Polyynes

Polyynes are linear chain molecules with alternating single and triple bond. Four polyynes di-acetylene (C_4H_2), tri-acetylene (C_6H_2), octatetrayne (C_8H_2), and decapentayne ($C_{10}H_2$) are part of the mechanism (Fig. 27). Polyynes are responsible for the formation of large carbonaceous molecules such as PAHs, fullerenes and soot and are considered to be highly reactive in polymerization reactions leading to soot nuclei formation [197]. The smallest polyyne di-acetylene is part of the core mechanism, whereas the three other polyynes are specifically included in the mechanism. Note, that the polyyne sub-model (C > 4) is important for calculations related to soot and can be removed otherwise.

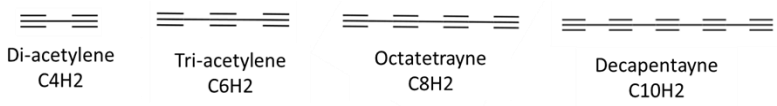

Fig. 27: Nomenclature of polyynes present in the model.

The importance of the aliphatic polyynes in soot nucleation process has been discussed in literature. For example, Krestinin [197] tested a kinetic model against pyrolysis experiments of set of hydrocarbons showing that the thermodynamic stability of C_2H_2 and polyynes increases with temperature in contrast to other hydrocarbons that tends to decline. They proposed a model that includes polymeric growth of polyyne by its addition to radical sites and further formation of aromatic structures were only assumed. So far, in literature on reaction mechanisms, not enough attention is given to allow thorough evaluation of reactions involving steps of large polyynes to soot nuclei formation. The major polyyne growth reactions that are included in the model are $C_{2n}H_2 + C_2H \rightarrow C_{2n+2}H_2 + H$ as well their decomposition reactions. Further consumption reactions of $C_{10}H_2$ are part of soot nuclei formation (part of soot models), and are outside scope of our mechanism.

The prediction of polyynes formation is tested in three different premixed flames namely, acetylene, benzene and styrene flames as shown in Fig. 28. Considering roughly factor of 2 measurement

uncertainty is possible for species where no direct calibration is available, the formation of all four polyynes are excellently reproduced by the model.

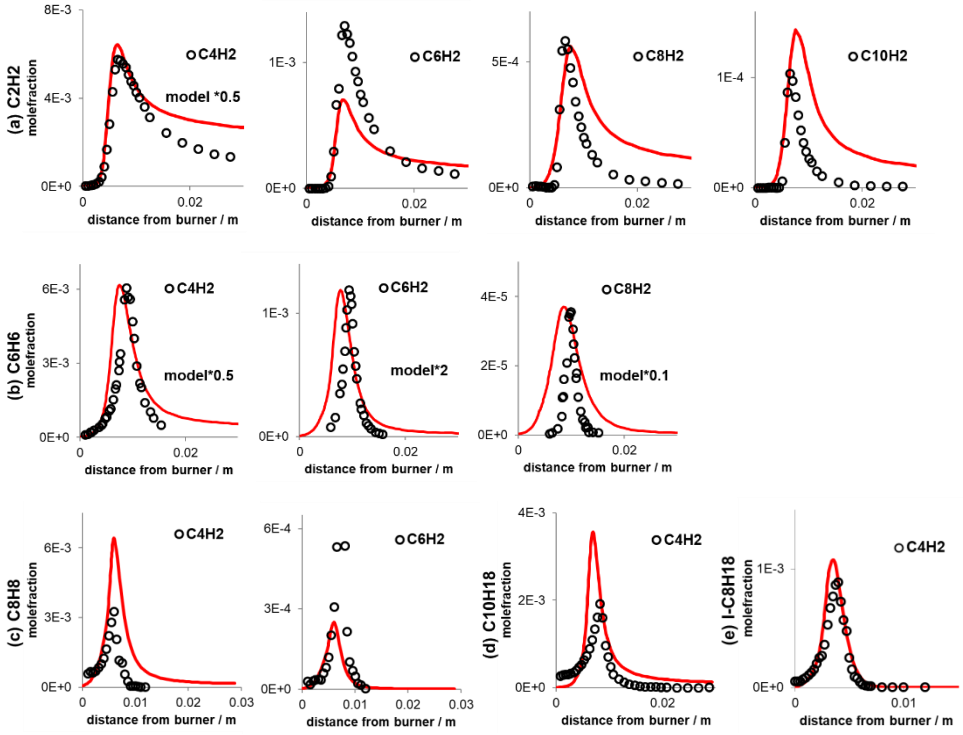

Fig. 28: Model prediction of polyynes measured in (a) acetylene flame ϕ = 2.4, 40 mbar. [136], (b) benzene flame, ϕ = 1.8, 0.026 atm [151], (c) styrene flame, ϕ = 1.7, 0.0395 atm [153], (d) decalin flame, ϕ = 1.8, 0.04 atm [150], and (e) iso-octane flame, ϕ = 1.47, 0.04 bar [147]. The details of the fuel composition in the figures are available in supplemental material.

3.7 Oxygenates – Alcohols and OMEs

Oxygenates are being increasingly studied for its potential as fuel or fuel blends specifically for road transportation purposes. For the scope of covering fuels from different sectors, our mechanism is extended to include straight chain alcohols varying from C_1-C_4, as well as oxymethylene ethers such as dimethyl ether DME, and OME_n with n = 1-5. The validation of these hydrocarbons is presented in Fig. 29 to Fig. 31.

The ignition delay times of methanol, ethanol and n-butanol are well predicted for different stoichiometries and at high pressures. Additionally, acetaldehyde and n-butanal, part of alcohol mechanism, are also tested against the experiments available in the literature. The measurements of ignition delay times in high temperature regime are available only for DME and OME1. The Fig. 29 shows comparison of the ignition delay time of DME and OME1 with in-house shock-tube data. The ignition delay times of both these species are excellently reproduced by the model for the three considered pressures.

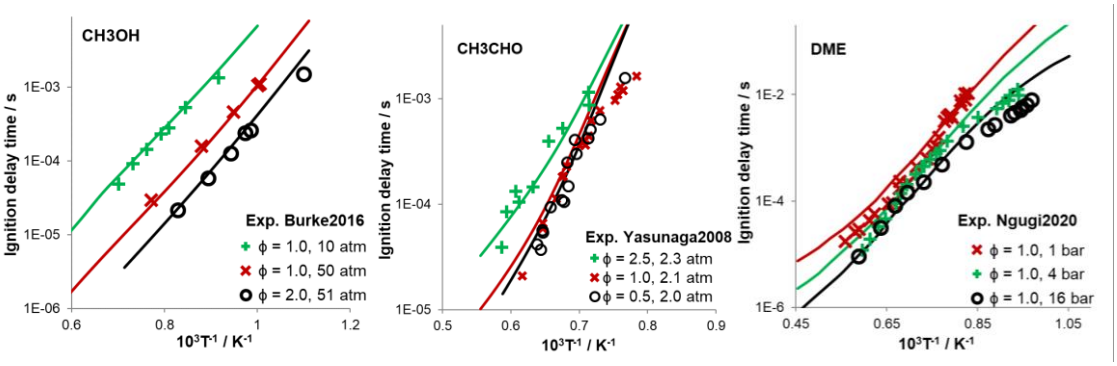

Fig. 29: Ignition delay times of oxygenates including alcohols, aldehydes and oxymethylene ethers. A complete validation data and the input conditions is available in the supplemental material. References: Burke2016 [63], Yasunaga2008 [64], Ngugi2020 [33].

The model predictions of laminar flame speed compared to the measurements are shown in Fig. 30. The flame speed of the alcohol and OME are excellently reproduced by the model, except for butanal, where higher model predictions are observed.

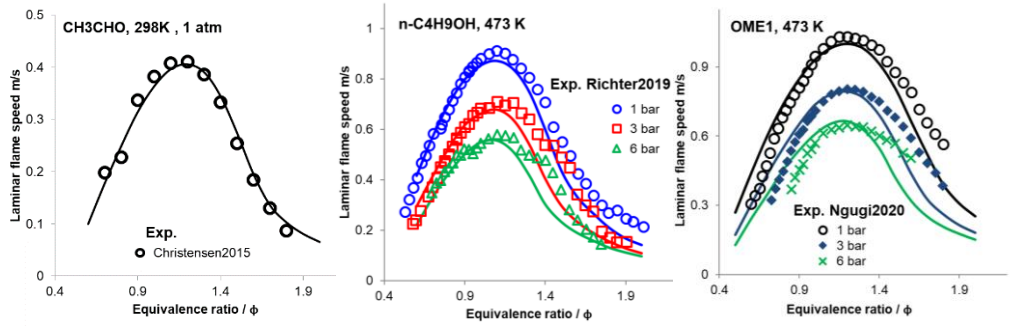

Fig. 30: Laminar flame speed of oxygenates including alcohols, aldehydes and oxymethyl ethers. A complete validation data and the input conditions is available in the supplemental material. References: Christensen2015 [120]. Richter2019 [69], Ngugi2020 [33].

Similarly, the species profiles in a burner stabilized laminar flames are available only for acetaldehyde, DME, OME1 and OME3. The major species formed in these flames are shown in Fig. 31. The consumption of fuel and formation of major combustion products are well reproduced by the model.

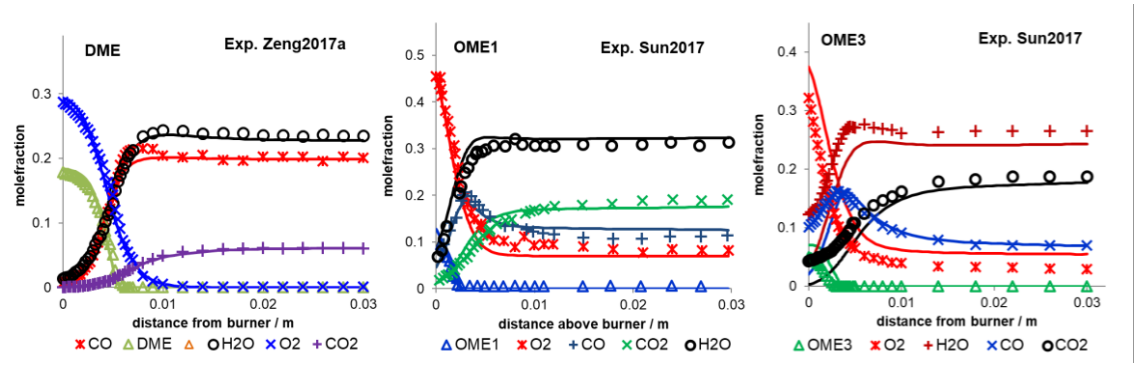

Fig. 31: Validation of speciation data in laminar flame of various oxygenates present in the mechanism. A complete validation data and the input conditions is available in the supplemental material. References: Zeng2017a [147], Sun2017 [131].

3.8 Model predictivity – Important intermediates

Different intermediates are formed during the combustion of hydrocarbons and their formation depends on the molecular structure of the hydrocarbon. In addition to global combustion behavior, the accuracy of the reaction model is further tested by comparing different intermediate species as they appear in the rate of production of parent fuel molecule with measurements obtained in the burner stabilized premixed flames as presented in Fig. 32. The major species are presented in previous sub-sections whereas the general decomposition channels of all the molecules presented in this section is given in Fig. 33.

Among the n-paraffins, n-heptane is shown in the Fig. 32. The consumption of n-heptane to form first fuel radical by H-abstraction reactions gives n-heptyl radicals which forms olefins such as n-heptene (nC_7H_{14}), pentene (C_5H_{10}) and propene (C_3H_6) through β-scission (Fig. 33). As shown in Fig. 32, the formation of these olefins is excellently reproduced by the modeled n-heptane flame. Smaller C_2 intermediates such as acetylene and ethane usually formed from the subsequent decomposition channels of olefins are also well predicted by the model.

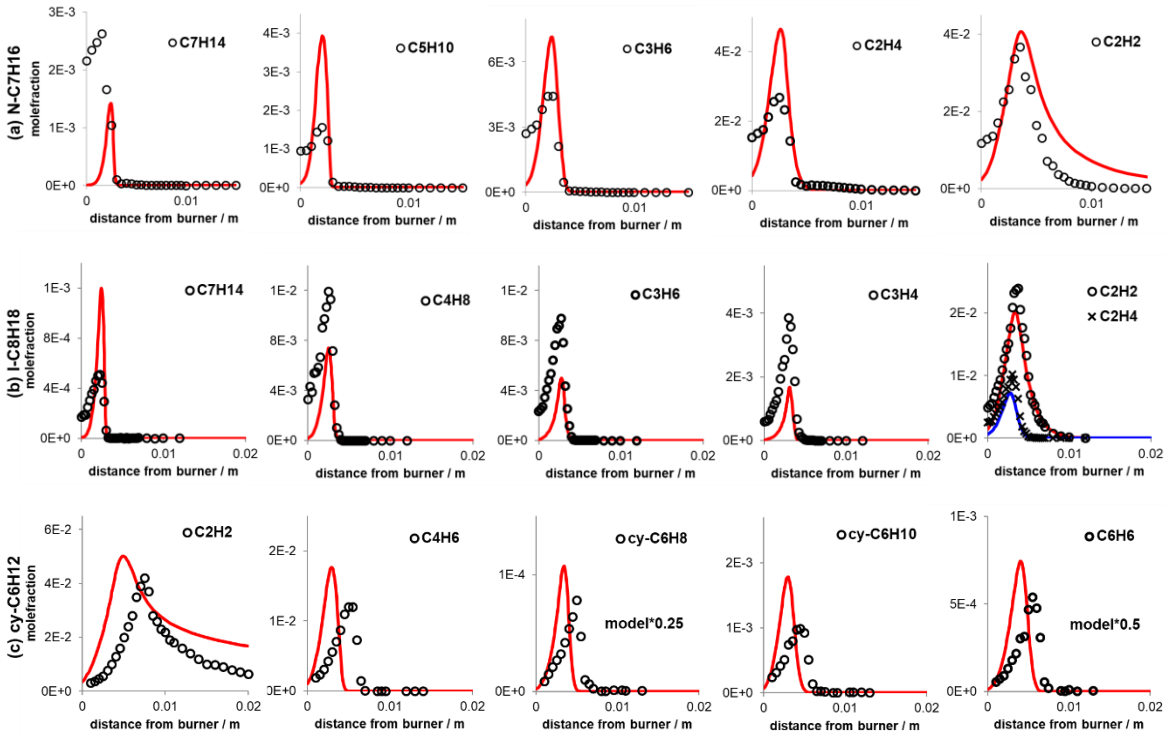

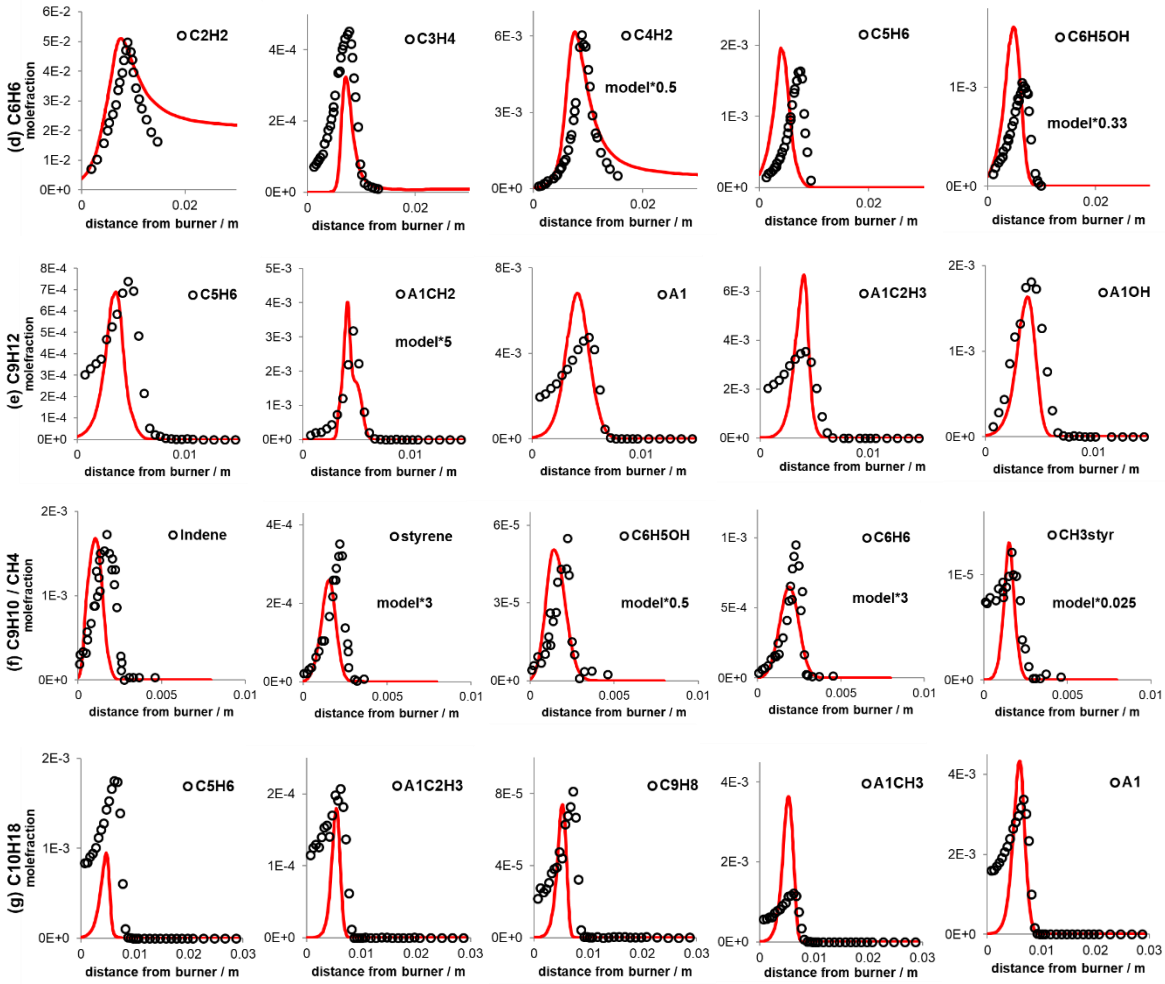

Fig. 32: Prediction of direct intermediate species formed from the fuel hydrocarbon in the stabilized flames presented earlier. (a) n-C_7H_{16}, ϕ = 1.69, 40 mbar [145], (b) i-C_8H_{18}, ϕ = 1.47, 40 mbar [147], (c) cy-C_6H_{12}, ϕ =2.0, 40 mbar [148], (d) C_6H_6, ϕ =1.8, 26 mbar [151], (e) C_9H_{12}, ϕ =1.79, 40 mbar [155], (f) CH_4/ C_9H_{10}, ϕ = 0.67, 67 mbar [154], (g) $C_{10}H_{18}$, ϕ =1.8, 40 mbar [150]. The details of the fuel composition are available in supplemental material.

The iso-octane decomposition leads to formation of octyl radicals. The fuel radical breakdown leads to the direct formation of species such as iC_7H_{14}, iC_4H_8, as well as C_3H_6. These species, along with the smaller hydrocarbons formed subsequently such as C_2H_2, C_2H_4, C_3H_4, are in excellent agreement with the measurement (Fig. 32).

In the cyclohexane flames, smaller hydrocarbons such C_4H_6, C_2H_4 are formed through ring opening of cyclohexyl radicals whereas benzene is formed by chemical cascading of cyclohexyl radical through cyC_6H_{10} → cyC_6H_9 → cyC_6H_8 → cyC_6H_7 → C_6H_6 route. Model prediction of intermediate species from both these channels are very well reproduced by the model as shown in Fig. 32.

The oxidation of simple aromatic hydrocarbon benzene is led by initial attach to O-atom leading to formation of phenoxy radical which further forms cyclopentadiene. The breakdown of cyclopentadiene to cyclopentadienyl radical give various smaller hydrocarbon species mainly in the

sequence C_5H_5 → C_4H_4 → C_3H_4(/C_4H_2) → C_2H_2. The formation of these species is shown in Fig. 32, where the modeled mole fractions are well reproduced when compared to the flame measurements.

The decomposition channel of n-propylbenzene present in the mechanism leads to formation of fuel radical by H-abstraction channel. The propylbenzyl radical decomposition leads to the formation of benzyl radical which subsequently forms cyclopentadiene through formation of phenyl radical in one channel and benzene through phenoxy radical → phenol → benzene in another channel. An important product of n-propylbenzene decomposition is direct formation of benzene and formation of styrene through phenyl-ethyl radical. The species cyclopentadiene, benzyl radical, benzene, styrene and phenol thus formed are in excellent agreement with the measurement as shown in Fig. 32.

The decomposition of cyclo-aromatics indane gives indanyl radical, which forms indene. The indene undergoes H-abstraction forming indenyl radical which then follows two channels. In one channel the ring opening leads to formation of styrene via phenyl vinyl radical whereas in second channel, styrene radical leads to formation of phenol and subsequently benzene. Additionally, the indanyl radical can also undergo ring opening leading to formation of methyl-styrene formation. Fig. 32 shows the model prediction of indene, styrene, phenol, benzene, and methyl-styrene concentrations against experiments and is well reproduced by the model.

Finally, the species formation in the bi-cycloparaffin decalin is shown in Fig. 33. The formation of decalyl radical can undergo decomposition leading to cyclohexene (cyC_6H_{10}) and further cyclohexadiene (cyC_6H_8) formation. Another route leads to toluene and cyclopentadiene, styrene via indene, or ethylbenzene formation. All these species lead to benzene. The model prediction of toluene, styrene, indene, benzene and cyclopentadiene are excellently reproduced as shown in Fig. 32.

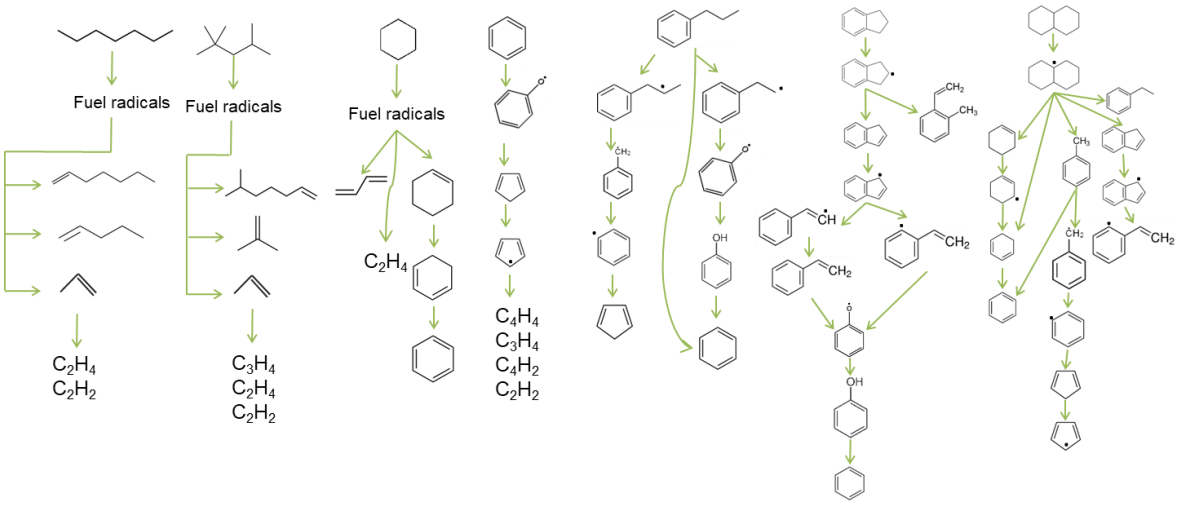

Fig. 33: General decomposition routes of various hydrocarbons discussed in the above flames.

3.9 Model predictivity – Comparison with literature mechanisms

In order to qualify the success of the model, our aim during the model development has been to prevail the quality of 3 factors: (1) model applicability for wide range of *T*, *p*, and Φ combustion conditions, (2) its reproducibility of the measured global combustion characteristics as well as speciation formed during the combustion in flame or reactors, (3) and equally important is, comparable predictability of our semi-detailed to the detailed models.

The superiority of the new mechanism not only lies in its predictive capability but also in the fact that it is a single mechanism. We consider the singleness of our mechanism as an important feature, that makes the modeling of various fuel surrogates including pollutants feasible with the same mechanism. This proves beneficial when analyzing the results for different fuels without being concerned about the deviation arising from chemistry when using different mechanisms. If one requires for same purpose two or more mechanisms, they are simply not additive and may require substantial revalidation efforts. Thus, a single mechanism provides advantage of direct use and keeps subsequent applicants flexible. Additionally, it is smallest compared to other mechanisms when number of species to the number of validated fuel components are considered. Reaction mechanisms such as LLNL mechanism [19], or automatic generated models are much more detailed and can provide better detailed chemistry however at the expense of high computational cost even for 1-D simulations, its application in CFD is not feasible. There are many mechanisms available in literature focused to one or few hydrocarbon molecules, but cannot be used for wide range of fuel surrogates.

With regard to CFD applications the entire model with 238 species is still large leading to long computational times. However, the reaction model proposed in this work is modular to address this issue. In more detail, one can easily remove components not required for the description of certain fuel surrogate or neat components. In terms of jet fuels surrogate for example, sub-mechanisms of

alcohol and oxymethylene ethers (usually important as gasoline/diesel surrogates) can be removed easily without affecting its predictability. Aromatics, polyynes can be removed in a similar way, when the focus of the study is not pollutant formation (soot precursors chemistry). Also, chemistry application in CFD is wide, where different CFD models necessitates varying degree of chemistry detailing, for example LES is computationally exhaustive therefore a reduced targeted model is more suitable. A model reduction and optimization for the specified conditions is possible through our in-house reduction tool LinTM [198]. These models highly depend on the boundary conditions and targets of different applications. For the most efficient computational application tailor-made reduced models are required and no general reduced model should be supplied. In addition, the size of our semi-detailed model is beneficial for the fast and efficient generation of these tailor-made reduced models.

The prediction of our model with the well-known literature mechanisms POLIMI [18], LLNL [19], JetSurf2.0 [20] and RWTH [21] that contains multiple hydrocarbon components are compared with the current mechanism. The comparison is available as supplemental material. In general, all models perform well. The differences or advantages between mechanism of present work and the mechanism close to our work POLIMI-mech [18] is not straightforward to summarize, so key thoughts are given here. Both models are semi-detailed with similar number of species, but different number of reactions. POLIMI-mech has roughly factor of 10 higher number of reactions than the present model resulting in a significant longer computing time for flames. Both reaction models contain many different hydrocarbon species, but the implemented fuel components vary. At the given point, the low temperature chemistry model available in POLIMI-mech is not present in our mechanism. To summarize, both models perform well and both address different aspects regarding technical fuels. In particular for semi-detailed models we believe in the advantage of multiple independent approaches even if targeting and capabilities are similar between DLR and POLIMI model. The strategy of our modular approach enables flexible use focusing on the features of interest.

4. Discussion

4.1 Influence of the molecular structure on global combustion characteristics

A fuel is composed of various hydrocarbon components with different underlying chemical characteristics. These different chemical characteristics influence the fuels' overall combustion characteristics. How does the global combustion properties of fuels behave? For a deeper understanding, a comparison of their individual hydrocarbon components is shown in Fig. 34 for different ignition delay times and laminar flame speeds. The ignition delay times of n- and iso-paraffins are similar at high temperatures whereas small variation is observed at lower temperatures considering the experimental setup allows measurements of ignition delay times up to 30 ms

depending on the temperature [29]. Compared to all cyclic compounds, except toluene which shows distinctive slower ignition times, all hydrocarbons shows similar values at higher temperatures. The less reactivity of alkylated aromatics (toluene, methylnaphthalene) are known due to formation of resonantly stable intermediates which persist in the intermediate temperatures before reacting further.

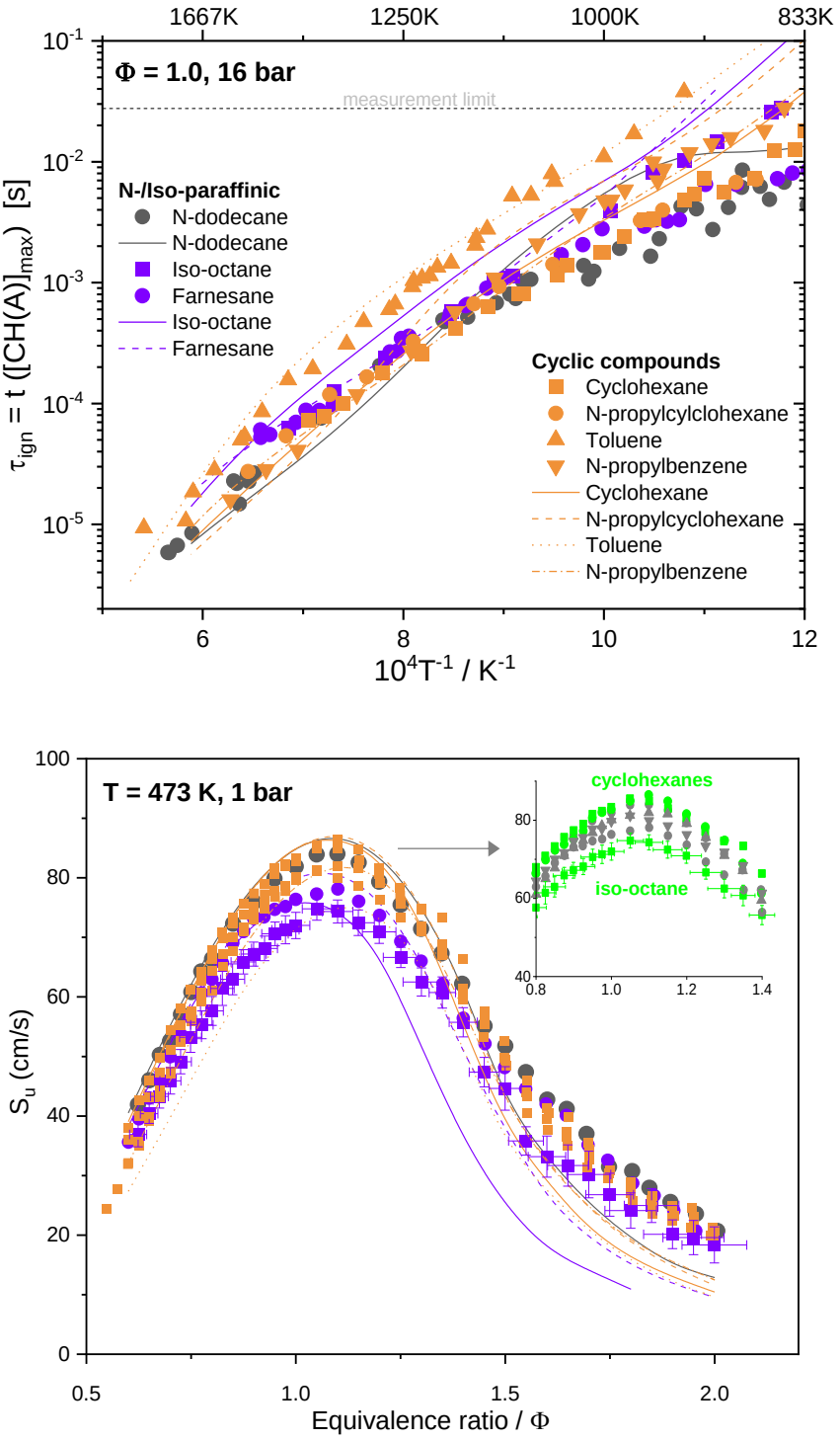

Fig. 34: Ignition delay times and laminar flame speeds of various hydrocarbons. Experiment: symbols [29], Model: curves. Inserted figure shows data of iso-octane and cyclohexanes (green) compared to other components (gray).

Compared to them, the flame speeds of most of the hydrocarbons are within the uncertainty limits of measurement as shown in Fig. 34. In the fuel lean or rich conditions, all hydrocarbon presented shows similar flame speeds. The maximum deviation is seen at around stoichiometric conditions. The exceptions are iso-octane and cyclohexanes with considerably lower flame speeds for iso-octane and higher flame speeds for the latter closer to stoichiometric conditions. On the lean and rich side these deviations are weaker with additional high measurement uncertainties to be considered on rich side.

A discussion on intermediates needs to be placed in the context of technical fuels and their hydrogen-carbon ratio. Since this is an in-depth analysis of its own and beyond the focus of this part here, the conclusion is given for completeness: although the formation of smaller intermediate species follows similar production routes in various fuels, they are specific to the fuel structure and cannot be generalized [26].

4.2 Iso-Paraffins: Significance of degree of branching

With increasing availability of iso-paraffinic fuels, which consist of highly branched paraffin molecules, it is interesting to see the influence of the degree of branching in iso-paraffins on the combustion chemistry. For example, the alcohol to jet ATJ-SPK fuel (Gevo) is consisted of highly branched molecules mainly consisting of ~80% iso-dodecane (2,2,4,6,6 pentamethylheptane, $iC_{12}H_{26}$), and iso-cetane (2,2,4,4,6,8,8 heptamethylnonane, $iC_{16}H_{34}$) [199]. Except iso-octane and iso-hexadecane, the combustion studies and models related to branched iso-paraffins are limited [2, 54, 186, 200, 201]. The number and position of alkyl branch on the parent paraffin molecule have great influence on the subsequent intermediates and products formation. With respect to soot precursors' formation, this influence can have different effect for fuels that are mainly iso-paraffinic, and for fuels with significant proportion of cyclic components as the latter may have dominance from the cyclic component chemistry. This has been observed in highly branched iso-paraffinic fuels such as ATJ-SPK that have higher sooting propensity compared to farnesane [31].

Based on 4 different iso-paraffins present in our model, we compare the differences among their global combustion characteristics and intermediates formation. Among the global characteristics, the maximum difference between the ignition delay times of iso-octane, farnesane and iso-paraffinic fuels such as ATJ-SPK is about factor of 2. Flame speed varies about 9% which is within the measurement uncertainties (Fig. 35a). The high temperature ignition delay times of octane [60] or heptane [202] isomers showed no substantial difference in the reactivity. Similarly, the position of branching of investigated octane isomers [203] showed no measurable influence on flame propagation. Compared to them at the DLR flow reactor conditions, model shows the intermediates and soot precursors formed in iso-octane are different than the other three iso-paraffins 2-methyldecane, 2,7 dimethyl-octane, and farnesane which has similar reactivity (Fig. 35b). In iso-

octane, the fuel radical decomposition leads mostly to formation of smaller hydrocarbons such as iso-butene and butyl radicals which are the precursors to the formation of C_2H_2, C_2H_4, C_4H_4, iC_4H_5 that leads to benzene from even route C_2+C_4 [159]. Compared to iso-octane, both farnesane and 2-methyldecane lead to various pool of fuel specific olefins and alkyl radicals >C_5, decomposing to various species (Fig. 35c). Fig. 35d shows this leads to less formation of above discussed benzene precursors and thereby less formation of benzene and naphthalene. In general, most of the PAHs are seen to be produced more in iso-octane compared to other three iso-paraffins.

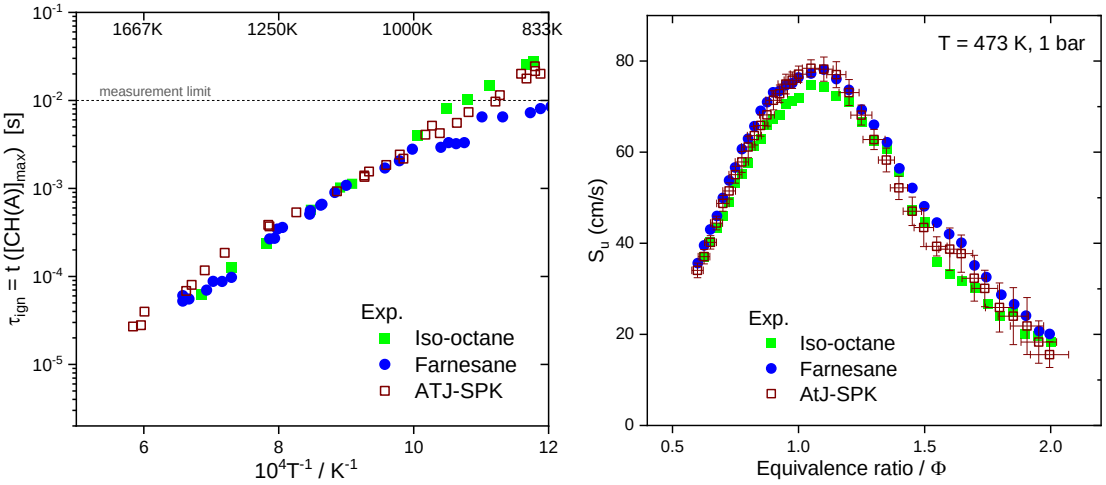

(a) Global combustion characteristics, measurements of ignition delay times and flame speeds, of iso-paraffins with varying degree of branching

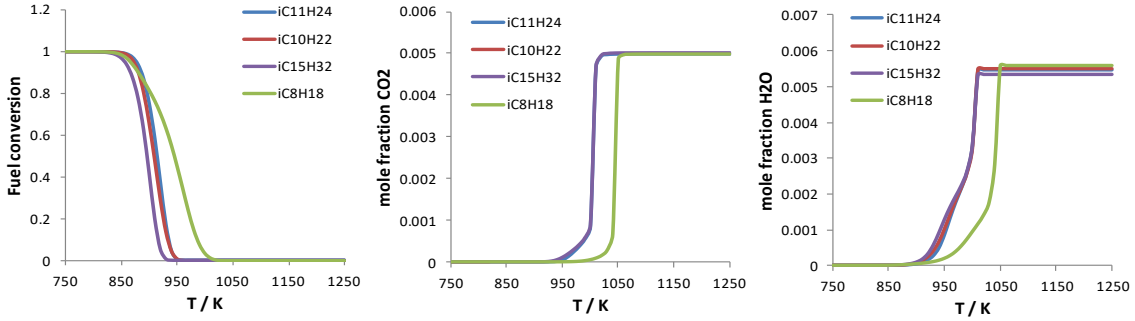

(b) chemical reactivity of iso-paraffins shown as modeled fuel conversion and major product formation at flow reactor conditions

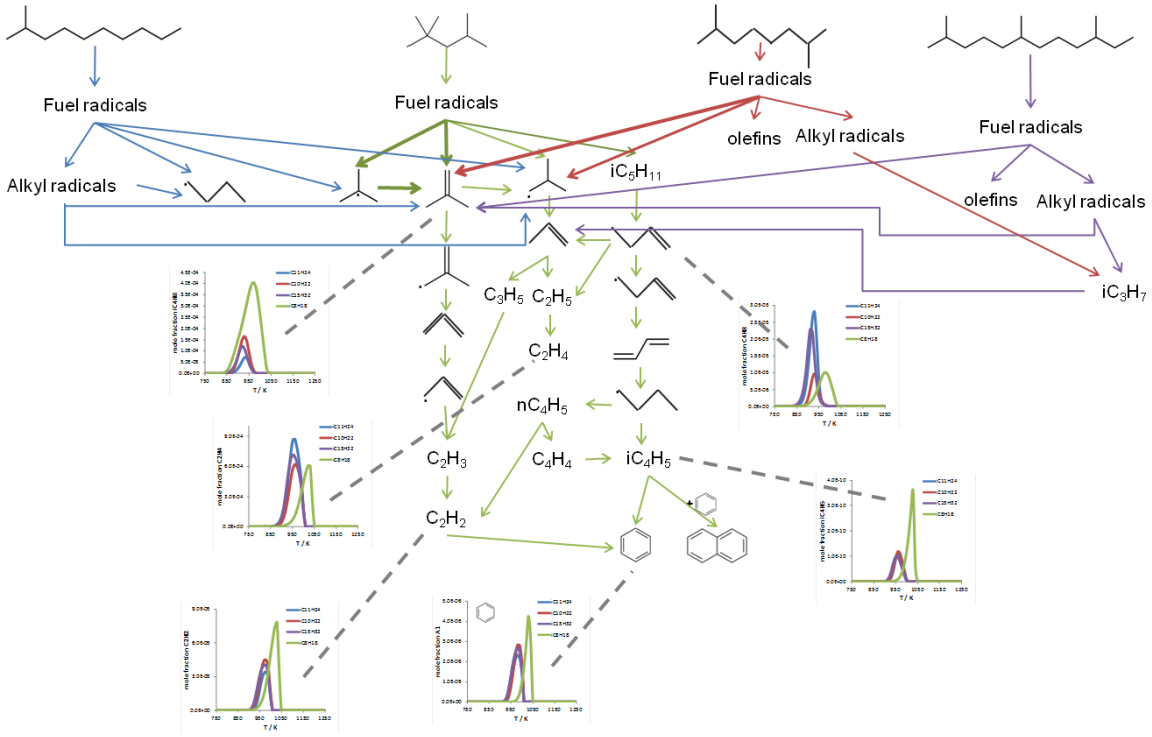

(c) Difference in decomposition routes and intermediate formations of four selected iso-paraffins

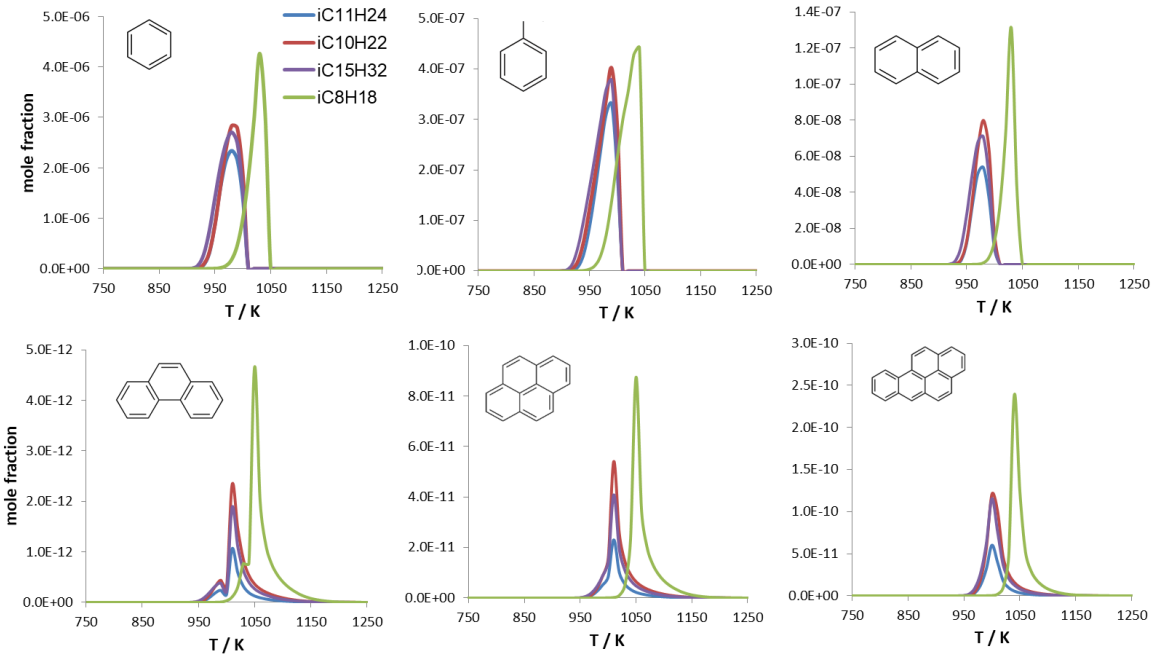

(d) Effect of degree of branching on soot precursors' formation

Fig. 35: Comparison of influence of degree of branching on reactivity and formation of soot intermediates.

From the analysis of fuel structure of octane isomers in premixed flames, Ji et al. [203] showed that due to the formation of H-scavenging resonantly stable intermediates such as propene, allyl, and iso-butene, the branched isomers present low reactivity. The fuel decomposition leads to C_1-C_4 intermediates ruling the overall reactivity of the flame and leaving fuel specific reactions of

secondary importance. A similar investigation on this effect and number of methyl substitution on octane diffusion flame structure [204] showed that the increase in methyl substitution increases production of iso-butene and propene and a reduction in ethene. The increased formation of stable intermediates and subsequently reduced reactivity in highly branched iso-octane compared other iso-paraffins, shown in above studies in different configurations, also supports our flow reactor observation (Fig. 35c). To this end, our study includes varying carbon chain length along with the degree of branching. In case of iso-octane and farnesane, both containing three methyl substitution presents different reactivity. Whereas, the reactivity of $iC_{10}H_{22}$, $iC_{11}H_{24}$, and $iC_{15}H_{32}$ is similar although the chain length and number of methyl substitution both are different.

In general, the reactivity of iso-paraffins is a complex combination of number of methyl substitution, its location on parent molecule, length of parent molecule that determines the fuel decomposition and thereby formation of intermediates and its global reactivity. Although the difference in global reactivity is not notable, the intermediate pool varies considerably and thereby the influence on the soot precursors formation needs further investigation.

4.3 Influence of molecular structure on the soot precursors' formation

Compared to their global characteristics, the formed soot precursor species can show different behavior and can be dependent on the molecular structure of the individual fuel component. Inspection of the experimental results of a large number of technical fuels [25] has proven a clear relation of most soot precursor amount with the fuels' degree of unsaturation i.e. IHD (index of hydrogen deficiency – a measure of unsaturation and cyclic structure present in fuel [205]). Similar findings can be drawn from actual soot measurement at full size engines, e.g. from ECLIF campaigns ground-test measurement of V2527-A5 engine of an Airbus A320 [206] have been reported or results from DemoSPK [207] measured at the Pratt & Whitney PW4158 engine of an Airbus A300 are seen to coincidence with the flow reactor results. More detailed examination for the ECLIF fuels can be found in [26] along with 26 different fuels with a particular focus on the influence of unsaturation and cyclic structure on the formation of individual small- to large-aromatics (up to 5-ring) formation.

The high temperature DLR flow reactor species measurements of different hydrocarbons are performed at the same carbon flow. Therefore, these data enable a direct comparison to investigate the influence of molecular structure on the soot precursors' formation. In the following we present and discuss the results obtained for selected neat components.

The formation of smaller aromatic species such as benzene or toluene is dependent on the individual formation paths and is influenced by the fuel's molecular stability. Compared to them, the three- to five-ring aromatics are usually formed from same route through earlier formed small aromatics. The

trend of increase in aromatic concentration with respect to IHD of the hydrocarbon is visible except in benzene formation where the larger fuel molecule does not readily decompose to smaller aromatics and thereby forming less one-ring benzene as in tetralin or methyl-naphthalene (Fig. 36). The closer relation of benzene mole fraction to the actual fuel structure was also observed for complex fuels (i.e. JS A1 and A1.3) and could be associated with the deduction of diaromatic components in A1.3 [17].

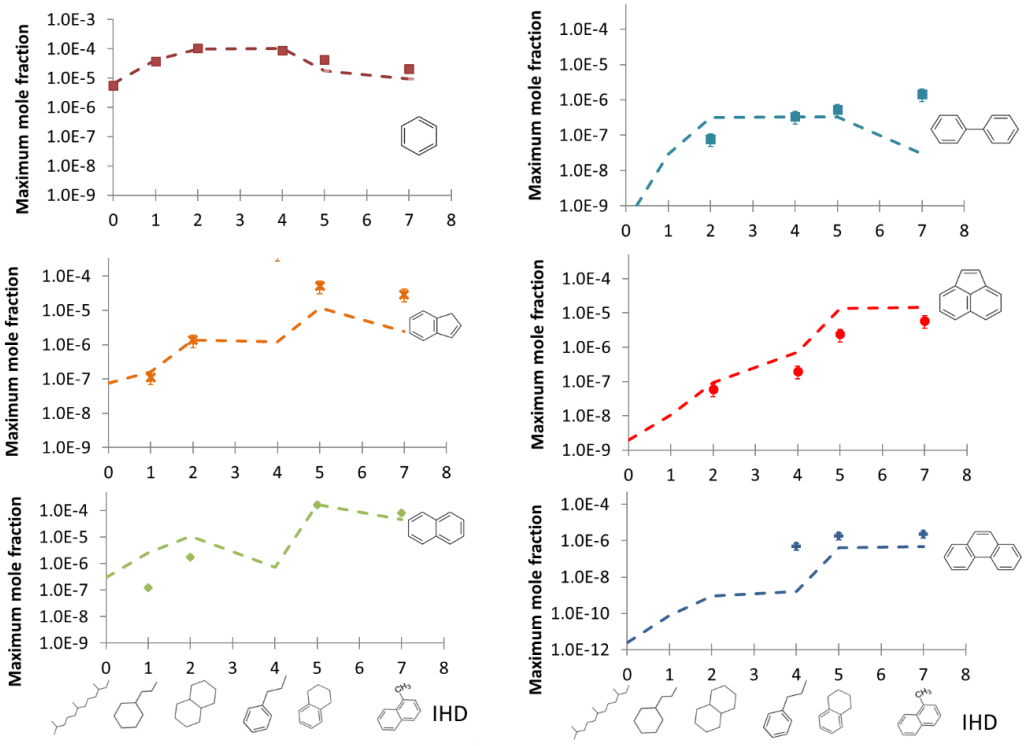

Fig. 36: Comparison of measured (symbol) and modeled (line) aromatic species maximum mole fractions obtained in neat hydrocarbons of different molecular structure (represented by their IHD), data are presented for Φ = 1.2. Measured data points are not available for all IHDs due to their values below measurement limit.

As for the technical pair [17] this trend continues for larger aromatics formed (3- to 5-ring) as shown in Fig. 37 also for the neat components. Here, only modeled predictions for fuel components are presented in absence of measurements.

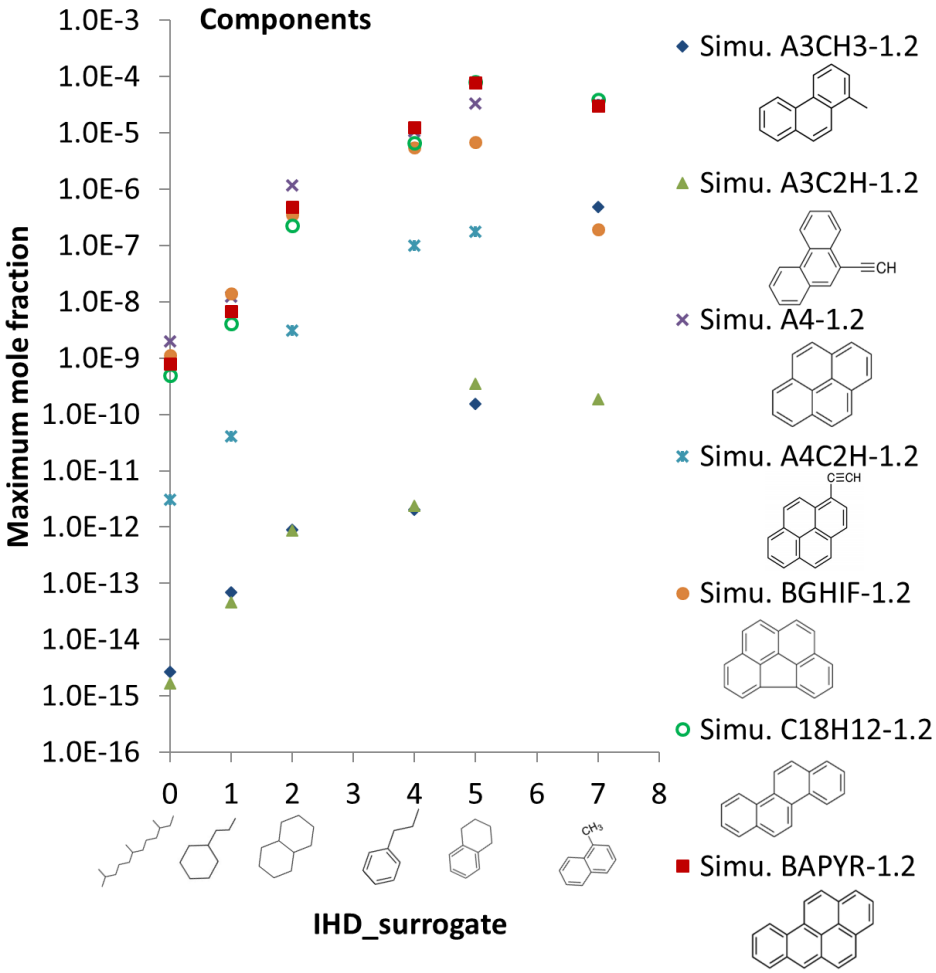

Fig. 37: Formation of larger aromatic species from neat hydrocarbons of different molecular structure at flow reactor condition. In absence of measurements, only modeled data are presented.

In general, from the above model experiment comparison, it is seen that most of the aromatics formed are linearly related to the cyclic compounds or in general to the unsaturation and cyclic structure present in a fuel. However, an overproportioned influence of diaromatic fuel constituents can be drawn from the experimental result [25]. A further examination of the particular soot precursor formation routes for the technical fuels can be found at the subsequent part of this series [26].

5. Conclusion

In Part II of our paper series [25, 26], we present a single reaction mechanism, suitable for modeling the combustion of a broad range of conventional and alternative fuels for all transportation sectors. Thereby, the combustion pathways of 70 validated hydrocarbons components of varying molecular structure are included in the model. The goal with this reaction model is to resolve compositional differences among the fuels and to supply parameters for subsequent fuel assessment and fuel optimization. This part focuses on the detailed model validation of neat hydrocarbon fuels before moving to application on technical fuels in Part III. The model validation here includes extensive

experimental global combustion characteristics such as ignition delay times measured in shock-tubes as well as laminar flame speed obtained from burners, for both in-house and literature data. Additionally, more intrinsic details of fuel decomposition to intermediates and product formation are investigated using new experiments obtained in DLR high temperature flow reactor, as well as burner stabilized flames and jet stirred reactor studies available in literature.

Using the well validated model, we present the influence of molecular structure on the global combustion characteristics and on the soot precursor's formation. With the help of four iso-paraffins of different branching and C-number, we study the significance of degree of branching. By that, we demonstrate the branching's low impact on global high temperature chemical kinetics, but a strong impact on the formation of aromatics or soot precursors, respectively. In general, it is seen that most of the soot precursors can be linearly related to the cyclic compounds present in the fuel.

The reaction mechanism for hydrocarbon combustion consisting of 238 species and 1814 reactions is supplied as supplemental material. The reaction mechanism is available for high temperatures (>900 K, pressures up to 60 atm) at the given moment with the option of low-temperature peroxy chemistry to be added in the future. We extent this study in Part III of this paper series, where 26 alternative and conventional aviation fuels are investigated.

6. Acknowledgment

The authors gratefully acknowledge especially the DLR projects ECLIF and Future Fuels for providing the framework of this comprehensive work.

This document contains supplemental material.

The reaction mechanism presented in this manuscript is uploaded with the paper.

References:

[1] Colket M, Edwards T, Williams S, Cernansky N, Miller DL, Egolfopoulos FN, et al. Development of an Experimental Database and Kinetic Models for Surrogate Jet Fuels. 45th AIAA Aerospace Sciences Meeting and Exhibit 2007; Paper No 2007-770.

[2] Dagaut P, Reuillon M, Cathonnet M. High Pressure Oxidation of Liquid Fuels from Low to High Temperature. 2. Mixtures of n-Heptane and iso-Octane. Combust Sci Technol 1994;103:315–336.

[3] Ranzi E. A Wide-Range Kinetic Modeling Study of Oxidation and Combustion of Transportation Fuels and Surrogate Mixtures. Energy Fuels 2006;20:1024-1032.

[4] Won S, Haas FM, Dooley S, Edwards T, Dryer FL. Reconstruction of chemical structure of real fuel by surrogate formulation based upon combustion property targets. Combust Flame 2017;183:39–49.

[5] Dooley S, Won SH, Heyne J, Farouk TI, Ju Y, Dryer FL, et al. The experimental evaluation of a methodology for surrogate fuel formulation to emulate gas phase combustion kinetic phenomena. Combust Flame 2012;159:1444−1466.

[6] Dryer FL, Jahangirian S, Dooley S, Won SH, Heyne J, Iyer VR, et al. Emulating the Combustion Behavior of Real Jet Aviation Fuels by Surrogate Mixtures of Hydrocarbon Fluid Blends: Implications for Science and Engineering. Energy Fuels 2014;28:3474-3485.

[7] Narayanaswamy K, Pitsch H, Pepiot P. A component library framework for deriving kinetic mechanisms for multi-component fuel surrogates: Application for jet fuel surrogates. Combust Flame 2016;165:288–309.

[8] Kerschgens B, Cai L, Pitsch H, Janssen A, Jakob M, Pischinger S. Surrogate fuels for the simulation of diesel engine combustion of novel biofuels. Int J Engine Res 2014;16:531-546.

[9] Cai L, Pitsch H. Optimized chemical mechanism for combustion of gasoline surrogate fuels. Combust Flame 2015;162:1623–1637.

[10] Honnet S, Seshadri K, Niemann U, Peters N. A surrogate fuel for kerosene. Proc Combust Inst 2009;32:485-492.

[11] Dooley S, Won SH, Chaos M, Heyne JS, Ju Y, Dryer FL, et al. A jet fuel surrogate formulated by real fuel properties, Combust Flame 2010;157:2333–2339.

[12] Westbrook C, Mehl M, Pitz WJ, Kukkadapu G, Wagnon SW, Zhang K. Multi-Fuel surrogate chemical kinetic mechanisms for real world applications. Phys Chem Chem Phys 2018;20:10588-10606.

[13] Luning Prak DJ, Jones MH, Trulove P, McDaniel AM, Dickerson T, Cowart JS. Physical and chemical analysis of Alcohol-to-Jet (ATJ) fuel and development of surrogate fuel mixtures. Energy Fuels 2015;29:3760−3769.

[14] Edwards T, Maurice LQ. Surrogate mixtures to represent complex aviation and rocket fuels. J Propul Power 2001;17:461–466.

[15] Huber ML, Lemmon EW, Diky V, Smith BL, Bruno TJ. Chemically authentic surrogate mixture model for the thermophysical properties of a coal-derived liquid fuel. Energy Fuels 2008;22:3249-3257.

[16] Kim D, Martz J, Abdul-Nour A, Yu X, Jansons M, Violi A. A six-component surrogate for emulating the physical and chemical characteristics of conventional and alternative jet fuels and their blends. Combust Flame 2017;179:86–94.

[17] Pelucchi M, Osswald P, Pejpichestakul W, Frassoldati A, Mehl M. On the combustion and sooting behavior of standard and hydro-treated jet fuels an experimental and modeling study on the compositional effects. Proc Combust Inst 2021;38 https://doi.org/10.1016/j.proci.2020.06.353.

[18] The CRECK Modeling Group, http://creckmodeling.chem.polimi.it/menu-kinetics.

[19] LLNL Mechanism, https://combustion.llnl.gov/mechanisms.

[20] Wang H, Dames E, Sirjean B, Sheen DA, Tango R, Violi A, et al. A high-temperature chemical kinetic model of n-alkane (up to n-dodecane), cyclohexane, and methyl-, ethyl-, npropyl and n-butyl-cyclohexane oxidation at high temperatures, JetSurF 2.0, Sept. 19, 2010 (http://melchior.usc.edu/JetSurF/JetSurF2.0).

[21] H. Pitsch group, Instituet für Technische Verbrennung, RWTH Aachen University, Germany.

[22] Esposito S, Cai L, Guenther M, Pitsch H, Pischinger S. Experimental comparison of combustion and emission characteristics between a market gasoline and its surrogate. Combust Flame 2020;214:306-322.

[23] Cai L, Jacob S, vom Lehn F, Langer R, Heufer KA, Pitsch H. Automatic mechanism generation for auto-ignition of the promising e-fuels oxymethylene ethers (OMEn, n = 2-4). Proc 1st Int Conf Smart Energy Carriers 2019.

[24] Wang K, Xu R, Parise T, Shao J, Movaghar A, Lee DJ, et al. A physics-based approach to modeling real-fuel combustion chemistry – IV. HyChem modeling of combustion kinetics of a bio-derived jet fuel and its blends with a conventional Jet A. Combust Flame 2018;198:477-489.

[25] Oßwald P, Zinsmeister J, Kathrotia T, Alves-Fortunato M, Burger V, van der Westhuizen R, Viljoen C, Lehto K, Sallinen R, Sandberg K, Aigner M, Le Clercq P, Köhler M. Combustion kinetics of alternative jet fuels, Part-I: Experimental flow reactor study. Accepted on 13.03.2021, Fuel (2021).

[26] Kathrotia T, Oßwald P, Zinsmeister J, Methling T, Köhler M. Combustion kinetics of alternative jet fuels, Part-III: Fuel modeling and surrogate strategy. Accepted on 13.03.2021, Fuel (2021).

[27] Oßwald P, Köhler M. An atmospheric pressure high-temperature laminar flow reactor for investigation of combustion and related gas phase reaction systems. Rev Sci Instrum 2015;86:105–109.

[28] Kéromnès A, Metcalfe WK, Heufer KA, Donohoe N, Das AK, Sung C, et al. An experimental and detailed chemical kinetic modeling study of hydrogen and syngas mixture oxidation at elevated pressures. Combust Flame 2013;160:995-1011.

[29] Richter S, Braun-Unkhoff M, Kathrotia T, Naumann C, Kick T, Slavinskaya N, Riedel U. Methods and tools for the characterisation of a generic jet fuel. CEAS Aeronaut J 2019;10:925–935.

[30] Slavinskaya N, Saffaripour M, Saibov E, Herzler J, Naumann C, Thomas L, Riedel U. Reaction models for i-C10H22 and i-C11H24 oxidation. 6th European Combustion Meeting 2013; Paper No P2-14.

[31] Richter S, Naumann C, Kathrotia T, Braun-Unkhoff M, Riedel U. Synthesized alternative kerosenes – Characterization through experiments and modeling, Proc 9th European Combustion Meeting 2019; Paper No S5_All_20.

[32] Richter S, Kathrotia T, Naumann C, Kick T, Slavinskaya N, Braun-Unkhoff M, Riedel U. Experimental and modeling study of farnesane. Fuel 2018;215:22-29.

[33] Ngugi J, Richter S, Braun-Unkhoff M, Naumann C, Riedel U. An investigation of fundamental combustion properties of the oxygenated fuels DME and OME1. ASME Turbo Expo 2020; Paper No GT2020-14702.

[34] Zhang Y, Huang Z, Wei L, Zhang J, Law CK. Experimental and modeling study on ignition delays of lean mixtures of methane, hydrogen, oxygen, and argon at elevated pressures. Combust Flame 2012;159:918–931.

[35] Petersen EL, Rohrig M, Davidson DF, Hanson RK, Bowman CT. High-pressure methane oxidation behind reflected shock waves. Sym (Int) Combust 1996;26:799-806.

[36] Eiteneer B, Frenklach M. Experimental and modeling study of shock-tube oxidation of acetylene. Int J Chem Kinet 2003;35:391–414.

[37] Brown CJ, Thomas GO. Experimental studies of shock-induced ignition and transition to detonation in ethylene and propane mixtures. Combust Flame 1999;117:861-870.

[38] Burcat A, Scheller K, Lifshitz A. Shock-tube investigation of comparative ignition delay times for C1-C5 alkanes. Combust Flame 1971;16:29–33.

[39] Curran H, Simme JM, Dagaut P, Voisin D, Cathonnet M. The ignition and oxidation of allene and propyne: Experiments and kinetic modelling. Proc Combust Inst 1996;26:613–620.

[40] Qin Z, Yang H, Gardiner WC Jr. Measurement and modeling of shock-tube ignition delay for propene. Combust Flame 2001;124:246–254.

[41] Kim K, Shin KS. Shock tube and modelling study of the ignition of propane. Bull Korean Chem Soc 2001;22:303-307.

[42] Fournet R, Bauge JC, Battin-Leclerc F. Experimental and modeling of oxidation of acetylene, propyne, allene, and 1,3-butadiene. Int J Chem Kinet 1999;31:361-379.

[43] Li Y, Zhou C, Somers KP, Zhang K, Curran HJ. The oxidation of 2-butene: A high pressure ignition delay, kinetic modeling study and reactivity comparison with isobutene and 1-butene. Proc Combust Inst 2017;36:403-411.

[44] Horning DC, Davidson DF, Hanson RK. Study of the High-temperature autoignition of n-alkane/O2/Ar mixtures. J Propul Power 2002;18:363–371.

[45] Healy D, Donato NS, Aul CJ, Petersen EL, Zinner CM, Bourque G, Curran HJ. n-Butane: Ignition delay measurements at high pressure and detailed chemical kinetic simulations. Combust Flame 2010;157:1526–1539.

[46] Cheng Y, Hu E, Deng F, Yang F, Zhang Y, Tang C, Huang Z. Experimental and kinetic comparative study on ignition characteristics of 1-pentene and n-pentane. Fuel 2016;172:263–272.

[47] Westbrook CK, Pitz WJ, Mehl M, Glaude P, Herbinet O, Bax S, et al. Experimental and kinetic modeling study of 2-methyl-2-butene: Allylic hydrocarbon kinetics. J Phys Chem A 2015;119:7462–7480.

[48] Yahyaoui M, Djebaïli-Chaumeix N, Dagaut P, Paillard CE, Gail S. Kinetics of 1-hexene oxidation in a JSR and a shock tube: experimental and modelling study. Combust Flame 2006;147:67–78.

[49] Davidson DF, Hanson RK. Fundamental kinetics database, utilizing shock tube measurements volume 4: Ignition delay time measurements 2014.

[50] Zhang K, Banyon C, Bugler J, Curran HJ, Rodriguez A, Herbinet O, et al. An updated experimental and kinetic modeling study of n-heptane oxidation. Combust Flame 2016;172:116–135.

[51] He J, Yong K, Zhang W, Li P, Zhang C, Li X. Shock tube study of ignition delay characteristics of n-nonane and n-undecane in argon. Energy Fuels 2016;30:8886−8895.

[52] Assad M, Leschevich VV, Penyazkov OG, Sevrouk KL, Tangirala VE, Joshi ND. Nonequilibrium phenomena: Plasma, combustion, atmosphere; Roy, G. D., Frolov, S. M., Starik, A. M., Eds.; Torus Press: Moscow 2009:210−220.

[53] Hu E, Yin G, Gao Z, Liu Y, Ku J, Huang Z. Experimental and kinetic modeling study on 2,4,4-trimethyl-1-pentene ignition behind reflected. Fuel 2017;195:97–104.

[54] Shen HS, Vanderover J, Oehlschlaeger MA. A shock tube study of iso-octane ignition at elevated pressures: The influence of diluent gases. Combust Flame 2008;155:739–755.

[55] Oehlschlaeger MA, Davidson DF, Herbon JT, Hanson RK. Shock tube measurements of branched alkane ignition times and OH concentration time histories. Int J Chem Kinet 2004;36:67–78.

[56] Dubois T, Chaumeix N, Paillard C. Experimental and modeling study of n-propylcyclohexane oxidation under engine-relevant conditions. Energy Fuels 2009;23:2453–2466.

[57] Comandini A, Dubois T, Abid S, Chaumeix N. Comparative study on cyclohexane and decalin oxidation. Energy Fuels 2014;28:714−724.

[58] Burcat A, Snyder C, Brabbs T. Ignition delay times of benzene and toluene with oxygen in argon mixtures, 1986;NASA Technical Memorandum 87312.

[59] Pengloan G, Dagaut P, Djebaili-Chaumeix N, Paillard CE, Cathonnet M, Combust Inst, French Section, Orléans, 2001.

[60] Wang H, Gerken WJ, Wang W, Oehlschlaeger MA, Experimental study of the high-temperature autoignition of tetralin. Energy Fuels 2013;27:5483-5487.

[61] Pfahl U, Fieweger K, Adomeit G, Self-ignition of diesel relevant hydrocarbon-air mixtures under engine conditions. Proc Combust Inst 1996;26:781–789.

[62] Noorani K, Akih-Kumgeh B, Bergthorson JM, Comparative high temperature shock tube ignition of C1−C4 primary alcohols, Energy Fuels 2010;24:5834–5843.

[63] Burke U, Metcalfe WK, Burke SM, Heufer KA, Dagaut P, Curran HJ. A detailed chemical kinetic modeling, ignition delay time and jet-stirred reactor study of methanol oxidation. Combust Flame 2016;165:125-136.

[64] Yasunaga K, Kubo S, Hoshikawa H, Kamesawa T, Hidaka Y. Shock-tube and modeling study of acetaldehyde pyrolysis and oxidation. Int J Chem Kinet 2008;40:73-102.

[65] Natarajan K, Bhaskaran KA. An experimental and analytical investigation of high temperature ignition of ethanol. Int Sym Shock Waves 1981;13:834-842.

[66] Davidson DF, Ranganath SC, Lam KY, Liaw M, Hong Z, Hanson RK. Ignition delay time measurements of normal alkanes and simple oxygenates. J Propul Power 2010;26:280–287.

[67] Black G, Curran HJ, Pichon S, Simmie JM, Zhukov V, Bio-butanol: Combustion properties and detailed chemical kinetic model. Combust Flame 2010;157:363–373.

[68] Richter S, Ermel J, Kick T, Braun-Unkhoff M, Naumann C, Riedel U. The influence of diluent gases on combustion properties of natural gas: A combined experimental and modeling study. J Eng Gas Turbines Power 2016;138:101503-101512.

[69] Richter S, Braun-Unkhoff M, Herzler J, Methling T, Naumann C, Riedel U. An investigation of combustion properties of a gasoline primary reference fuel surrogate blended with butanol. ASME Turbo Expo 2019; Paper No GT2019-90911.

[70] McLean IC, Smith DB, Taylor SC. The use of carbon monoxide/hydrogen burning velocities to examine the rate of the CO+OH reaction. Proc Combust Inst 1994;25:749-757.

[71] Lowry W, de Vries J, Krejci M, Petersen EL, Serinyel Z, Metcalfe WK, et al. Laminar flame speed measurements and modeling of pure alkanes and alkane blends at elevated pressures. J Eng Gas Turbines Power 2011;133:091501.

[72] Rozenchan G, Zhu DL, Law CK, Tse SD. Outward propagation, burning velocities, and chemical effects of methane flames up to 60 atm. Proc Combust Inst 2002;29:1461-1470.

[73] Gu XJ, Haq MZ, Lawes M, Woolley R. Laminar burning velocity and Markstein lengths of methane–air mixtures. Combust Flame 2000;121:41-58.

[74] Kochar Y, Seitzman J, Lieuwen T, Metcalfe WK, Burke SM, Curran HJ, et al. Laminar flame speed measurements and modeling of alkane blends at elevated pressures with various diluents. ASME Turbo Expo 2011; Paper No GT2011-45122.

[75] Davis SG, Law CK. Determination of and fuel structure effects on laminar flame speeds of C1 to C8 hydrocarbons, Comb Sci Tech 1998;140:427-449.

[76] Hassan MI, Aung KT, Faeth GM. Measured and predicted properties of laminar premixed methane/air flames at various pressures, Combust Flame 1998;115:539-550.

[77] Vagelopoulos CM, Egolfopoulos FN, Direct experimental determination of laminar flame speeds, Sym (Int) Combust 1998;27:513-519.

[78] Vagelopoulos CM, Egolfopoulos FN, Law CK. Further considerations on the determination of laminar flame speeds with the counterflow twin-flame technique. Sym (Int) Combust 1994;25:1341-1347.

[79] Egolfopoulos FN, Zhu DL, Law CK. Experimental and numerical determination of laminar flame speeds: mixtures of C2-hydrocarbons with oxygen and nitrogen. Proc Combust Inst 1990;23:471-478.

[80] Taylor SC. PhD Thesis. Burning velocity and the influence of flame stretch. University of Leeds 1991.

[81] Scholte TG, Vaags PB. The burning velocity of hydrogen-air mixtures and mixtures of some hydrocarbons with air. Combust Flame 1959;3:495–501.

[82] Shen X, Yang X, Santner J, Sun J, Ju Y. Experimental and kinetic studies of acetylene flames at elevated pressures. Proc Combust Inst 2015;35:721–728.

[83] Jomaas G, Zheng XL, Zhu DL, Law CK. Experimental determination of counterflow ignition temperatures and laminar flame speeds of C2-C3 hydrocarbons at atmospheric and elevated pressures. Proc Combust Inst 2005;30:193-200.

[84] Ravi S, Sikes TG, Morones A, Keesee CL, Petersen EL. Comparative study on the laminar flame speed enhancement of methane with ethane and ethylene addition. Proc Combust Inst 2015;35:679–686.

[85] Hassan MI, Aung KT, Kwon KC, Faeth GM. Properties of laminar premixed hydrocarbon/air flames at various pressures. J. Propul Power 1994;14:479-488.

[86] Kochar Y, Vaden S, Lieuwen T, Seitzman J. Laminar flame speed of hydrocarbon fuels with preheat and low oxygen content. 2010, Paper No AIAA-2010-778.

[87] Konnov AA, Dyakov IV, De Ruyck J. Measurement of adiabatic burning velocity in ethane-oxygen-nitrogen and in ethane-oxygen-argon mixtures, Exp Therm Fluid Sci 2003;27:379–384.

[88] Aung KT, Tseng LK, Ismail MA, Faeth GM. Response to comment by SC Taylor and DB Smith on Laminar burning velocities and markstein numbers of hydrocarbon/air flames, Brief Communication, Combust Flame 1995;102:526–530.

[89] Bosschaart KJ, De Goey LPH, Burgers JM. The laminar burning velocity of flames propagating in mixtures of hydrocarbons and air measured with the heat flux method. Combust Flame 2004;136:261–269.

[90] Dyakov IV, De Ruyck J, Konnov AA. Probe sampling measurements and modeling of nitric oxide formation in ethane+air flames. Fuel 2007;86:98–105.

[91] Saeed K, Stone R. Laminar burning velocities of propene–air mixtures at elevated temperatures and pressures. J Energy Inst 2007;80:73–82.

[92] Burke SM, Metcalfe W, Herbinet O, Battin-Leclerc F, Haasc FM, Santner J, et al. Combust Flame 2015;162:296–314.

[93] Razus D, Oancea D, Brinzea V, Mitu M, Movileanu C. Experimental and computed burning velocities of propane-air mixtures. Energy Convers Manag 2010;51:2979–2984.

[94] Tang C, Zheng J, Huang Z, Wang J. Study on nitrogen diluted propane–air premixed flames at elevated pressures and temperatures, Energy Convers Manag 2010;51:288–295.

[95] Law CK, Kwon OC. Effects of hydrocarbon substitution on atmospheric hydrogen-air flame propagation. Int J Hydrog Energy 2010;29:867–879.

[96] Zhao Z, Kazakov A, Li J, Dryer FL. The initial temperature and N2 dilution effect on the laminar flame speed of propane/air. Combust Sci Technol 2004;176:1705–1723.

[97] Zhou M, Garner CP. Direct measurements of burning velocity of propane-air using particle image velocimetry. Combust Flame 1996;106:363–367.

[98] van Maaren A, de Goey LPH. Stretch and the adiabatic burning velocity of methane-and propane-air flames. Combust Sci Technol 1994;102:309–314.

[99] Tseng LK, Ismail MA, Faeth GM. Laminar burning velocities and Markstein numbers of hydrocarbon/air flames. Combust Flame 1993;95:410–426.

[100] Metghalchi M, Keck JC. Laminar burning velocity of propane-air mixtures at high temperature and pressure. Combust Flame 1980;38:143–154.

[101] Gibbs GJ, Calcote HF. Effect of molecular structure on burning velocity. J Chem Eng Data 1959;4:226–237.

[102] Dugger GL. Effect of initial mixture temperature on flame speed of methane-air, propane-air, and ethylene-air mixtures. NACA-Report-1061, 1952.

[103] Zhao P, Yuan W, Sun H, Li Y, Kelley AP, Zheng X, Law CK. Laminar flame speeds, counterflow ignition, and kinetic modeling of the butene isomers. Proc Combust Inst 2015;35: 309–316.

[104] Zhou C, Li Y, O'Connor E, Somers KP, Thion S, Keesee C, et al. A comprehensive experimental and modeling study of isobutene oxidation. Combust Flame 2016;167:353-379.

[105] Hirasawa T, Sung CJ, Joshi A, Yang Z, Wang H, Law CK. Determination of laminar flame speeds using digital particle image velocimetry: Binary Fuel blends of ethylene, n-Butane, and toluene. Proc Combust Inst 2002;29:1427–1434.

[106] Cheng Y, Hu E, Lu X, Li X, Gong J, Li Q, Huang Z. Experimental and kinetic study of pentene isomers and n-pentane in laminar flames. Proc Combust Inst 2017;36:1279–1286.

[107] Fan X, Wang G, Li Y, Wang Z, Yuan W, Zhao L. Experimental and kinetic modeling study of 1-hexene combustion at various pressures. Combust Flame 2016;173:151–160.

[108] Kelley AP, Smallbone AJ, Zhu D, Law CK. Laminar flame speeds of C5 to C8 n-alkanes at elevated pressures and temperatures. AIAA Aerospace Sciences Meeting. 2010, Paper No 2010-774.

[109] Ji C, Dames E, Wang YL, Wang H, Egolfopoulos FN. Propagation and extinction of premixed C5–C12 n-alkane flames. Combust Flame 2010;157:277–287.

[110] Bikas G, Peters N. Kinetic modelling of n-decane combustion and autoignition: Modeling combustion of n-decanem. Combust Flame 2001;126:1456–1475.

[111] Comandini A, Dubois T, Chaumeix N. Laminar flame speeds of n-decane, n-butylbenzene, and n-propylcyclohexane mixtures. Proc Combust Inst 2015;35:671–678.

[112] Kumar K, Freeh JE, Sung CJ, Huang Y. Laminar flame speeds of preheated iso-octane/O2/N2 and n-heptane/O2/N2 mixtures. J Propul Power 2007;23:428–436.

[113] Hui X, Sung CJ. Laminar flame speeds of transportation-relevant hydrocarbons and jet fuels at elevated temperatures and pressures. Fuel 2013;109:191–200.

[114] Kim HH, Won SH, Santner J, Chen Z, Ju Y. Measurements of the critical initiation radius and unsteady propagation of n-decane/air premixed flames. Proc Combust Inst 2013;34:929–936.

[115] Munzar JD, Akih-Kumgeh B, Denman BM, Zia A, Bergthorson JM. An experimental and reduced modeling study of the laminar flame speed of jet fuel surrogate components. Fuel 2013;113:586–597.

[116] Singh D, Nishiie T, Qiao L. Experimental and kinetic modeling study of the combustion of n-decane, Jet-A, and S-8 in laminar premixed flames. Combust Sci Technol 2011;183:1002–1026.

[117] Li B, Liu N, Zhao R, Zhang H, Egolfopoulos FN. Flame propagation of mixtures of air with high molecular weight neat hydrocarbons and practical jet and diesel fuels. Proc Combust Inst 2013;34:727–733.

[118] Hu E, Yin G, Ku J, Gao Z, Huang Z. Experimental and kinetic study of 2,4,4-trimethyl-1-pentene and iso-octane in laminar flames. Proc Combust Inst 2018;37:1709–1716.

[119] Galmiche B, Halter F, Foucher F. Effects of high pressure, high temperature and dilution on laminar burning velocities and Markstein length of iso-octane/air mixtures. Combust Flame 2012;159:3286–3299.

[120] Christensen M, Abebe MT, Nilsson EJK, Konnov AA. Kinetics of premixed acetaldehyde + air flames. Proc Combust Inst 2015;35:499–506.

[121] Veloo P, Dagaut P, Togbe C, Dayma G, Sarathy SM, Westbrook CK, Egolfopoulos FN. Experimental and modeling study of the oxidation of n- and iso-butanal. Combust Flame 2013;160:1609–1626.

[122] Vancoillie J, Christensen M, Nilsson EJK, Verhelst S, Konnov AA. Temperature dependence of the laminar burning velocity of methanol flames. Energy Fuels 2012;26:1557−1564.

[123] Egolfopoulos FN, Du DX, Law CK. A comprehensive study of methanol kinetics in freely-propagating and burner-stabilized flames, flow and static reactors, and shock tubes. Combust Sci Technol 1992;83:33−75.

[124] Veloo PS, Wang YL, Egolfopoulos FN, Westbrook CK. A comparative experimental and computational study of methanol, ethanol, and n-butanol flames. Combust Flame 2010;157:1989−2004.

[125] Egolfopoulos FN, Du DX, Law CK. A study on ethanol oxidation kinetics in laminar premixed flames, flow reactors, and shock tubes. Proc Comb Inst 1992;24:833–841.

[126] Liao SY, Jiang DM, Huang ZH, Zeng K, Cheng Q. Determination of the laminar burning velocities for mixtures of ethanol and air at elevated temperatures. Appl Therm Eng 2007;27:374–380.

[127] de Vries J, Lowry WB, Serinyel Z, Curran HJ, Petersen EL. Laminar flame speed measurements of dimethyl ether in air at pressures up to 10 atm. Fuel 2011;90:331-338.

[128] Wang YL, Holley AT, Ji C, Egolfopoulos FN, Tsotsis TT, Curran HJ. Propagation and Extinction of Premixed Dimethyl-Ether/Air Flames. Proc Combust Inst 2009;32:1035-1042.

[129] Daly CA, Simmie JM, Wuermel J, DjebaIli N, Paillard C. Burning velocities of dimethyl ether and air. Combust Flame 2001;125:1329-1340.

[130] Qin X, Ju Y. Measurements of burning velocities of dimethyl ether and air premixed flames at elevated pressures. Proc Combust Inst, 2005;30:233-240.

[131] Sun W, Wang G, Li S, Zhang R, Yang B, Yang J, et al. Speciation and the laminar burning velocities of poly(oxymethylene) dimethyl ether 3 (POMDME3) flames: An experimental and modeling study. Proc Combust Inst 2017;36:1269–1278.

[132] Heimel S, Weast RC. Effect of initial mixture temperature on the burning velocity of benzene-air, n-heptane-air, and isooctane-air mixtures. Sym (Int) Combust 1957;6:296-302.

[133] Hui X, Das AK, Kumar K, Sung CJ, Dooley S, Dryer FL. Laminar flame speeds and extinction stretch rates of selected aromatic hydrocarbons. Fuel 2012;97:695–702.

[134] Osswald P. (2014) Unpublished data.

[135] Castaldi MJ, Vincitore AM, Senkan SM, Microstructures of premixed hydrocarbon flames – methane. Comb Sci Technol 1995;107:1–19.

[136] Bierkandt T, Kasper T, Akyildiz E, Lucassen A, Oßwald P, Koehler M, Hemberger P, Flame structure of a low-pressure laminar premixed and lightly sooting acetylene flame and the effect of ethanol addition. Proc Combust Inst 2015;35:803–811.

[137] Castaldi MJ, Marinov NM, Melius CF, Huang J, Senkan SM, Pitz WJ, et al. Experimental and modeling investigation of aromatic and polycyclic aromatic hydrocarbon formation in a premixed ethylene flame. Sym (Int) Combust 1996;26:693-702.

[138] Hansen N, Miller JA, Taatjes CA, Wang J, Cool TA, Law ME, et al. Photoionization mass spectrometric studies and modeling of fuel-rich allene and propyne flames. Proc Combust Inst 2007;31:1157–1164.

[139] Atakan B, Hartlieb AT, Brand J, Kohse-Hoeinghaus K. An experimental investigation of premixed fuel-rich low-pressure propene/oxygen/argon flames by laser spectroscopy and molecular beam mass spectrometry. Sym (Int) Combust 1998;27:435–444.

[140] Cool TA, Nakajima K, Taatjes CA, McIlroy A, Westmoreland PR, Law ME, et al. Studies of a fuel-rich propane flame with photoionization mass spectrometry. Proc Combust Inst 2005;30:1681–1688.

[141] Schenk M, Leon L, Moshammer K, Oßwald P, Zeuch T, Seidel L, et al. Detailed mass spectrometric and modeling study of isomeric butene flames. Combust Flame 2013;160:487–503

[142] Marinov NM, Pitz WJ, Westbrook CK, Vincitore AM, Castaldi MJ, Senkan SM, et al. Aromatic and polycyclic aromatic hydrocarbon formation in a laminar premixed n-butane flame. Combust Flame 1998;114:192–213.

[143] Ruwe L, Moshammer K, Hansen N, Kohse-Hoeinghaus K. Consumption and hydrocarbon growth processes in a 2-methyl-2-butene flame. Combust Flame 2017;175:34–46.

[144] Nawdiyal A, Hansen N, Zeuch T, Seidel L, Mauss F. Experimental and modelling study of speciation and benzene formation pathways in premixed 1-hexene flames. Proc Combust Inst 2015;35:325–332.

[145] Seidel L, Moshammer K, Wang X, Zeuch T, Kohse-Höinghaus K, Mauss F. Comprehensive kinetic modeling and experimental study of a fuel-rich, premixed n-heptane flame. Combust Flame 2015;162:2045–2058.

[146] Doute C, Delfau J, Akrich R, Vovelle C. Chemical structure of atmospheric pressure premixed n-decane and kerosene flames. Combust Sci Technol 1995;106:327-344.

[147] Zeng M, Wullenkord J, Graf I, Kohse-Höinghaus K. Influence of dimethyl ether and diethyl ether addition on the flame structure and pollutant formation in premixed iso-octane flames. Combust Flame 2017;184:41–54.

[148] Li W, Law ME, Westmoreland PR, Kasper T, Hansen N, Kohse-Höinghaus K. Multiple benzene-formation paths in a fuel-rich cyclohexane flame. Combust Flame 2011;158:2077–2089.

[149] Pousse E, Porter R, Biet J, Warth V, Glaude PA, Fournet R, Battin-Leclerc F. Lean methane premixed laminar flames doped by components of diesel fuel II: n-Propylcyclohexane. Combust Flame 2010;157:75–90.

[150] Zeng M, Li Y, Yuan W, Li T, Wang Y, Zhou Z, et al. Experimental and kinetic modeling study of laminar premixed decalin flames. Proc Combust Inst 2017;36:1193–1202.

[151] Bittner JD, Howard JB. Composition profiles and reaction mechanisms in a near-sooting premixed benzene/oxygen/argon flame. Proc Combust Sym 1981:18:1105-1116.

[152] Detilleux V, Vandooren J. Experimental and kinetic modeling evidences of a c7h6 pathway in a rich toluene flame. J Phys Chem A 2009;113:10913–10922.

[153] Yuan W, Li Y, Dagaut P, Yang J, Qi F. Experimental and kinetic modeling study of styrene combustion. Combust Flame 2015;162:1868–1883.

[154] Pousse E, Tian ZY, Glaude PA, Fournet R, Battin-Leclerc F. A lean methane premixed laminar flame doped with components of diesel fuel part III: Indane and comparison between n-butylbenzene, n-propylcyclohexane and indane. Combust Flame 2010;157:1236–1260.

[155] Wang Z, Li Y, Zhang F, Zhang L, Yuan W, Wang Y, Qi F. An experimental and kinetic modeling investigation on a rich premixed n-propylbenzene flame at low pressure. Proc Combust Inst 2013;34:1785–1793.

[156] Leplat N, Vandooren J. Experimental investigation and numerical simulation of the structure of CH3CHO/O2/Ar flames at different equivalence ratios. Combust Sci Technol 2010;182:436–448.

[157] Cool TA, Wang J, Hansen N, Westmoreland PR, Dryer FL, Zhao Z, et al. Photoionization mass spectrometry and modeling studies of the chemistry of fuel-rich dimethyl ether flame. Proc Combust Inst 2007;31:285–293.

[158] Köhler M, Oßwald P, Xu H, Kathrotia T, Hasse C, Riedel U. Speciation data for fuel-rich methane oxy-combustion and reforming under prototypical partial oxidation conditions. Chem Eng Sci 2016;139:249–260.

[159] Kathrotia T, Oßwald P, Köhler M, Slavinskaya N, Riedel U. Experimental and mechanistic investigation of benzene formation during atmospheric pressure flow reactor oxidation of n-hexane, n-nonane, and n-dodecane below 1200 K. Combust Flame 2018;194:426–438.

[160] Osswald P, Whitside R, Schäffer J, Köhler M. An experimental flow reactor study of the combustion kinetics of terpenoid jet fuel compounds: farnesane, p-menthane and p-cymene. Fuel 2017;187:43-50.

[161] Ristori A, Dagaut P, Cathonnet M. The oxidation of n-hexadecane: Experimental and detailed kinetic modeling. Combust Flame 2001;125:1128-1137.

[162] Dagaut P, Cathonnet M. The ignition, oxidation, and combustion of kerosene: A review of experimental and kinetic modeling. Prog Energy Combust Sci 2006;32:48–92.

[163] Dagaut P, Daly C, Simmie JM, Cathonnet M. The oxidation and ignition of dimethylether from low to high temperature (500–1600 K): Experiments and kinetic modelling. Sym (Int) Combust 1998;27:361–369.

[164] Dagaut P. On the kinetics of hydrocarbons oxidation from natural gas to kerosene and diesel fuel. Phys Chem Chem Phys 2002;4:2079–2094.

[165] Herbinet O, Husson B, Serinyel Z, Cord M, Warth V, Fournet R, et al. Experimental and modeling investigation of the low-temperature oxidation of n-heptane, Combust Flame 2012;159:3455–3471.

[166] Le Cong T, P. Dagaut P. Oxidation of H2/CO2 mixtures and effect of hydrogen initial concentration on the combustion of CH4 and CH4/CO2 mixtures: Experiments and modelling. Proc Combust Inst 2009;32:427–435.

[167] Mati K, Ristori A, Pengloan G, Dagaut P. Oxidation of 1-methylnaphthalene at 1–13 atm: Experimental study in a JSR and detailed chemical kinetic modeling, Combust Sci Technol 2007;179:1261-1285.

[168] Leplat N, Dagaut P, Togbe C, Vandooren J. Numerical and experimental study of ethanol combustion and oxidation in laminar premixed flames and in jet-stirred reactor. Combust Flame 2011;158:705–725.

[169] Rotavera B, Dievart P, Togbe C, Dagaut P, Petersen EL. Oxidation kinetics of n-nonane: Measurements and modeling of ignition delay times and product concentrations. Proc Combust Inst 2011;33:175–183.

[170] Sun W, Tao T, Lailliau M, Hansen N, Yang B, Dagaut P. Exploration of the oxidation chemistry of dimethoxymethane: Jet-stirred reactor experiments and kinetic modelling. Combust Flame 2018;193:491–501.

[171] Tan Y, Dagaut P, Cathonnet M, Boettner J. Acetylene oxidation in a JSR from 1 to 10 atm and comprehensive kinetic modeling, Combust Sci Technol 1994;102:21-55.

[172] Moréac G, Dagaut P, Roesler JF, Cathonnet M. Nitric oxide interactions with hydrocarbon oxidation in a jet-stirred reactor at 10 atm. Combust Flame 2006;145:512–520.

[173] Dagaut P, Ristori A, Frassoldati A, Faravelli T, Dayma G, Ranzi E. Experimental and semi-detailed kinetic modeling study of decalin oxidation and pyrolysis over a wide range of conditions. Proc Combust Inst 2013;34:289–296.

[174] Dagaut P, Ristori A, Frassoldati A, Faravelli T, Dayma G, Ranzi E. Experimental study of tetralin oxidation and kinetic modeling of its pyrolysis and oxidation. Energy Fuels 2013;27:1576−1585.

[175] Kathrotia T, Braun-Unkhoff M, Richter S, Naumann C, Slavinskaya N, Methling T, Riedel U. Reaction model development for synthetic jet fuels: Surrogate fuels as a flexible tool to predict their performance. ASME Turbo Expo 2018; Paper No GT2018-76997.

[176] Slavinskaya NA, Riedel U, Saibov E, Herzler J, Naumann C, Saffaripour M, Thomas L. Kinetic surrogate model for GTL kerosene, Aerospace Sciences Meeting Paper No 2014-0126.

[177] Goos E, Burcat A, Ruscic B. New NASA thermodynamic polynomials database with active thermochemical tables updates, Report ANL 05/20 TAE 960, 2011.

[178] Green WH, Allen JW, Beat A, Buesser R, Ashcraft W, Beran GJ, et al., RMG-Reaction Mechanism Generator, https://rmg.mit.edu/.

[179] Smith GP, Diagnostics for detailed kinetic modeling. Applied combustion diagnostics. Kohse-Höinghaus & Jeffries, ed. Taylor & Francis, 2001.

[180] Brown NJ, Revzan KL. Comparative sensitivity analysis of transport properties and reaction rate coefficients. Int J Chem Kinet. 2005;37:538–553.

[181] Gao CW, Liu M, Green WH. Uncertainty analysis of correlated parameters in automated reaction mechanism generation. Int J Chem Kinet. 2020;52:266–282.

[182] Mohamed SY, Cai L, Khaled F, Banyon C, Wang Z, Al Rashidi MJ, Pitsch H, Curran HJ, Farooq A, Sarathy SM. Modeling ignition of a heptane isomer: Improved thermodynamics, reaction pathways, kinetics, and rate rule optimizations for 2-methylhexane. J Phys Chem A. 2016;120:2201–2217.

[183] Burke MP, Dryer FL, Ju Y. Assessment of kinetic modeling for lean H2/CH4/O2/ diluent flames at high pressures. Proc Combust Inst 2011;33:905–912.

[184] Westbrook CK, Pitz WJ, Herbinet O, Curran HJ, Silke EJ. A comprehensive detailed chemical kinetic reaction mechanism for combustion of n-alkane hydrocarbons from n-octane to n-hexadecane. Combust Flame 2009;156:181–199.

[185] Kelley AP, Smallbone AJ, Zhu D, Law CK. Laminar flame speeds of C5 to C8 n-alkanes at elevated pressures: Experimental determination, fuel similarity, and stretch sensitivity. Proc Combust Inst 2011;33:963–970.

[186] Curran HJ, Gaffuri P, Pitz WJ, Westbrook CK. A comprehensive modeling study of iso-octane oxidation, Combust Flame 2002;129:253-280.

[187] Silke EJ, Pitz WJ, Westbrook CK, Ribaucour M. Detailed chemical kinetic modeling of cyclohexane oxidation. J Phys Chem A 2007;111:3761-3775.

[188] Agosta A, Cernansky NP, Miller DL, Faravelli T, Ranzi E. Reference components of jet fuels: Kinetic modeling and experimental results. Exp Therm Fluid Sci 2004;28:701–708.

[189] Gulati KS, Walker RW. Addition of cyclohexane to slowly reacting H2-O2 mixtures at 480°C. J Chem Soc, Faraday Trans 2, 1989;85:1799-1812.

[190] Bennett PJ, Gregory D, Jackson RA. Mechanistic studies on the combustion of isotopically labelled cyclohexanes within a single cylinder internal combustion engine. Combust Sci Technol 1996;115:83-103.

[191] Sirjean B, Buda F, Hakka H, Glaude PA, Fournet R, Warth V, et al. The autoignition of cyclopentane and cyclohexane in a shock tube. Proc Combust Inst 2007;31:277–284.

[192] Lemaire O, Ribaucour M, Carlier M, Minetti R. The production of benzene in the low-temperature oxidation of cyclohexane, cyclohexene, and cyclohexa-1,3-diene, Combust Flame 2001;127:1971–1980.

[193] Voisin D, Marchal A, Reuillon M, Boettner J, Cathonnet M. Experimental and kinetic modeling study of cyclohexane oxidation in a JSR at high pressure. Combust Sci Technol 1998;138:137–158.

[194] Law ME, Westmoreland PR, Cool TA, Wang J, Hansen N, Taatjes CA, Kasper T. Benzene precursors and formation routes in a stoichiometric cyclohexane flame. Proc Combust Inst 2007;31:565–573.

[195] McEnally CS, Pfefferle LD. Experimental study of fuel decomposition and hydrocarbon growth processes for cyclohexane and related compounds in nonpremixed flames. Combust Flame 2004;136:155–167.

[196] Slavinskaya N, Frank P. A modelling study of aromatic soot precursors formation in laminar methane and ethene flames. Combust Flame 2009;156:1705–1722.

[197] Krestinin AV. Detailed modeling of soot formation in hydrocarbon pyrolysis. Combust Flame 2000;121:513–524.

[198] Methling T., Braun-Unkhoff M., Riedel U. A novel linear transformation model for the analysis and optimisation of chemical kinetics. Combust. Theor. Model. 2017;21:503–528.

[199] Zschocke A, Scheuermann S, Ortner J. High biofuel blends in aviation (HBBA), 2012.

[200] Oehlschlaeger MA, Steinberg J, Westbrook CK, Pitz WJ. The autoignition of iso-cetane at high to moderate temperatures and elevated pressures: Shock tube experiments and kinetic modeling, Combust Flame 2009;156:2165-2172.

[201] Sarathy SM, Westbrook CK, Mehl M, Pitz WJ, Togbe C, Dagaut P, et al. Comprehensive chemical kinetic modeling of the oxidation of 2-methylalkanes from C7 to C20, Combust Flame 2011;158:2338-2357.

[202] Smith JM, Simmie JM, Curran HJ. Autoignition of heptanes; Experiments and modeling. Int J Chem Kinet 2005;37:728–736.

[203] Ji C, Sarathy SM, Veloo PS, Westbrook CK, Egolfopoulos FN. Effects of fuel branching on the propagation of octane isomers flames. Combust Flame 2012;159:1426–1436.

[204] Sarathy SM, Niemann U, Yeung C, Gehmlich R, Westbrook CK, Plomer M, et al. A counterflow diffusion flame study of branched octane isomers. Proc Combust Inst 2013;34:1015–1023.

[205] Kathrotia T, Riedel U. Predicting the soot emission tendency of real fuels - A relative assessment based on an empirical formula. Fuel 2020;261:116482.

[206] Schripp T, Anderson B, Crosbie E, Moore R, Herrmann F, Oßwald P, et al. Impact of alternative jet fuels on engine exhaust composition during the 2015 ECLIF ground based measurements campaign. Environ Sci Technol 2018;52:4969–78.

[207] Schripp T, Grein T, Zinsmeister J, Oßwald P, Köhler M, Müller-Langer F, et al. Technical application of a ternary alternative jet fuel blend – Chemical characterization and impact on jet engine exhaust composition, Fuel 2021;288:119606.

Supplemental Material

to

Combustion Kinetics of Alternative Jet Fuels, Part-II: Reaction Model for Fuel Surrogate

Trupti Kathrotia*, Patrick Oßwald, Clemens Naumann, Sandra Richter, Markus Köhler

German Aerospace Center (DLR), Institute of Combustion Technology,

Pfaffenwaldring 38-40, 70569 Stuttgart, Germany

*Corresponding author: Trupti.Kathrotia@dlr.de

Table of Contents

1. Complete validation data set: fuel composition, combustion conditions and references of experimental data presented in the following figures and tables.

6.1 Core C_1-C_5 chemistry

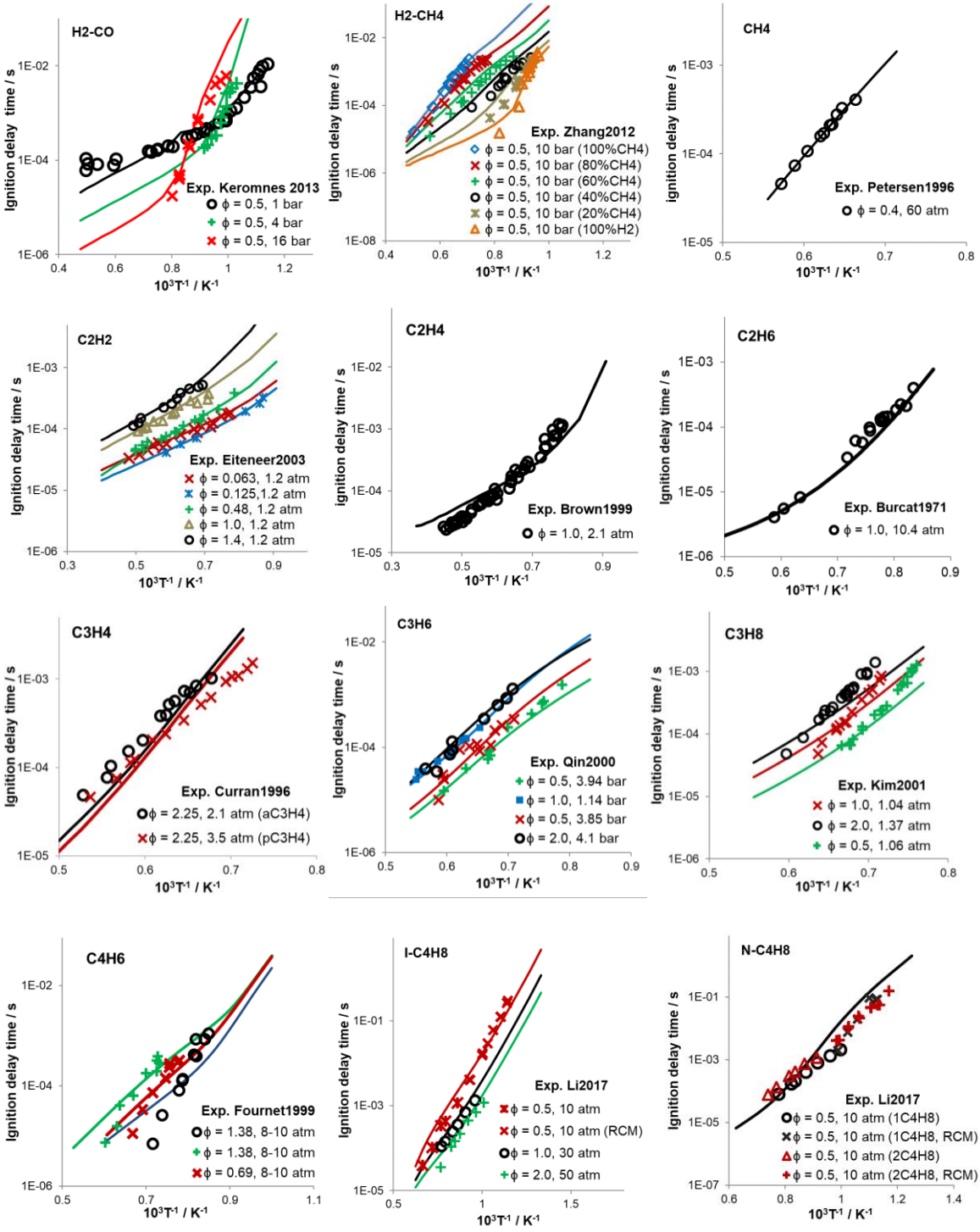

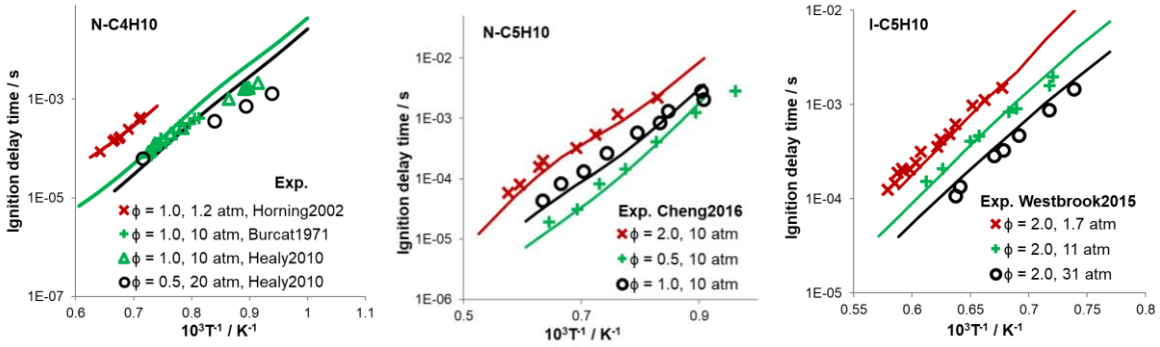

Fig. 1: Validation of ignition delay times of various hydrocarbons from C_1 to C_5 available in the core mechanism.

Fuel	Ref	Conditions
H_2-CO	in-house (Keromnes2013)	φ = 0.5, 1.74% H_2 + 1.74% CO + 3.47% O_2 + 93.06% Ar, 1, 4, 16 atm
H_2-CH_4	Zhang2012	φ = 0.5, 0-100% CH_4 + H_2 mixtures, 10 bar
CH_4	Petersen1996	φ = 0.4, 0.5% CH_4 + 2.5% O_2 + 97% Ar, 60 atm
C_2H_2	Eiteneer2003	φ = 0.063, 0.25% C_2H_2 + 10% O_2 + 89.75% Ar, 1.2 atm φ = 0.125, 0.5% C_2H_2 + 10% O_2 + 89.5% Ar, 1.2 atm φ = 0.48, 0.5% C_2H_2 + 2.6% O_2 + 96.9% Ar, 1.2 atm φ = 1.0, 0.5% C_2H_2 + 1.25% O_2 + 98.25% Ar, 1.2 atm φ = 1.4, 0.5% C_2H_2 + 0.89% O_2 + 98.61% Ar, 1.2 atm
C_2H_4	Brown1999	φ = 1.0, 1% C_2H_4 + 3% O_2 + 96% Ar, 2.1atm
C_2H_6	Burcat1971	φ = 1.0, 4.54% C_2H_6 + 15.91% O_2 + 79.55% Ar, 10.4 atm
C_3H_4	Curran1996	φ = 2.25, 1% aC_3H_4 + 2% O_2 + 97% Ar, 2.1atm φ = 2.25, 1% pC_3H_4 + 2% O_2 + 97% Ar, 3.5 atm
C_3H_6	Qin2001	φ = 0.5, 1.6% C_3H_6 + 14.4% O_2 + 84.0% Ar, 3.94 bar φ = 1.0, 1.6% C_3H_6 + 7.2% O_2 + 91.2% Ar, 1.14 bar φ = 0.5, 0.8% C_3H_6 + 7.2% O_2 + 92% Ar, 3.85 bar φ = 2.0, 1.6% C_3H_6 + 3.6% O_2 + 94.8% Ar, 4.1bar
C_3H_8	Kim2001	φ = 1.0, 2% C_3H_8 + 10% O_2 + 88% Ar, 1.04 atm φ = 2.0, 4% C_3H_8 + 10% O_2 + 86% Ar, 1.37 atm φ = 0.5, 2% C_3H_8 + 20% O_2 + 78% Ar, 1.06 atm
C_4H_6	Fournet1999	φ = 1.38: 3% C_4H_6 + 12% O_2 + 85% Ar, 8-10 atm φ = 1.38: 1% C_4H_6 + 4% O_2 + 95% Ar, 8-10 atm φ = 0.69: 1% C_4H_6 + 8% O_2 + 91% Ar, 8-10 atm
N-C_4H_8	Li2017	φ = 0.5: 1.72% C_4H_8 + 20.64% O_2 + 77.64% N_2, 10 atm
I-C_4H_8	Li2017	φ = 0.5: 1.72% C_4H_8 + 20.64% O_2 + 77.64% N_2, 10 atm φ = 1.0: 3.38% C_4H_8 + 20.29% O_2 + 76.33% N_2, 10 atm φ = 2.0: 6.54% C_4H_8 + 19.63% O_2 + 73.83% N_2, 10 atm
N-C_4H_{10}	Horning2002 Burcat1971 Healy2010 Healy2010	φ = 1.0: 1.0% nC_4H_{10} + 6.5% O_2 + 92.5% Ar, 1.2 atm φ = 1.0: 2.5% nC_4H_{10} + 16.25% O_2 + 81.25% Ar, 10 atm φ = 1.0: 2.5% nC_4H_{10} + 16.25% O_2 + 81.25% Ar, 10 atm φ = 0.5: 1.595% nC_4H_{10} + 20.7% O_2 + 77.71% Ar, 20 atm
N-C_5H_{10}	Cheng2016	φ = 0.5: 0.5% nC_5H_{10} + 7.5% O_2 + 92% Ar, 10 atm φ = 1.0: 0.5% nC_5H_{10} + 3.75% O_2 + 95.75% Ar, 10 atm φ = 2.0: 0.5% nC_5H_{10} + 1.875% O_2 + 97.625% Ar, 10 atm
I-C_5H_{10}	Westbrook2015	φ = 2.0: 0.21053% iC_5H_{10} + 0.78947% O_2 + 99% Ar, 1.7, 11, 31 atm

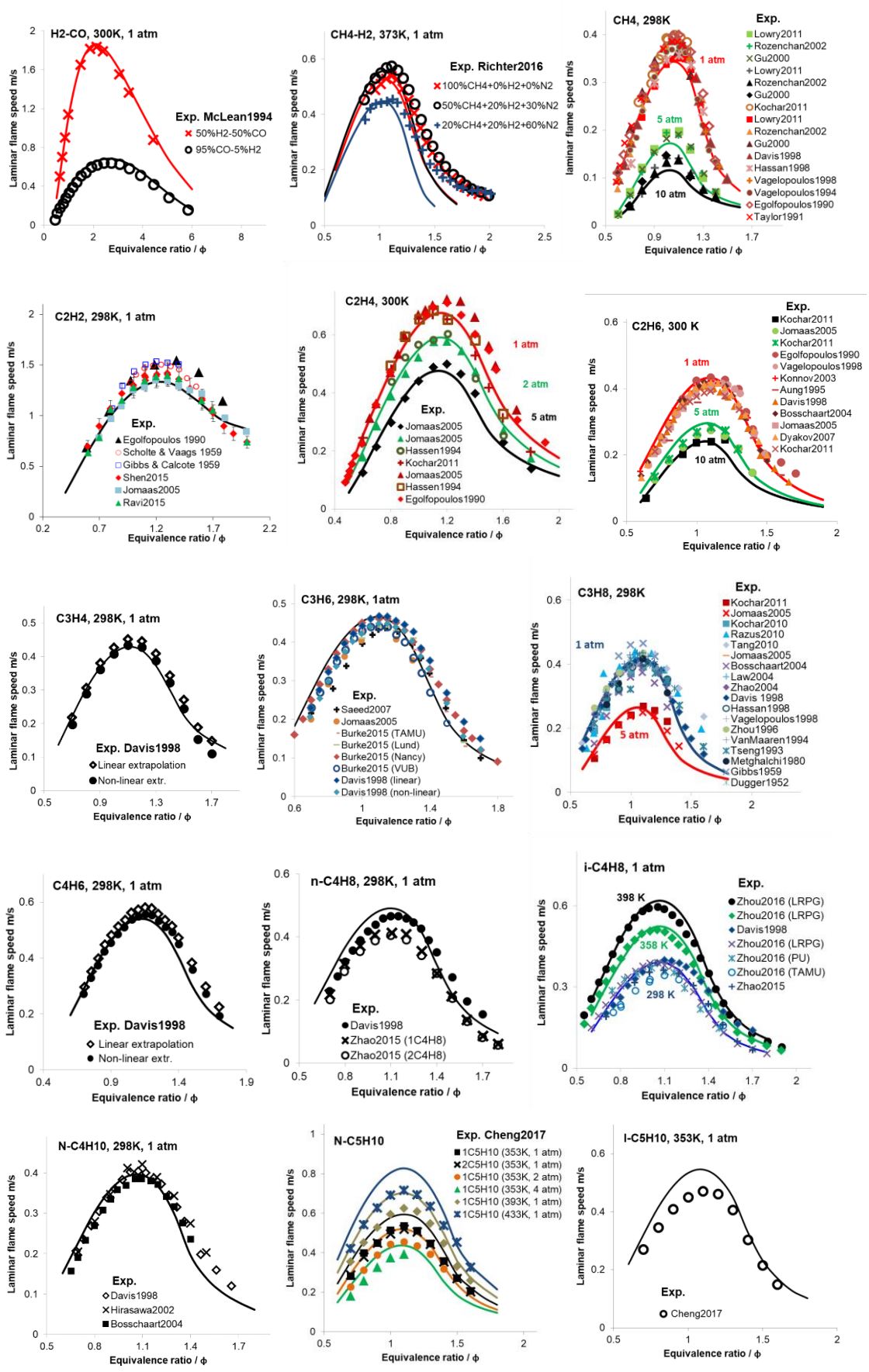

Fig. 2: Validation of laminar flame speed of various hydrocarbons from C_1 to C_5 present in the core mechanism.

Fuel	Ref	Conditions
H_2-CO	McLean1994	300K; 1 atm
CH_4-H_2	In-house (Richter2016)	373K; 1 atm
CH_4	Lowry2011, Rozenchan2002, Gu2000, Kochar2011, Davis1998, Hassan1998, Vagelopoulos1998, Vagelopoulos1994, Egolfopoulos1990, Taylor1991	298K; 1, 5, 10 atm
C_2H_2	Egolfopoulos1990, Scholte1959, Gibbs1959, Shen2015, Jomaas2005, Ravi2015	298K; 1 atm
C_2H_4	Jomaas2005, Hassan1994, Kochar2011, Egolfopoulos1990	300K; 1, 2, 5 atm
C_2H_6	Kochar2010, Jomaas2005, Egolfopoulos1990, Vagelopoulos1998, Konnov2003, Aung1995, Davis1998, Bosschaart2004, Dyakov2007	300K; 1, 5, 10 atm
C_3H_4	Davis1998	298 K; 1 atm
C_3H_6	Saeed2007, Jomaas2005, Burke2015, Davis1998	298 K; 1 atm
C_3H_8	Kochar2010, Jomaas2005, Razus2010, Tang2010, Bosschaart2004, Law2004, Zhao2004, Davis1998, Hassan1998, Vagelopoulos1998, Zhou1996, VanMaaren1994, Tseng1993, Metghalchi1980, Gibbs1959, Dugger1952	298 K; 1, 5 atm
C_4H_6	Davis1998	298 K; 1 atm
N-C_4H_8	Davis1998, Zhao2015	298 K; 1 atm
I-C_4H_8	Davis1998, Zhao2015, Zhou2016	298, 358, 398 K; 1 atm
N-C_4H_{10}	Davis1998, Hirasawa2002, Bosschaart2004	298 K; 1 atm
N-C_5H_{10}	Cheng2017	353, 393, 433 K; 1, 2, 4 atm
I-C_5H_{10}	Cheng2017	353 K; 1 atm

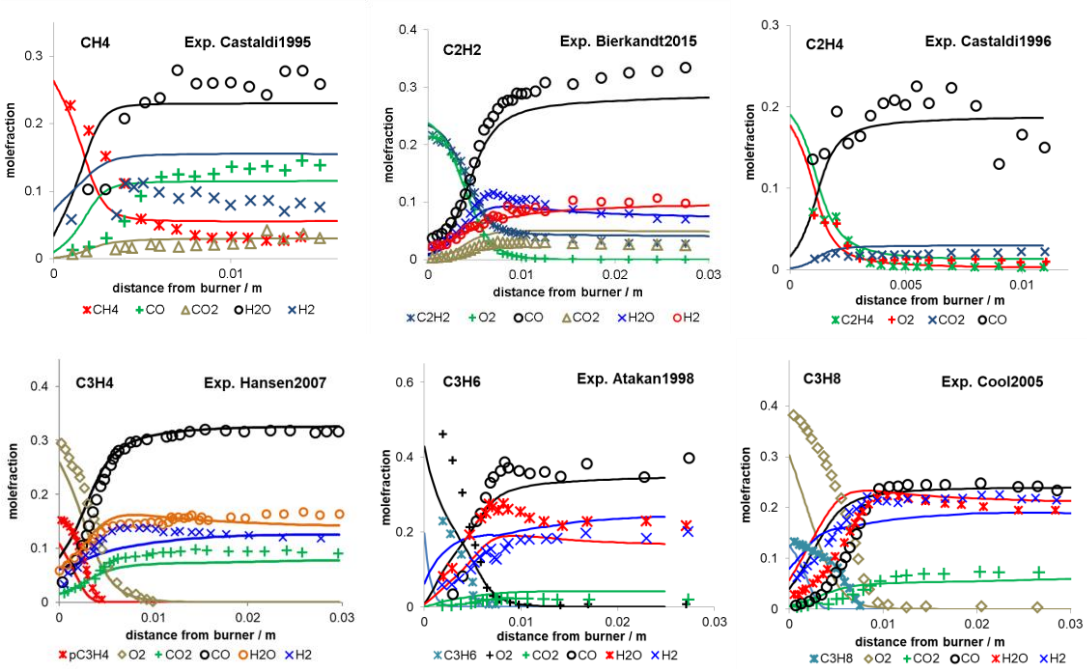

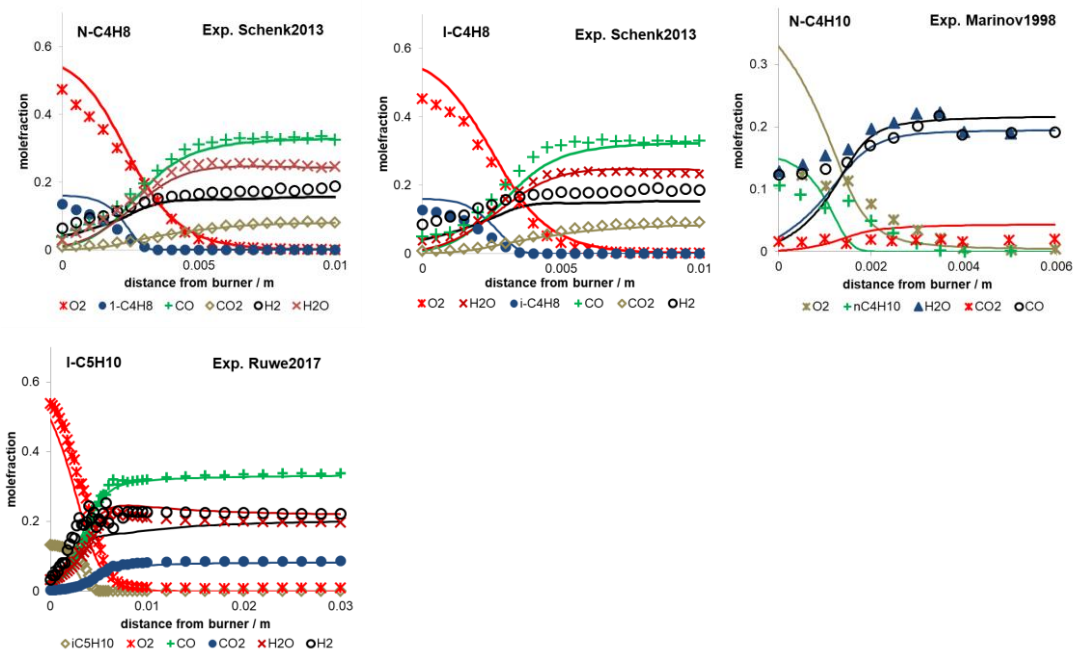

Fig. 3: Validation of speciation data in laminar flame of various hydrocarbons from C_1 to C_5 present in the core mechanism.

Fuel	Ref	Conditions
CH_4	Castaldi1995	φ = 2.6, 30.9% CH_4 + 23.78% O_2 + 45.3% Ar, 1 atm
C_2H_2	Bierkandt2015	φ = 2.4, 24.5% C_2H_2 + 25.5% O_2 + 50.0% Ar, 0.04atm
C_2H_4	Castaldi1996	φ = 3.06, 21.3% C_2H_4 + 20.9% O_2 + 57.8% Ar, 1 atm
C_3H_4	Hansen2007	φ = 1.8, 18.37% C_3H_4 + 40.83% O_2 + 40.8% Ar; 0.0333 atm
C_3H_6	Atakan1998	φ = 2.32, 25.5% C_3H_6 + 49.5% O_2 + 25% Ar, 0.05 atm
C_3H_8	Cool2005	φ = 1.8, 15.25% C_3H_8 + 42.37% O_2 + 42.37% Ar, 0.04atm
n-C_4H_8	Schenk2013	φ = 1.7, 16.5% nC_4H_8 + 58.5% O_2 + 25% Ar, 0.04 bar
i-C_4H_8	Schenk2013	φ = 1.7, 16.5% iC_4H_8 + 58.5% O_2 + 25% Ar, 0.04 bar
n-C_4H_{10}	Marinov1998	φ = 2.6, 15.67% nC_4H_{10} + 39.64% O_2 + 45.04% Ar, 1 atm
i-C_5H_{10}	Ruwe2017	φ = 1.8, 14.5% iC_5H_{10} + 60.5% O_2 + 25% Ar, 0.04 bar

6.2 n-Paraffins

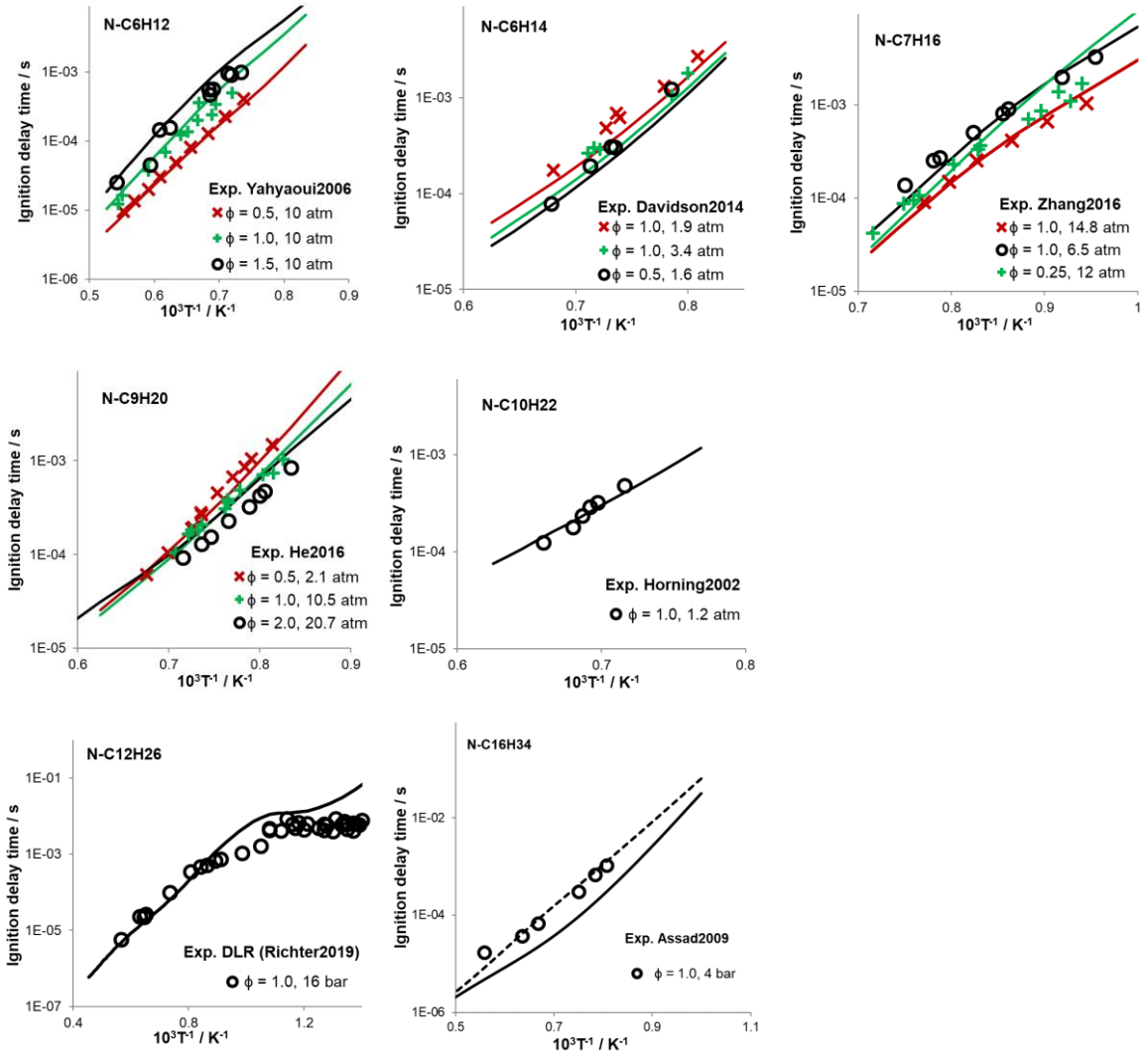

Fig. 4: Validation of ignition delay times of various hydrocarbons from nC_6-nC_{16}-paraffins available in the mechanism.

Fuel	Ref	Conditions
N-C_6H_{12}	Yahyaoui2006	φ =0.5, 0.1% nC_6H_{12} + 1.8%O_2 + 98.1% Ar, 10 atm φ = 1.0, 0.1% nC_6H_{12} + 0.9%O_2 + 99% Ar, 10 atm φ = 1.5, 0.1% nC_6H_{12} + 0.6%O_2 + 99.3% Ar, 10 atm
N-C_6H_{14}	Davidson2014	φ = 0.5, 0.21% nC_6H_{14} + 4%O_2 + 95.79% Ar, 1.6 atm φ = 1.0, 0.42% nC_6H_{14} + 4%O_2 + 95.58% Ar, 1.9, 3.4 atm
N-C_7H_{16}	Zhang2016	φ = 0.25, 0.47 nC_7H_{16}, 20.9 O_2 + 78.6 N_2, 12 atm φ = 1.0, 1.87% nC_7H_{16}, 20.61 O_2 + N2 77.52 N_2, 6.5, 14.8 atm
N-C_9H_{20}	He2016	φ = 0.5: 0.143% nC_9H_{20} + 4% O_2 + 95.857% Ar, 2.1atm φ = 0.286% nC_9H_{20} + 4% O_2 + 95.714% Ar, 10.5 atm φ = 0.571% nC_9H_{20} + 4% O_2 + 95.429% Ar, 20.7 atm
N-$C_{10}H_{22}$	Horning2002	φ = 1.0: 0.2% $C_{10}H_{22}$ + 3.1% O_2 + 96.7% Ar, 1.2 atm
N-$C_{12}H_{26}$	In-house (Richter2019)	φ = 1.0: 0.6% $nC_{12}H_{26}$ +9.9% O_2 + 89.6% N_2, 16 bar
N-$C_{16}H_{34}$	Assad2009	φ = 1.0: 0.8% $nC_{16}H_{34}$ + 20.8% O_2 + 78.3% N_2, 4 bar

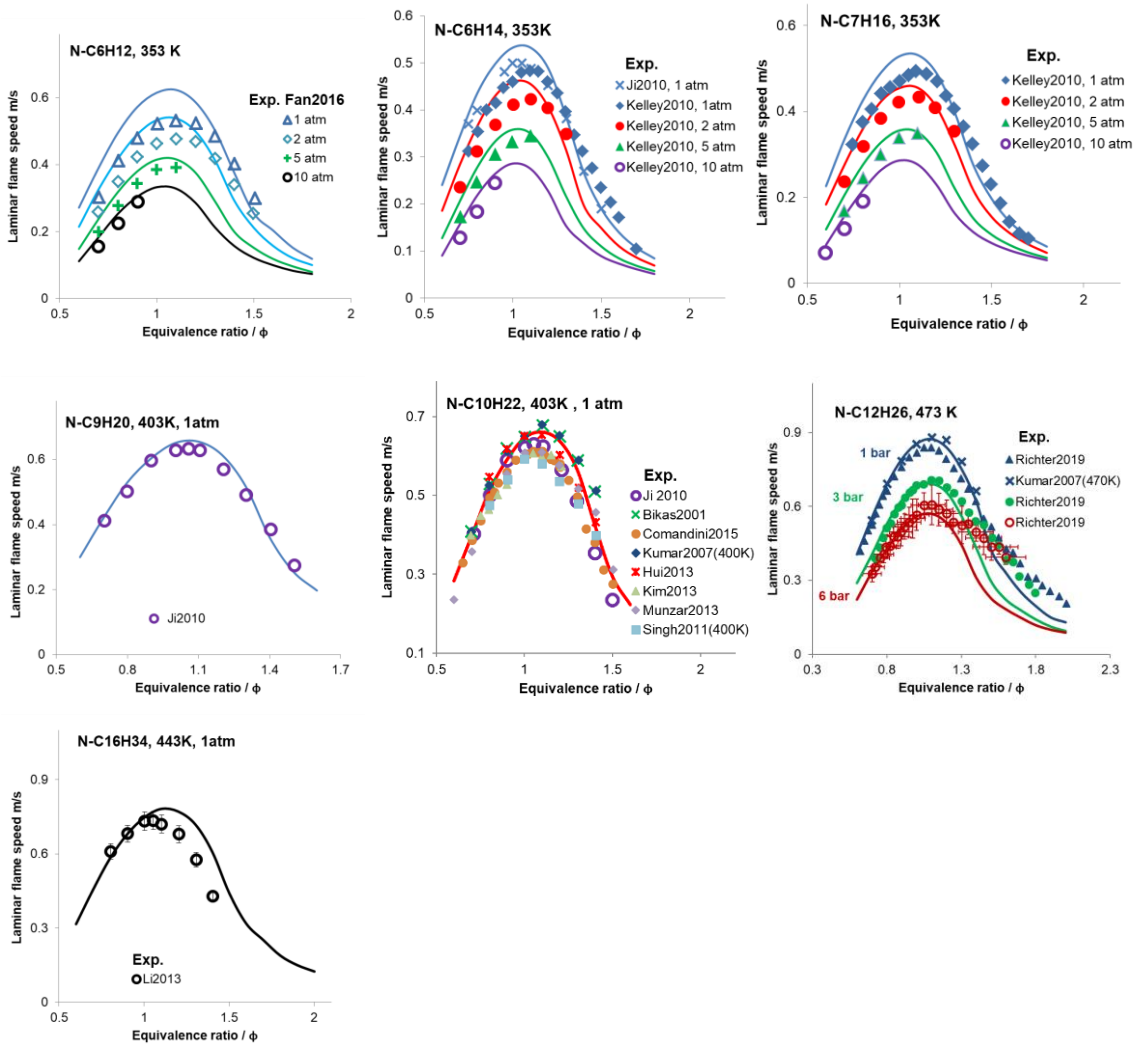

Fig. 5: Model validation of laminar flame speed as function of fuel stoichiometry for n-paraffins with carbon number C_6 to C_{16}.

Fuel	Ref	Conditions
N-C_6H_{12}	Fan2016	353 K; 1, 2, 5, 10 atm
N-C_6H_{14}	Kelley2010, Ji2010	353 K; 1, 2, 5, 10 atm
N-C_7H_{16}	Kelley2010	353 K; 1, 2, 5, 10 atm
N-C_9H_{20}	Ji2010	403 K; 1 atm
N-$C_{10}H_{22}$	Ji2010, Bikas2001, Comandini2015, Kumar2007, Hui2013, Kim2013, Munzar2013, Singh2011	403 K; 1 atm
N-$C_{12}H_{26}$	In-house (Richter2019), Kumar2007	473 K; 1, 3, 6 atm
N-$C_{16}H_{34}$	Li2013	443 K; 1 atm

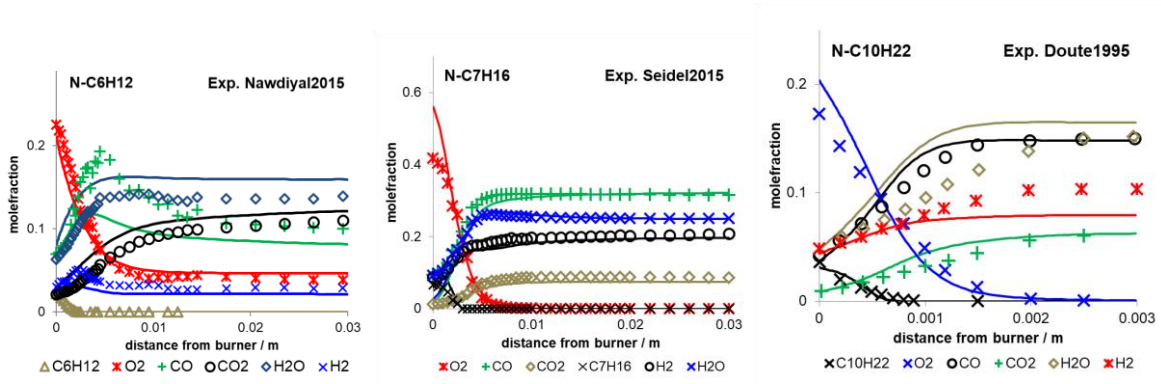

Fig. 6: Validation of speciation data in laminar flame of n-hexene, n-heptane, and n-decane present in the reaction mechanism.

Fuel	Ref	Conditions
N-C_6H_{12}	Nawdiyal2015	φ = 1.0, 4% 1-C_6H_{12} + 36% O_2 + 60.0% Ar, 0.02 atm
N-C_7H_{16}	Seidel2015	φ = 1.69, 10% nC_7H_{16} + 65% O_2 + 25% Ar, 0.04 bar
N-$C_{10}H_{22}$	Doute1995	φ = 1.7, 3.2% n$C_{10}H_{22}$ + 28.6 O_2 + 68.2% N_2, 1atm

6.3 Iso-paraffins

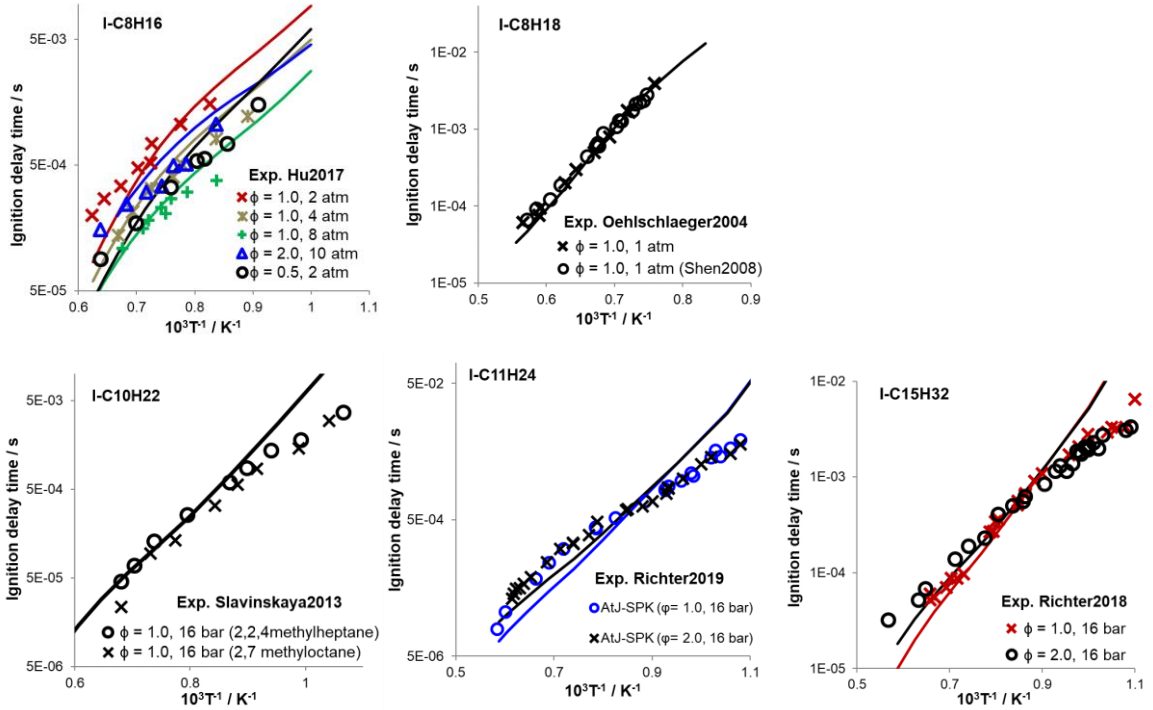

Fig. 7: Validation of ignition delay times of various iso-paraffins present in the mechanism.

Fuel	Ref	Conditions
I-C_8H_{16}	Hu2017	φ = 1.0: 1% iC_8H_{16} + 12% O_2 + 87% Ar, 2,4,8 atm φ = 2.0: 1% iC_8H_{16} + 6% O_2 + 93% Ar, 10 atm φ = 0.5: 1% iC_8H_{16} + 24% O_2 + 75% Ar, 2 atm
I-C_8H_{18}	Shen2008 Oehlschlaeger2004	φ = 1.0, 0.5% iC_8H_{18} + 6.5% O_2 + 93% Ar, 1 atm
I-$C_{10}H_{22}$	in-house (Slavinskaya2013)	φ = 1.0, 0.64% i$C_{10}H_{22}$ + 9.87O_2 + 89.5 N_2, 16 bar
I-$C_{11}H_{24}$	in-house (Richter2019a)	φ = 1.0, 0.58% i$C_{11}H_{24}$ + 9.88% O_2 + 89.53% N_2, 16 bar φ = 2.0, 1.15% i$C_{11}H_{24}$ + 9.77% O_2 + 89.08 % N_2, 16 bar

$I\text{-}C_{15}H_{32}$	in-house (Richter2018)	φ = 1.0, 0.43% $iC_{15}H_{32}$ + 9.91% O_2 + 89.66% N_2, 16 bar φ = 2.0, 0.85% $iC_{15}H_{32}$ + 9.83% O_2 + 89.32 % N_2, 16 bar

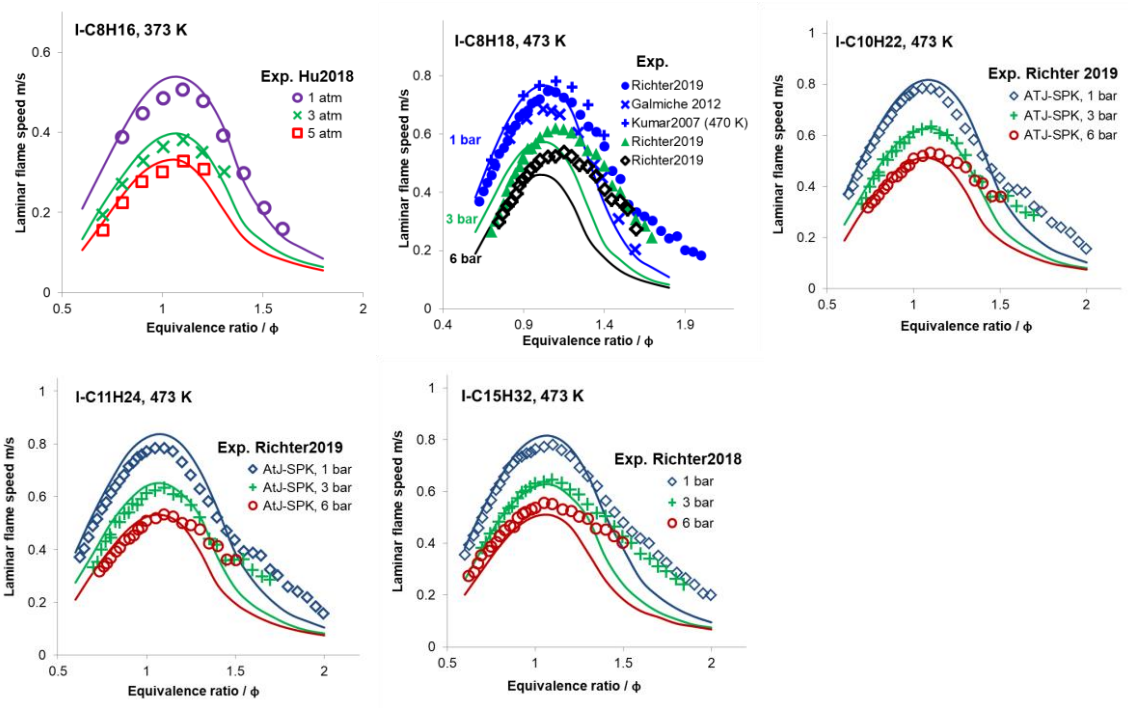

Fig. 8: Model validation of laminar flame speed as function of fuel stoichiometry for various iso-paraffins.

Fuel	Ref	Conditions
$I\text{-}C_8H_{16}$	2,4,4-trimethyl-1-pentene, Hu2018	373 K; 1, 3, 5 atm
$I\text{-}C_8H_{18}$	Iso-octane, In-house (Richter2019), Kumar2007, Galmiche2012	473 K; 1, 3, 6 bar
$I\text{-}C_{10}H_{22}$	ATJ-SPK, In-house (Richter2019a)	473 K; 1, 3, 6 bar
$I\text{-}C_{11}H_{24}$	ATJ-SPK, In-house (Richter2019a)	473 K; 1, 3, 6 bar
$I\text{-}C_{15}H_{32}$	Farnesane, In-house (Richter2018)	473 K; 1, 3, 6 bar

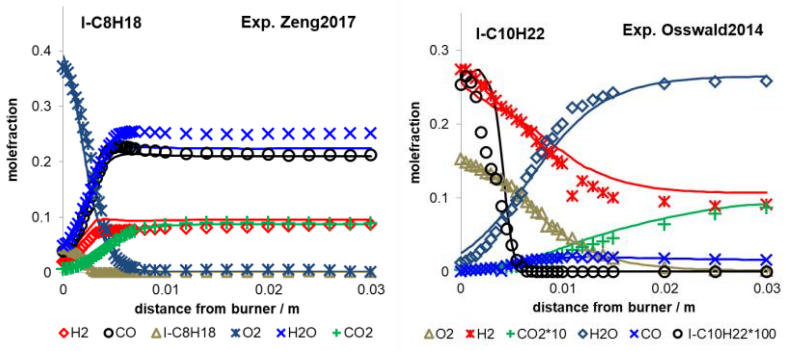

Fig. 9: Validation of speciation data in laminar flame of $i\text{-}C_8H_{18}$ (iso-octane) and $i\text{-}C_{10}H_{22}$ (exp.:1-methyl nonane, model: 2,7 dimethyl-octane) present in the mechanism.

Fuel	Ref	Conditions
$I\text{-}C_8H_{18}$	Zeng2017a	φ = 1.47, 5.25% iC_8H_{18} + 44.75% O_2 + 50% Ar; 0.04 bar
$I\text{-}C_{10}H_{22}$ (1-methylnonane)	In-house (Osswald2014)	φ = 1.5, 0.23% $iC_{10}H_{22}$ + 35% H_2 + 14% O_2 + 49% Ar, 0.02 bar

6.4 Cyclo-paraffins

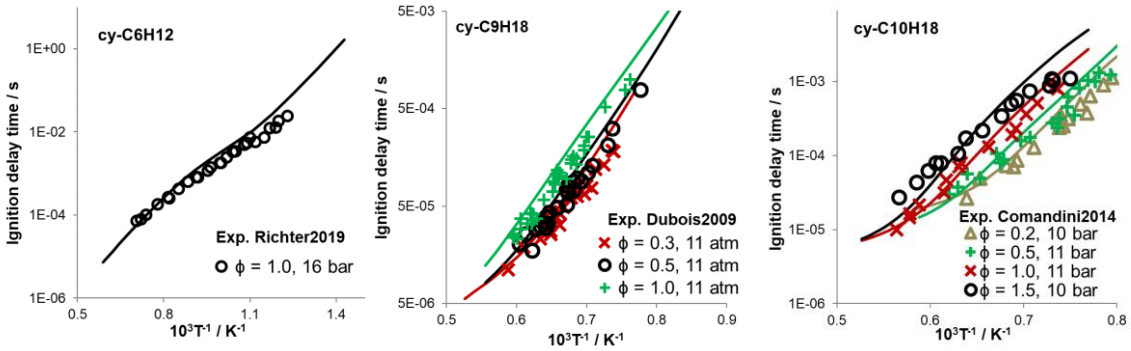

Fig. 10: Validation of ignition delay times of various cy-paraffins available in the mechanism.

Fuel	Ref	Conditions
cy-C_6H_{12}	in-house (Richter2019)	φ = 1.0, 1.1% cyC_6H_{12} +9.8% O_2 + 89.1% N_2, 16 bar
cy-C_9H_{18}	Dubois2009	φ = 0.3, 0.215% cyC_9H_{18} + 0.98% O_2 + 99% Ar, 11 atm φ = 0.5, 0.36% cyC_9H_{18} + 0.97% O_2 + 99% Ar, 11 atm φ = 1.0, 0.69% cyC_9H_{18} + 0.93% O_2 + 99% Ar, 11 atm
cy-$C_{10}H_{18}$	Comandini2014	φ = 0.2, 0.014% cy$C_{10}H_{18}$ + 0.986% O_2 + 99% N_2, 10 bar φ = 0.5, 0.033% cy$C_{10}H_{18}$ + 0.967% O_2 + 99% N_2, 11 bar φ = 1.0, 0.065% cy$C_{10}H_{18}$ + 0.935% O_2 + 99% N_2, 11 bar φ = 1.5, 0.094% cy$C_{10}H_{18}$ + 0.906% O_2 + 99% N_2, 10 bar

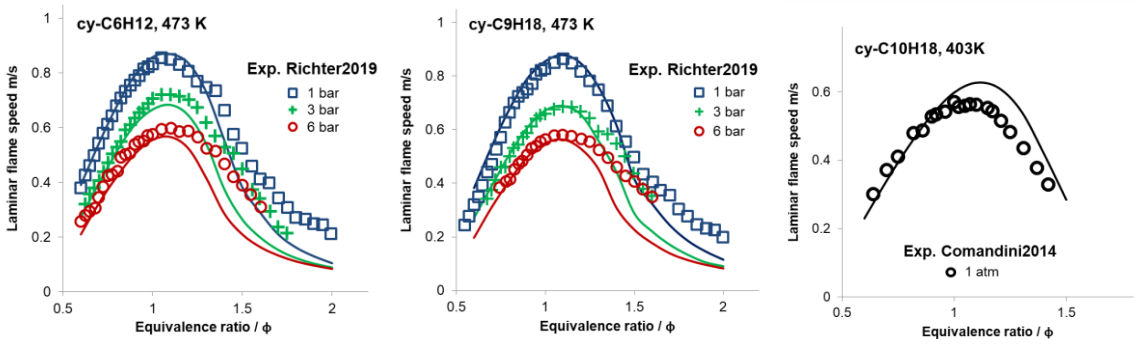

Fig. 11: Model validation of laminar flame speed as function of fuel stoichiometry for various cy-paraffins.

Fuel	Ref	Conditions
cy-C_6H_{12}	Cyclohexane, Richter2019	473 K; 1, 3, 6 bar
cy-C_9H_{18}	n-Propylcyclohexane, Richter2019	473 K; 1, 3, 6 bar
cy-$C_{10}H_{18}$	Decalin, Comandini2014	403 K; 1 atm

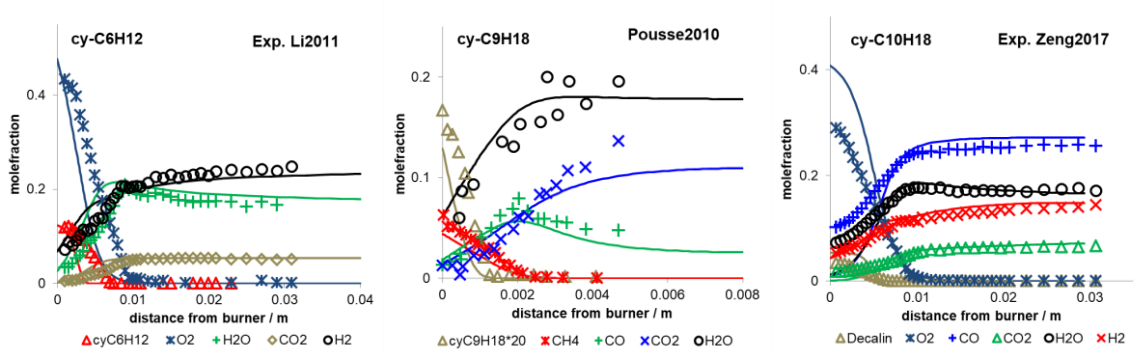

Fig. 12: Validation of speciation data in laminar flame of cyclohexane, n-propylcyclohexane, and decalin present in the mechanism.

Fuel	Ref	Conditions
cy-C_6H_{12}	Li2011	φ = 2.0, 12.727% cyC_6H_{12} + 57.27% O_2 + 30% Ar, 0.04 bar
cy-C_9H_{18}	Pousse2010	φ = 0.68, 0.81% cyC_9H_{18} + 7.1% CH_4 + 36.8% O_2 + 55.29% Ar, 0.07 atm
cy-$C_{10}H_{18}$	Zeng2017	φ = 1.8, 5.52% Decalin + 44.48% O_2 + 50% Ar; 0.04 atm

6.5 Aromatics and PAH (including cyclo-aromatics)

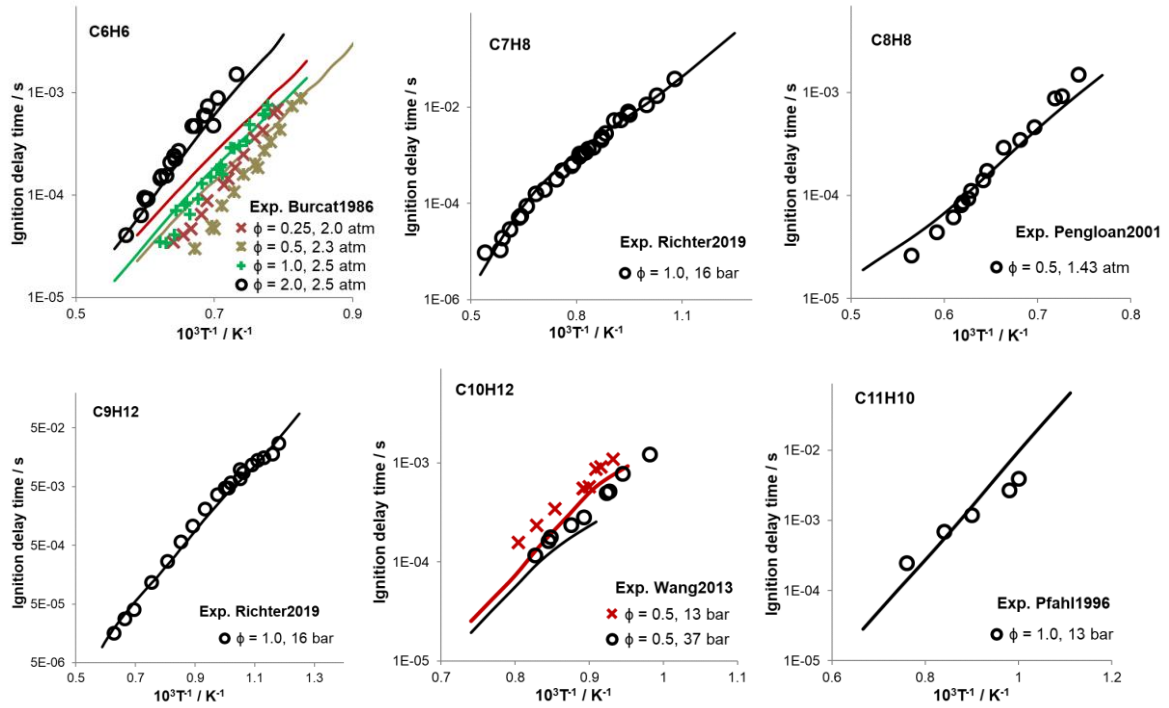

Fig. 13: Validation of ignition delay times of various aromatics available in the mechanism.

Fuel	Ref	Conditions
Benzene	Burcat1986	φ = 0.25, 0.00419% C_6H_6 + 0.1257% O_2 + 0.8701 Ar, 2.0 atm φ = 0.5, 0.0135 % C_6H_6 + 0.2031% O_2 + 0.7833 Ar, 2.3 atm φ = 1.0, 0.0169 % C_6H_6 + 0.12675% O_2 + 0.85635 Ar, 2.5 atm φ = 2.0, 0.01358 % C_6H_6 + 0.0509% O_2 + 0.9355 Ar, 2.5 atm
Toluene	Richter2019	φ = 1.0: 1.1% C_7H_8 + 9.8% O_2 + 89.1% N_2, 16 bar
Styrene	Pengloan2001	φ = 0.5, 0.25% C_8H_8 + 5% O_2 + 94.75% Ar, 1.43 atm
n-$C_6H_5C_3H_7$	Richter2019	φ = 1.0, 0.82% C_9H_{12} + 9.84% O_2 + 89.34% N_2, 16 bar
Tetralin	Wang2013	φ = 0.5, 0.8% $C_{10}H_{12}$ + 20.67% O_2 + 78.36% N_2, 13, 37 bar φ = 1.0, 1.6% $C_{10}H_{12}$ + 20.7% O_2 + 77.7% N_2, 13 bar
Methylnaphthalene	Pfahl1996	φ = 1.0, 1.5% MN + 20.7% O_2 + 77.8% N_2, 13 bar

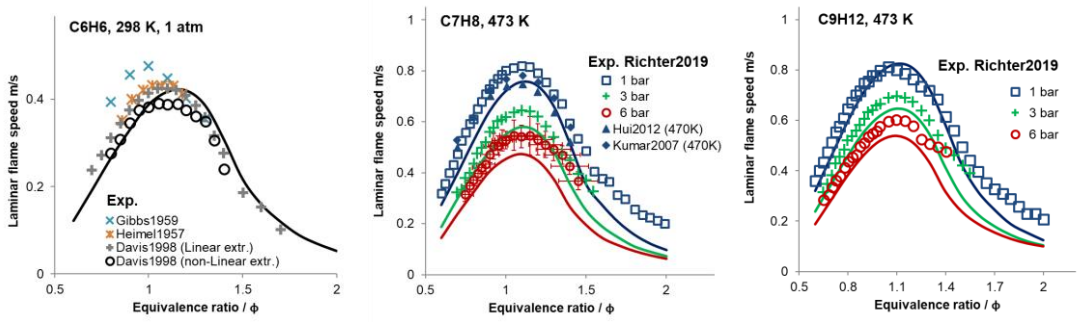

Fig. 14: Model validation of laminar flame speed as function of fuel stoichiometry for various aromatics.

Fuel	Molecule, Ref	Conditions
C_6H_6	Benzene, Davis1998, Heimel1957, Gibbs1959	298 K; 1 atm
C_7H_8	Toluene, Richter2019 Kumar2007, Hui2012	473 K; 1, 3, 6 bar 470 K; 1 bar
n-$C_6H_5C_3H_7$	n-propylbenzene, Richter2019	473 K; 1, 3, 6 bar

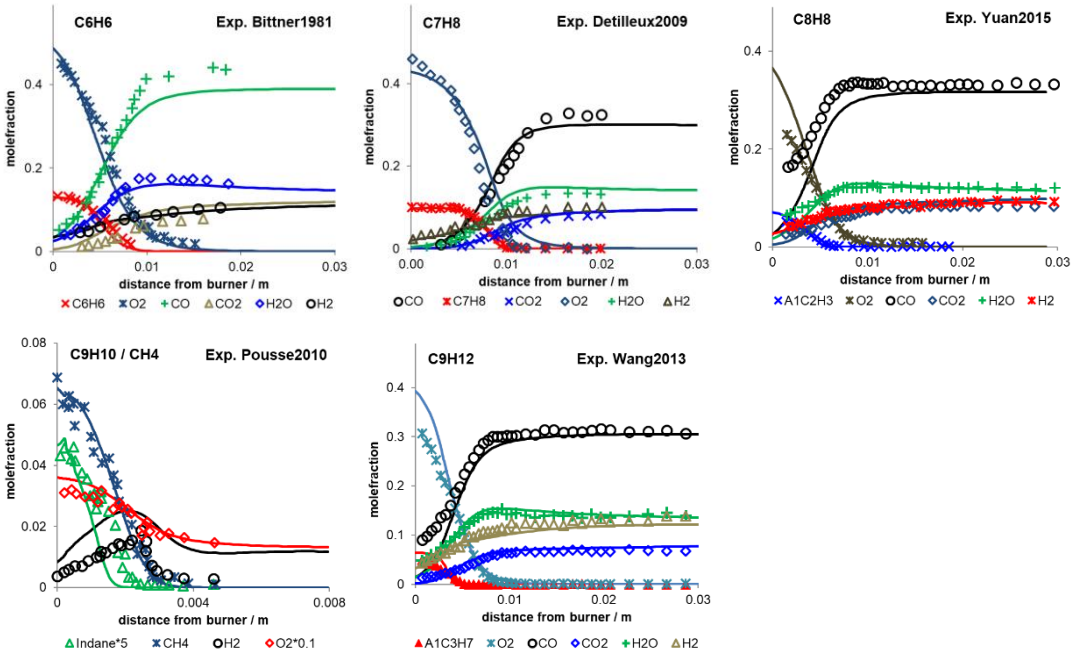

Fig. 15: Validation of speciation data in laminar flame of benzene, toluene, styrene, indane, and n-propylbenzene present in the mechanism.

Fuel	Ref	Conditions
Benzene	Bittner1981	φ = 1.8, 13.5% C_6H_6 + 56.5% O_2 + 30% Ar, 0.026 atm
Toluene	Detilleux2009	φ = 2.0, 9.9% C_7H_8 + 44.5% O_2 + 45.6% Ar, 0.05atm
Styrene	Yuan2015	φ = 1.7, 7.27% C_8H_8 + 42.73% O_2 + 50% Ar, 0.04 bar
Indane	Pousse2010a	φ = 0.67, 0.9% C_9H_{10} + 7.1% CH_4 + 36.8% O_2 + 55.2% Ar, 0.066 atm, due to unclear input data of flow rate, an estimated rate of 0.5 gm/s is taken for model simulation
n-$C_6H_5C_3H_7$	Wang2013z	φ = 1.79, 6.5% C_9H_{12} + 43.52% O_2 + 50% Ar, 0.04 bar

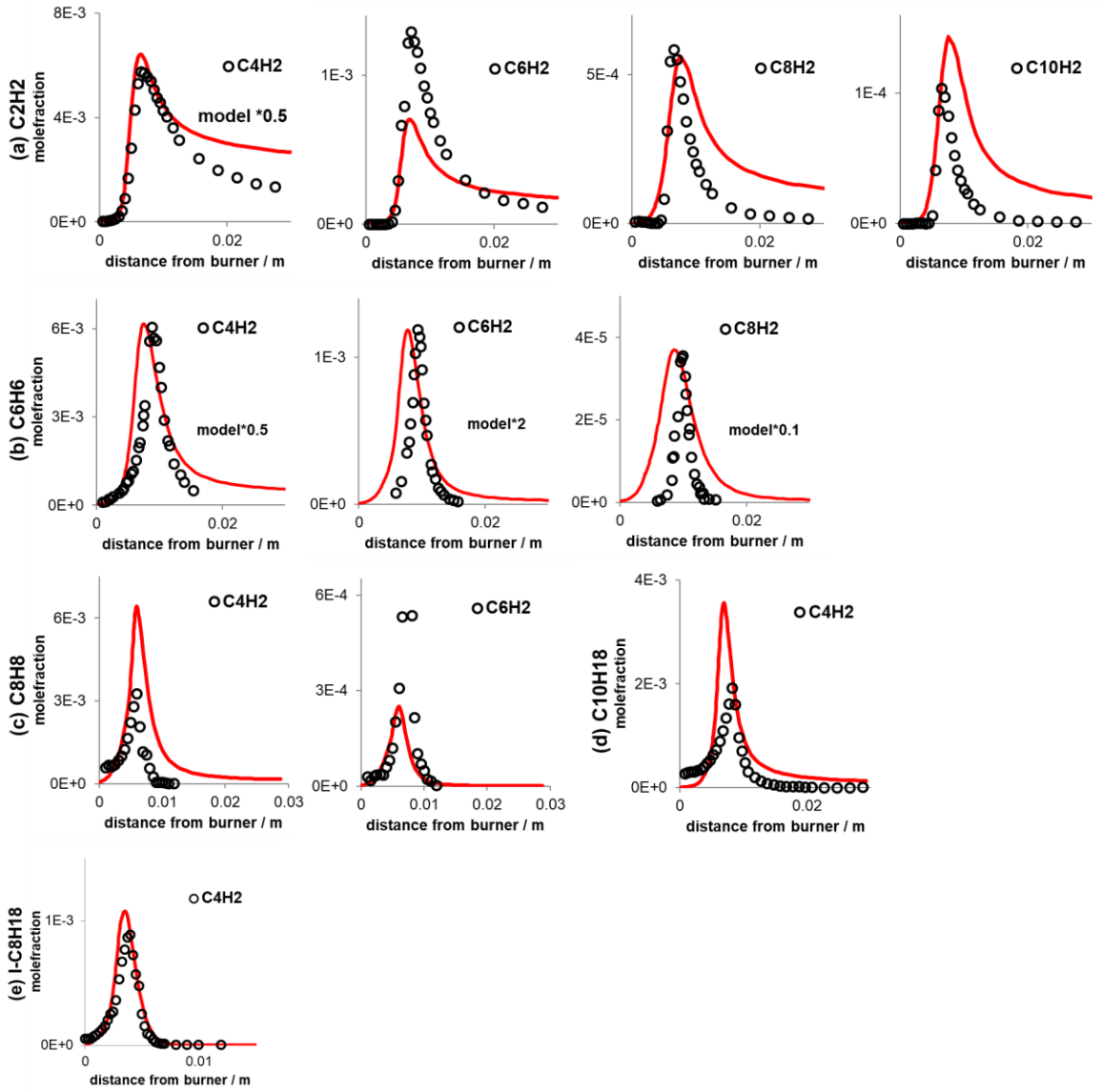

Fig. 16: Model prediction of polyynes measured in (a) acetylene flame ϕ = 2.4, 40 mbar. [Bierkandt2015], (b) benzene flame, ϕ = 1.8, 0.026 atm [Bittner1981], (c) styrene flame ϕ = 1.7, 0.0395 atm [Yuan2015], (d) Decalin flame, ϕ = 1.8, 0.04 atm., [Zeng2017] and (e) iso-octane flame ϕ = 1.47, 0.04 bar [Zeng2017a].

Fuel	Ref	Conditions
C_2H_2	Bierkandt2015	φ = 2.4, 24.5% C_2H_2 + 25.5% O_2 + 50.0% Ar, 0.04atm
C_6H_6	Bittner1981	φ = 1.8, 13.5% C_6H_6 + 56.5% O_2 + 30% Ar, 0.026 atm
C_8H_8	Yuan2015	φ = 1.7, 7.27% C_8H_8 + 42.73% O_2 + 50% Ar, 0.04 bar
$C_{10}H_{18}$	Zeng2017	φ = 1.8, 5.52% Decalin + 44.48% O_2 + 50% Ar; 0.04 atm
I-C_8H_{18}	Zeng2017a	φ = 1.47, 5.25% I-C_8H_{18} + 44.75% O_2 + 50% Ar; 0.04bar

6.6 Oxygenates – Alcohols and OME intermediates

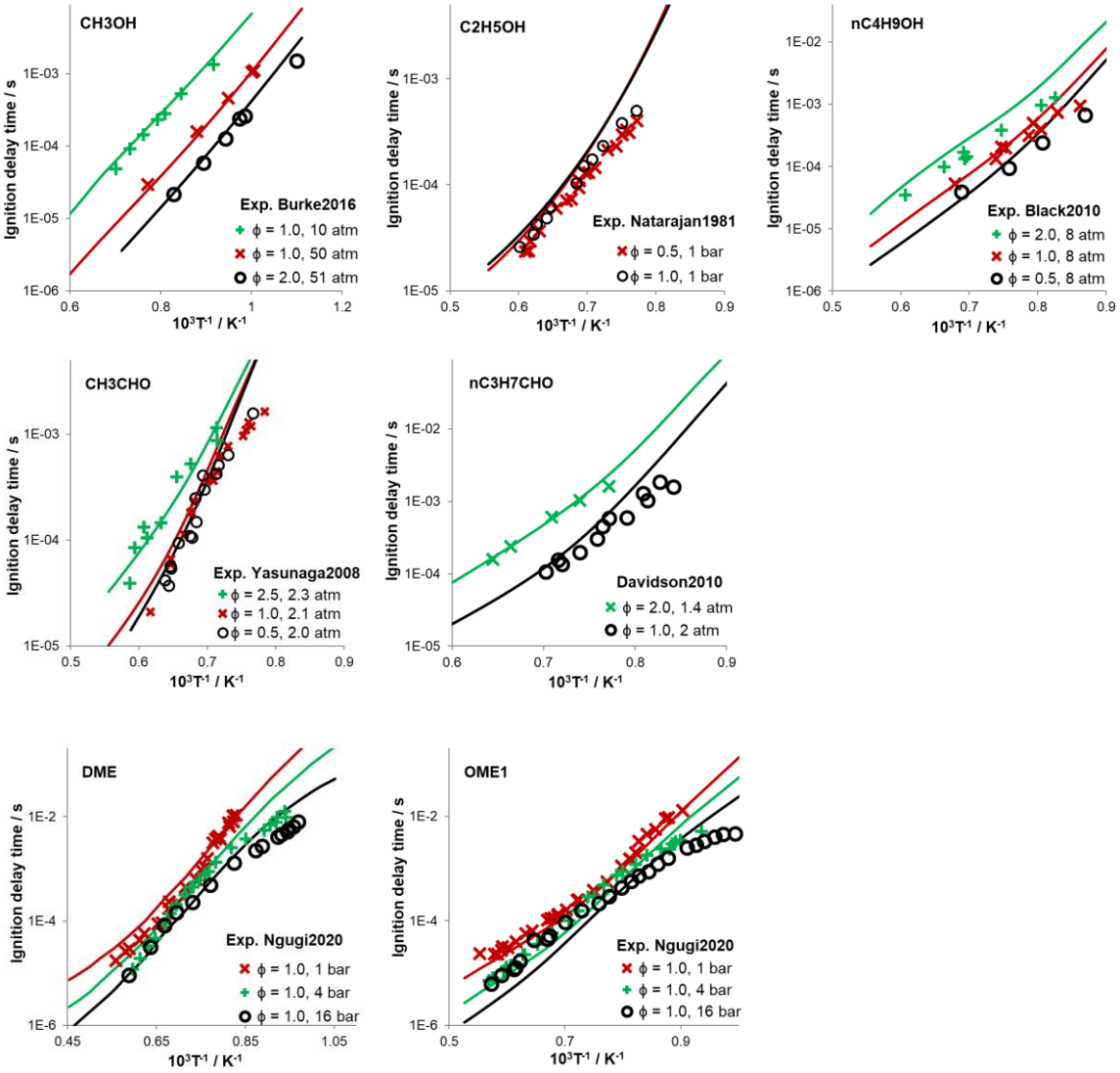

Fig. 17: Ignition delay times of oxygenates including alcohols, aldehydes and oxymethylene ethers.

Fuel	Ref	Conditions
CH_3OH	Noorani2010 Burke2016	φ = 1.0, 3.1% CH_3OH + 4.65%O_2 + 92.25% Ar, 10 atm φ = 1.0, 5.7% CH_3OH + 8.55%O_2 + 85.75% Ar, 50 atm φ = 2.0, 21.88% CH_3OH + 16.41%O_2 + 61.71% N_2, 51 atm
CH_3CHO	Yasunaga2008	φ = 0.5, 1% CH_3CHO + 5%O_2 + 94% Ar, 2.0 atm φ = 1.0, 2% CH_3CHO + 5%O_2 + 93% Ar, 2.1 atm φ = 2.5, 2% CH_3CHO + 2%O_2 + 96% Ar, 2.3 atm
C_2H_5OH	Natarajan1981	φ = 0.5: 1.43% C_2H_5OH + 8.57% O_2 + 90% Ar, 1 bar φ = 1.0: 2.5% C_2H_5OH + 7.5% O_2 + 90% Ar, 1 bar
nC_3H_7CHO	Davidson2010	φ = 1.0, 1% nC_3H_7CHO + 5.5% O_2 + 93.7% Ar, 2 atm φ = 2.0, 1% nC_3H_7CHO + 2.75% O_2 + 96.3% Ar, 1.4 atm
nC_4H_9OH	Black2010	φ = 0.5, 0.6% nC_4H_9OH + 7.2% O_2 + 92.2% Ar, 8 atm φ = 1.0, 0.6% nC_4H_9OH + 3.6% O_2 + 95.8% Ar, 8 atm φ = 2.0, 0.6% nC_4H_9OH + 1.8% O_2 + 97.6% Ar, 8 atm
DME	in-house (Ngugi2020)	φ = 1.0, 1.3% DME + 3.9% O_2 + 94.8% N_2, 1,4, 16 bar
OME1	in-house (Ngugi2020)	φ = 1.0, 0.95% OME1 + 3.8% O_2 + 95.2% N_2, 1,4, 16 bar

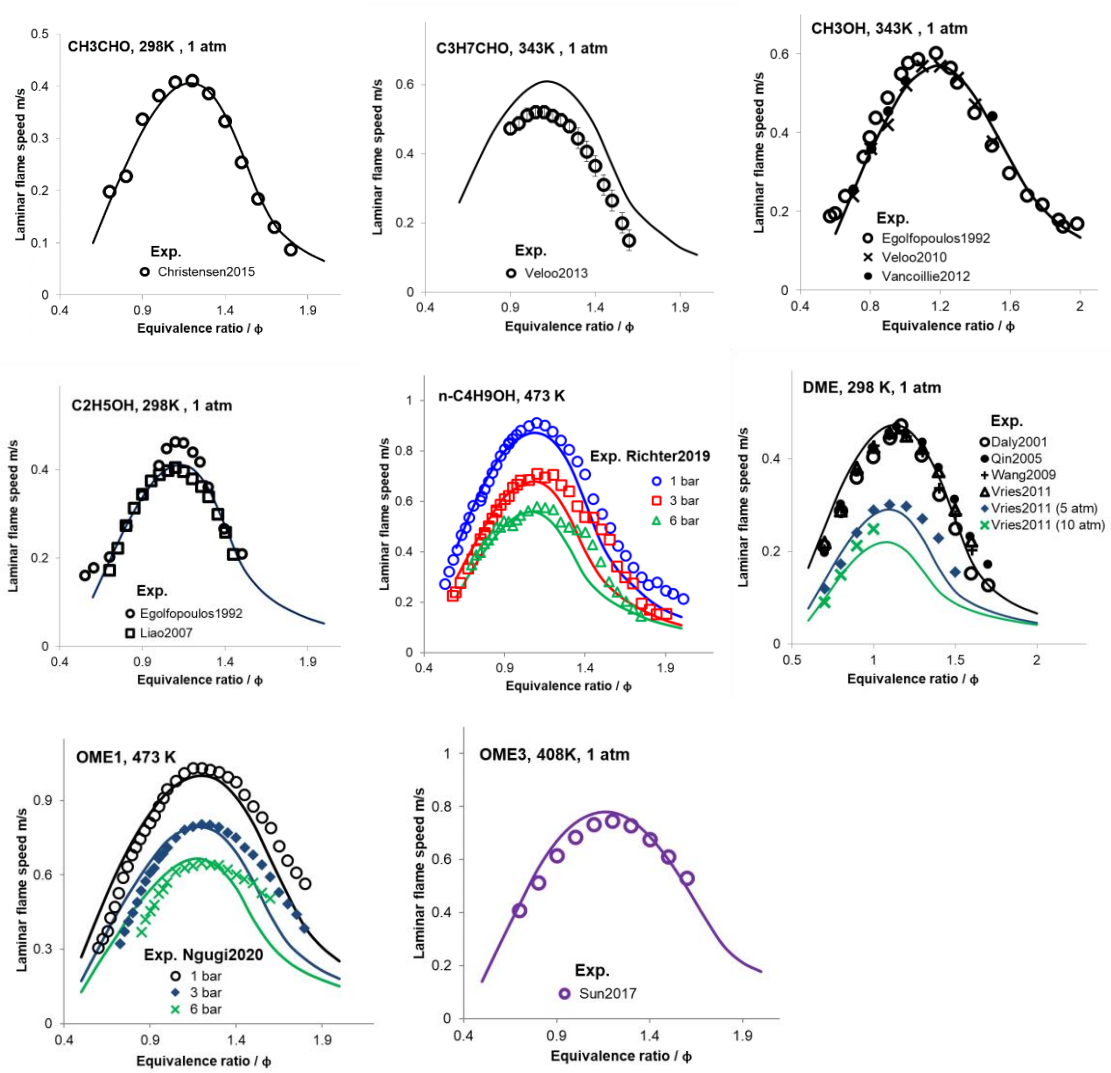

Fig. 18: Laminar flame speed of oxygenates including alcohols, aldehydes and oxy methyl ethers.

Fuel	Ref	Conditions
CH_3CHO	Christensen2015	298 K; 1 atm
C_3H_7CHO	Veloo2013	343 K; 1 atm
CH_3OH	Vancoillie2012, Egolfopoulos1992, Veloo2010	343 K; 1atm
C_2H_5OH	Egolfopoulos1992a, Liao2007	298 K; 1 atm
C_4H_9OH	Richter2019b	473 K; 1, 3, 6 bar
DME	Vries2011, Wang2009, Daly2001, Qin2005	298 K; 1, 5, 10 atm
OME1	Ngugi2020	473 K; 1, 3, 6 bar
OME3	Sun2017	408 K; 1 atm

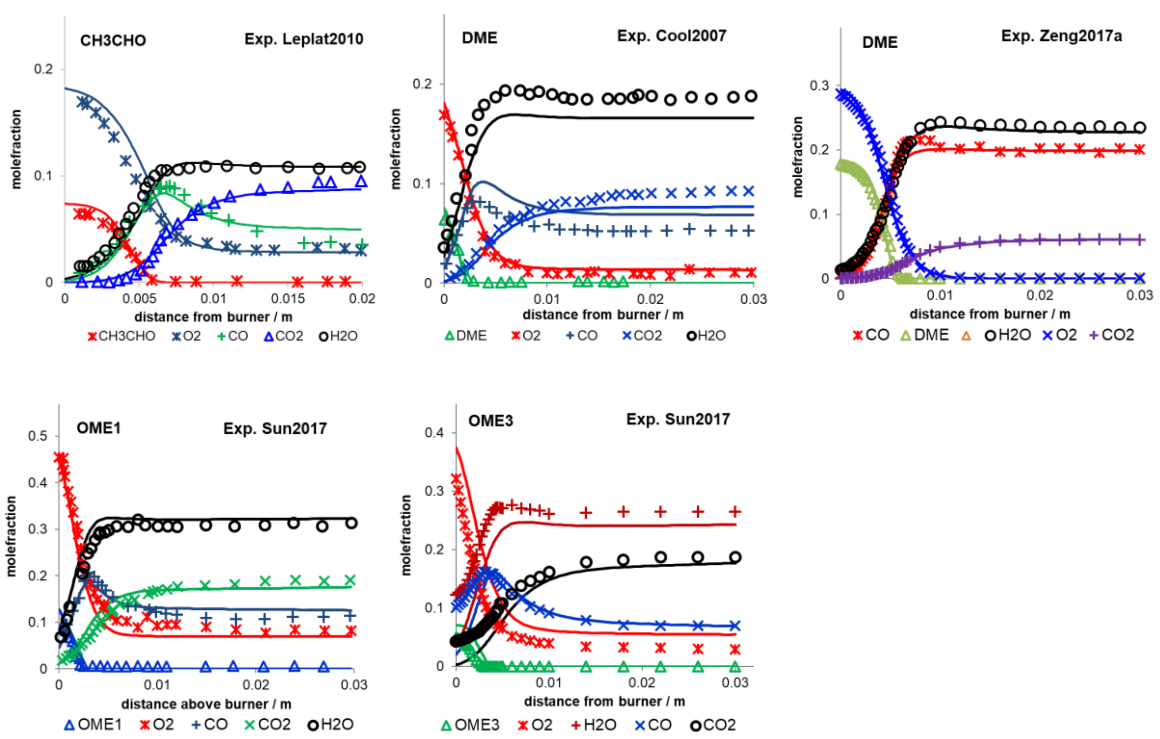

Fig. 19: Validation of speciation data in laminar flame of various oxygenates present in the mechanism.

Fuel	Ref	Conditions
CH_3CHO	Leplat2010	φ = 1.0, 7.5% CH_3CHO + 18.7% O_2 + 73.8% Ar, 0.05 atm
DME	Cool2007 Zeng2017a	φ = 1.2, 8.5% DME + 21.2% O_2 + 70.3% Ar, 0.04 bar φ = 1.84, 19.03% DME + 30.98% O_2 + 50% Ar; 0.04 bar
OME1	Sun2017	φ = 1.0, 15% OME1 + 60% O_2 + 25% Ar, 0.033 bar
OME3	Sun2017	φ = 1.0, 7.15% OME3 + 42.85% O_2 + 50% Ar; 0.033 bar

6.7 Speciation in laminar burner stabilized flames

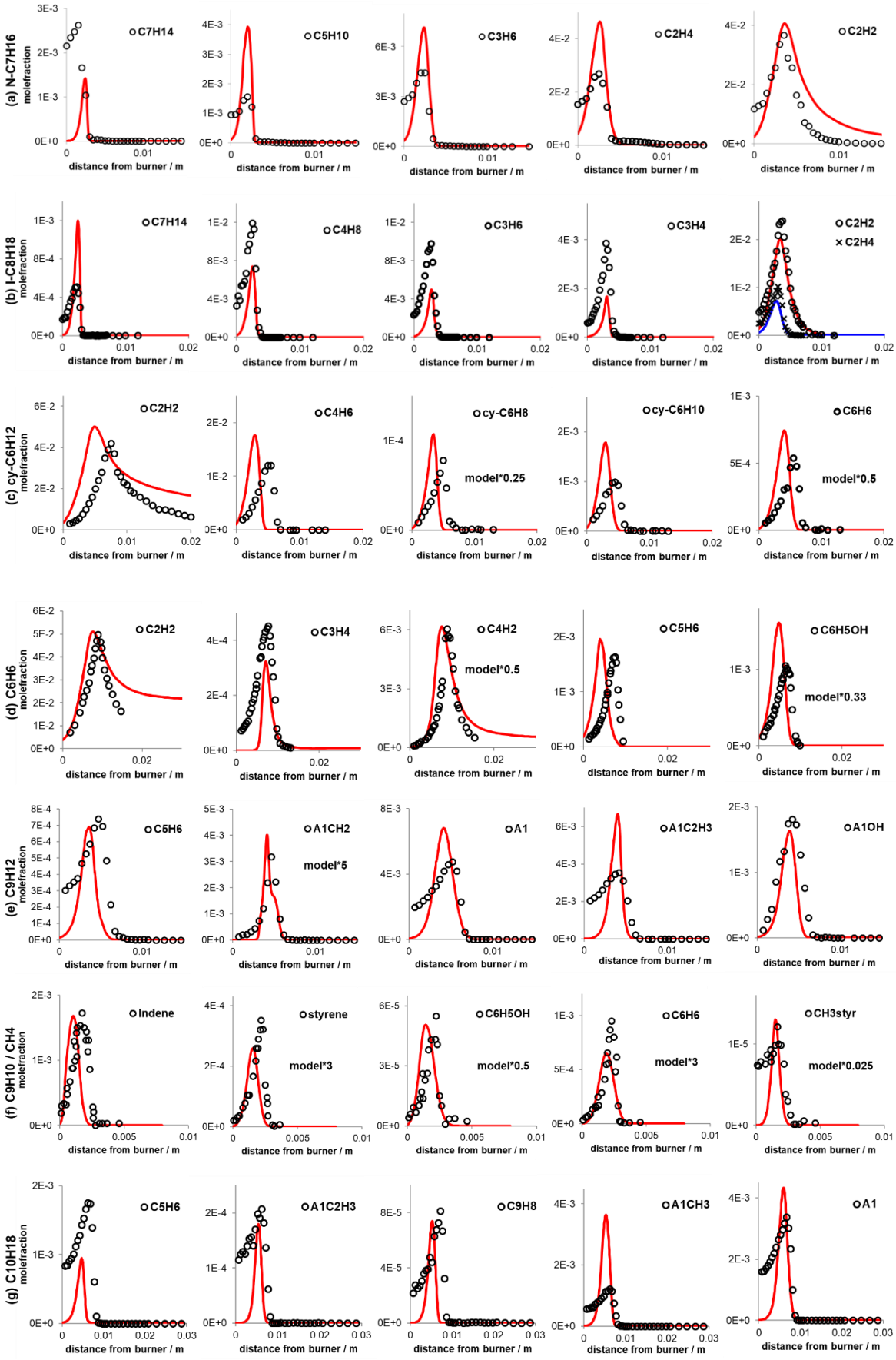

Fig. 20: Prediction of direct intermediate species formed from the fuel hydrocarbon in the stabilized flames presented earlier. (a) n-C_7H_{16}, φ = 1.69, 40 mbar [Seidel2015], (b) i-C_8H_{18}, φ = 1.47, 40 mbar

[Zeng2017a], (c) cy-C_6H_{12}, φ =2.0, 40 mbar [Li2011], (d) C_6H_6, φ =1.8, 26 mbar [Bittner1981], (e) C_9H_{12}, φ =1.79, 40 mbar [Wang2013z], (f) CH_4/C_9H_{10}, φ =0.67, 67 mbar [Pousse2010a], (g) $C_{10}H_{18}$, φ =1.8, 40 mbar [Zeng2017].

Fuel	Ref	Conditions
N-C_7H_{16}	Seidel2015	φ = 1.69, 10% nC_7H_{16} + 65% O_2 + 25% Ar, 0.04 bar
I-C_8H_{18}	Zeng2017a	φ = 1.47, 5.25% I-C_8H_{18} +44.75% O_2 + 50%Ar; 0.04 bar
cy-C_6H_{12}	Li2011	φ = 2.0, 12.727% cyC_6H_{12} + 57.27% O_2 + 30% Ar, 0.04 bar
C_6H_6	Bittner1981	φ = 1.8, 13.5% C_6H_6 + 56.5%O_2 +30%Ar, 0.026 atm
n-$C_6H_5C_3H_7$	Wang2013z	φ = 1.79, 6.5% C_9H_{12} + 43.52%O_2 + 50%Ar, 0.04 bar
C_9H_{10}	Pousse2010a	φ = 0.67, 0.9% Indane + 7.1%CH_4 + 36.8%O_2 + 55.2% Ar, 0.066 atm
$C_{10}H_{18}$	Zeng2017	φ = 1.8, 5.52% Decalin + 44.48% O_2 + 50% Ar; 0.04 atm

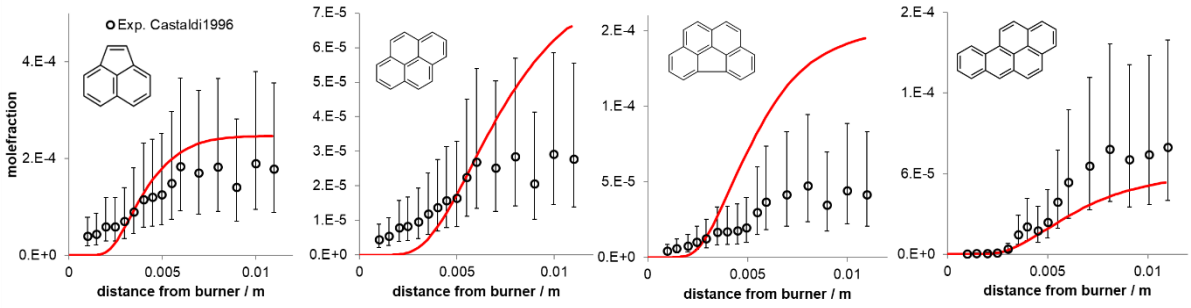

Fig. 21: Predictions of 4- and 5- ring aromatics in atmospheric laminar burner stabilized flame C_2H_4-O_2-Ar (Φ = 3.06) Exp. [Castaldi1996].

6.8 Speciation in jet-stirred reactors

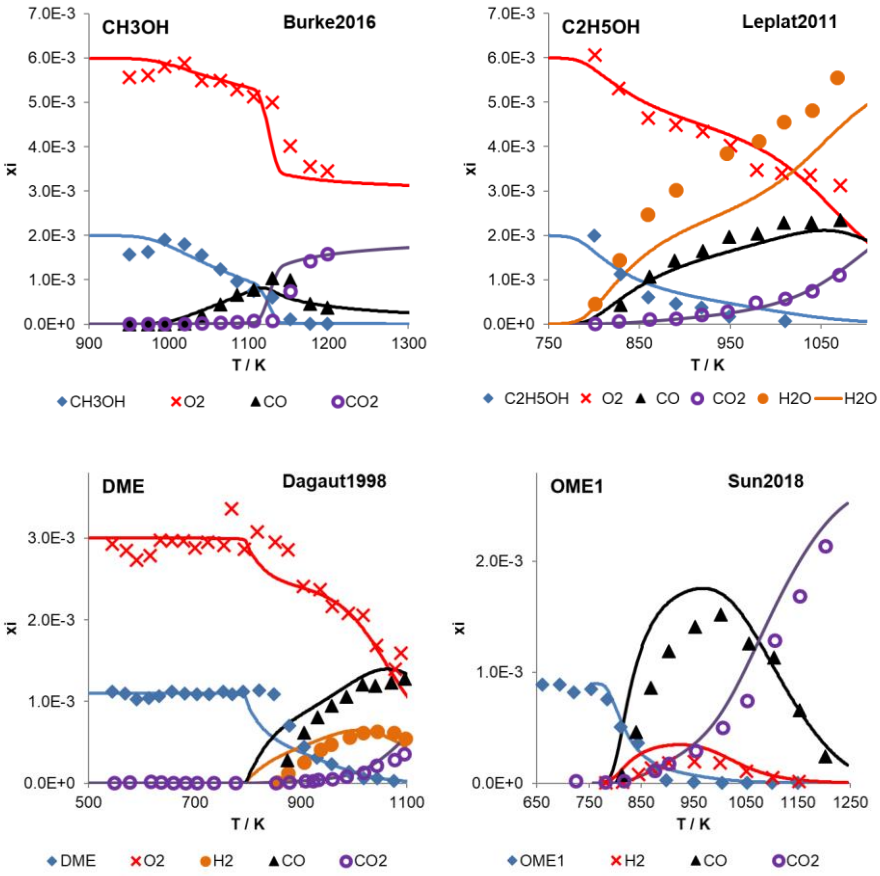

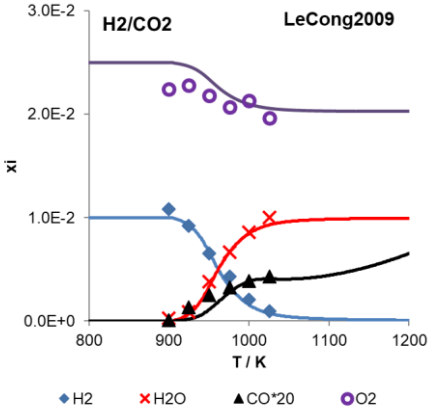
H2/CO2
LeCong2009
xi
T / K
H2
H2O
CO*20
O2

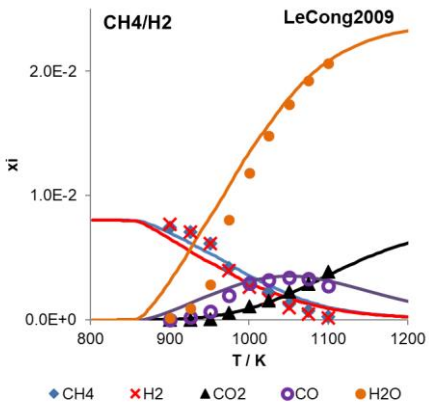
CH4/H2
LeCong2009
xi
T / K
CH4
H2
CO2
CO
H2O

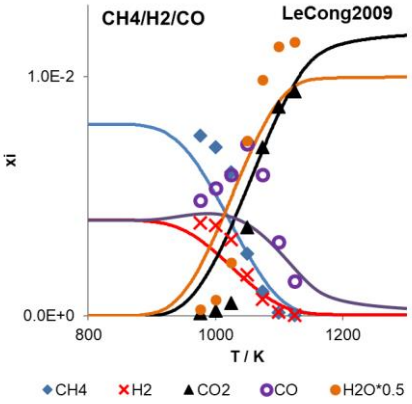
CH4/H2/CO
LeCong2009
xi
T / K
CH4
H2
CO2
CO
H2O*0.5

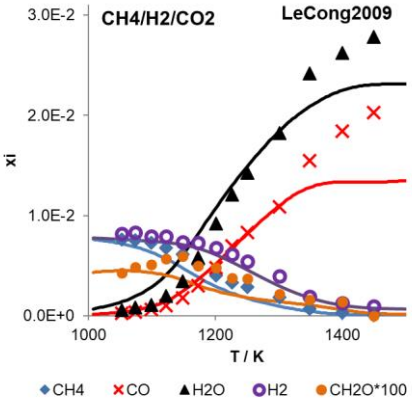
CH4/H2/CO2
LeCong2009
xi
T / K
CH4
CO
H2O
H2
CH2O*100

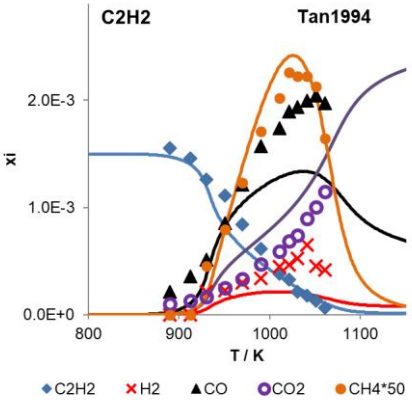
C2H2
Tan1994
xi
T / K
C2H2
H2
CO
CO2
CH4*50

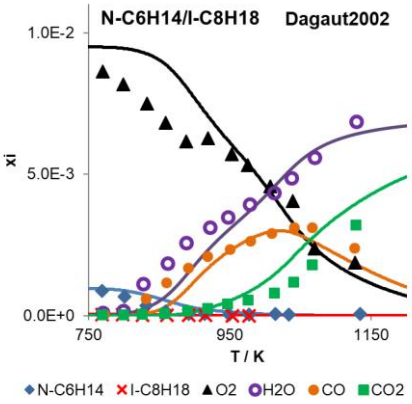
N-C6H14/I-C8H18
Dagaut2002
xi
T / K
N-C6H14
I-C8H18
O2
H2O
CO
CO2

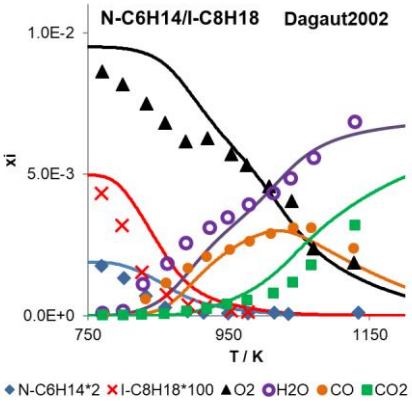
N-C6H14/I-C8H18
Dagaut2002
xi
T / K
N-C6H14*2
I-C8H18*100
O2
H2O
CO
CO2

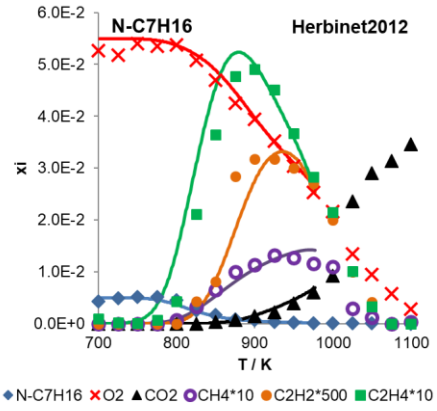
N-C7H16
Herbinet2012
xi
T / K
N-C7H16
O2
CO2
CH4*10
C2H2*500
C2H4*10

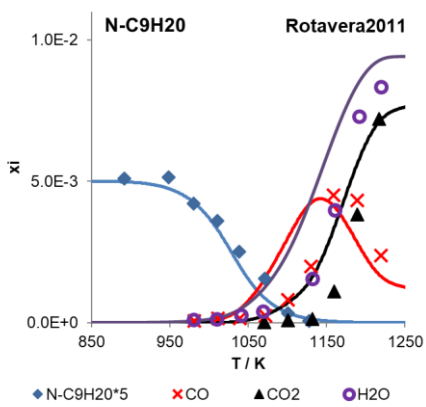
N-C9H20
Rotavera2011
xi
T / K
N-C9H20*5
CO
CO2
H2O

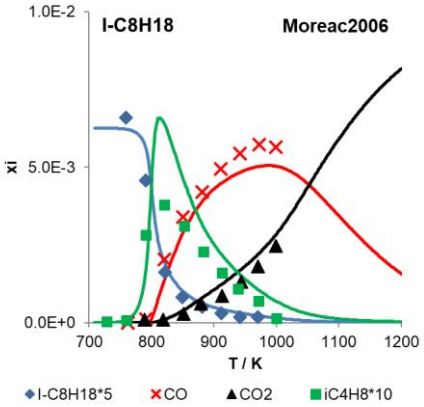
I-C8H18
Moreac2006
xi
T / K
I-C8H18*5
CO
CO2
iC4H8*10

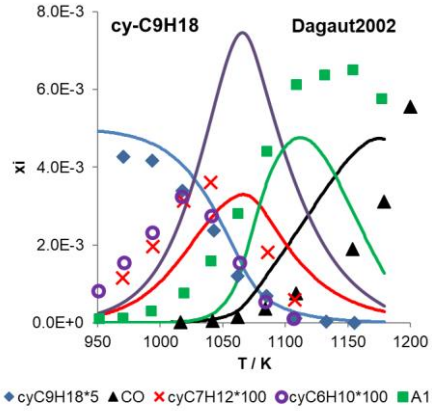
cy-C9H18
Dagaut2002
xi
T / K
cyC9H18*5
CO
cyC7H12*100
cyC6H10*100
A1

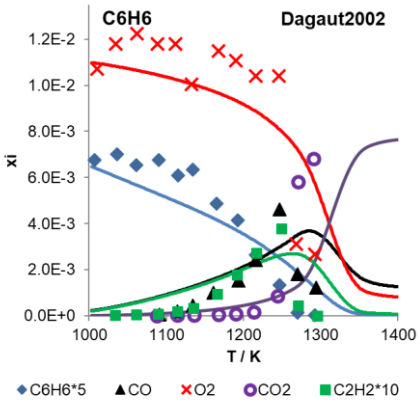
C6H6
Dagaut2002
xi
T / K
C6H6*5
CO
O2
CO2
C2H2*10

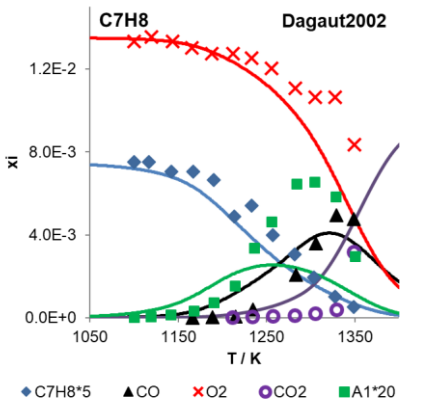
C7H8
Dagaut2002
xi
T / K
C7H8*5
CO
O2
CO2
A1*20

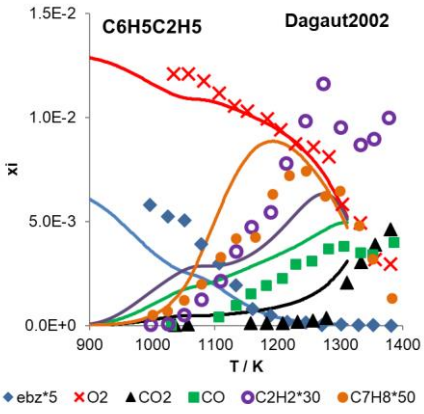
C6H5C2H5
Dagaut2002
xi
T / K
ebz*5
O2
CO2
CO
C2H2*30
C7H8*50

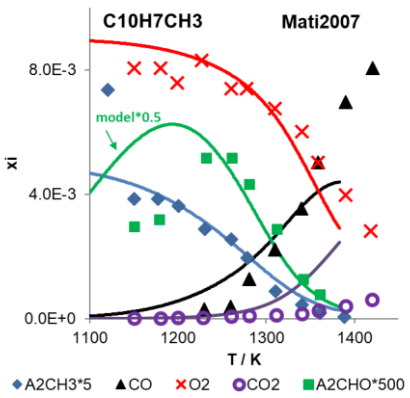
C10H7CH3
Mati2007
model*0.5
xi
T / K
A2CH3*5
CO
O2
CO2
A2CHO*500

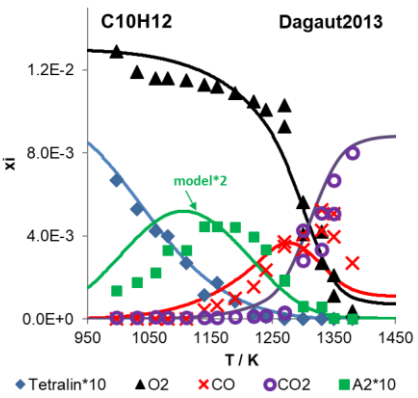
C10H12
Dagaut2013
model*2
xi
T / K
Tetralin*10
O2
CO
CO2
A2*10

Fig. 22: Predictions of major species in jet-stirred reactor

Fuel	Ref	Conditions
CH_3OH	Burke2016	φ = 0.5, 0.2% CH_3OH + 0.6% O_2 in N_2, 1 atm, τ = 0.05 s
C_2H_5OH	Leplat2011	φ = 1.0, 0.2% C_2H_5OH + 0.6% O_2 in N_2, 10 atm, τ = 0.7 s
DME	Dagaut1998	φ = 1.0, 0.11% DME + 0.3% O_2 in N_2, 10 atm, τ = 1.0 s
OME1	Sun2018	φ = 0.5, 0.09% OME1 + 0.7% O_2 in N_2, 10 atm, τ = 0.7 s
H_2-CO_2	LeCong2009	φ = 0.2, 1% H_2 + 30% CO_2 + 2.5% O_2 in N_2, 1 atm, τ = 0.12 s
CH_4-H_2	LeCong2009	φ = 0.3, 0.8% CH_4 + 0.8% H_2 + 6.7% O_2 in N_2, 10 atm, τ = 0.25 s
CH_4-H_2-CO	LeCong2009	φ = 0.3, 0.8% CH_4 + 0.4% H_2 + 0.4% CO + 6.7% O_2 in N_2, 1 atm, τ = 0.12 s
CH_4-H_2-CO_2	LeCong2009	φ = 1.5, 0.8% CH_4 + 0.8% H_2 + 20% CO_2 + 1.3% O_2 in N_2, 1 atm, τ = 0.12 s
C_2H_2	Tan1994	φ = 1.0, 0.15% C_2H_2 + 0.375% O_2 in N_2, 1 atm, τ = 0.12 s
N-C_6H_{14} + I-C_8H_{18}	Dagaut2002	φ = 1.0, 0.095% N-C_6H_{14} + 0.005% I-C_8H_{14} + 0.95% O_2 in N_2, 10 atm, τ = 0.7 s
N-C_7H_{16}	Herbinet2012	φ = 1.0, 0.5% N-C_7H_{16} + 5.5% O_2 in He, 1.06 atm, τ = 2.0 s
N-C_9H_{20}	Rotavera2011	φ = 1.0, 0.1% N-C_9H_{20} + 1.4% O_2 in N_2, 1 atm, τ = 0.07 s
I-C_8H_{18}	Moreac2006	φ = 1.0, 0.125% I-C_8H_{18} + 1.56% O_2 in N_2, 10 atm, τ = 1 s
cy-C_9H_{18}	Dagaut2002	φ = 1.0, 0.1% cyC_9H_{18} + 1.35% O_2 in N_2, 1 atm, τ = 0.07 s
C_6H_6	Dagaut2002	φ = 1.0, 0.15% C_6H_6 + 1.125% O_2 in N_2, 1 atm, τ = 0.07 s
C_7H_8	Dagaut2002	φ = 1.0, 0.15% C_7H_8 + 1.35% O_2 in N_2, 1 atm, τ = 0.1 s
$C_6H_5C_2H_5$	Dagaut2002	φ = 1.0, 0.13% ebz + 1.3% O_2 in N_2, 1 atm, τ = 0.12 s
$C_{10}H_{12}$	Dagaut2013	φ = 1.0, 0.1% tetralin + 1.3% O_2 in N_2, 1 atm, τ = 0.1 s
$C_{10}H_{11}$	Mati2007	φ = 1.5, 0.1% Methylnaphthalene + 0.9% O_2 in N_2, 1 atm, τ = 0.1 s

2. Comparison for selected fuels (and conditions) validation of current model with previous model version.

The conditions and the references are same as presented in the main paper. The data are presented for selected conditions were deviation was found among previous models with respect to measurements. The straight lines are calculations from current model and the previous model prediction are shown as dashed lines.

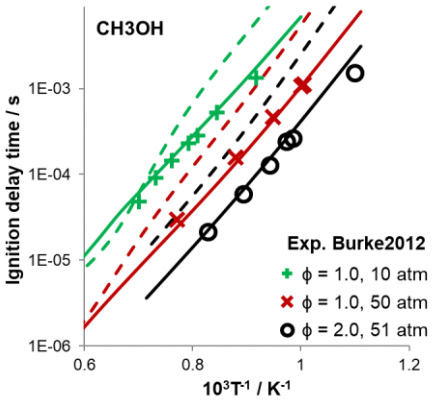
CH3OH
Ignition delay time / s
1E-03
1E-04
1E-05
1E-06
0.6
0.8
1
1.2
10³T⁻¹ / K⁻¹
Exp. Burke2012
ϕ = 1.0, 10 atm
ϕ = 1.0, 50 atm
ϕ = 2.0, 51 atm

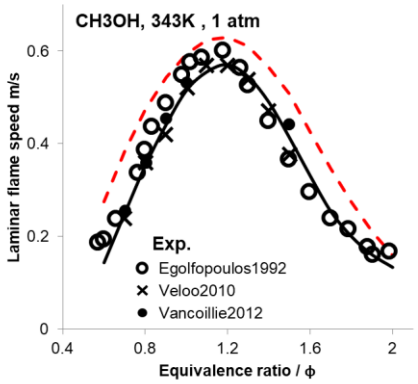
CH3OH, 343K , 1 atm
Laminar flame speed m/s
0.6
0.4
0.2
0
0.4
0.8
1.2
1.6
2
Equivalence ratio / ϕ
Exp.
Egolfopoulos1992
Veloo2010
Vancoillie2012

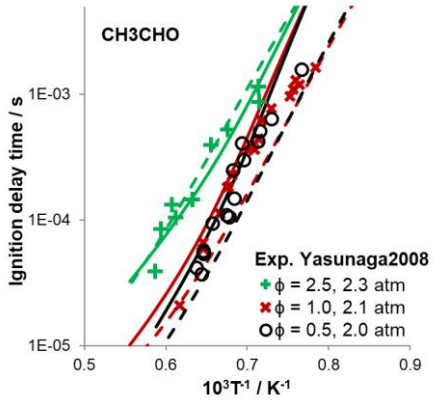
CH3CHO
Ignition delay time / s
1E-03
1E-04
1E-05
0.5
0.6
0.7
0.8
0.9
10³T⁻¹ / K⁻¹
Exp. Yasunaga2008
ϕ = 2.5, 2.3 atm
ϕ = 1.0, 2.1 atm
ϕ = 0.5, 2.0 atm

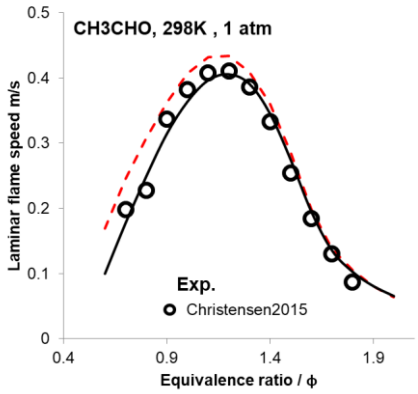
CH3CHO, 298K , 1 atm
Laminar flame speed m/s
0.5
0.4
0.3
0.2
0.1
0
0.4
0.9
1.4
1.9
Equivalence ratio / ϕ
Exp.
Christensen2015

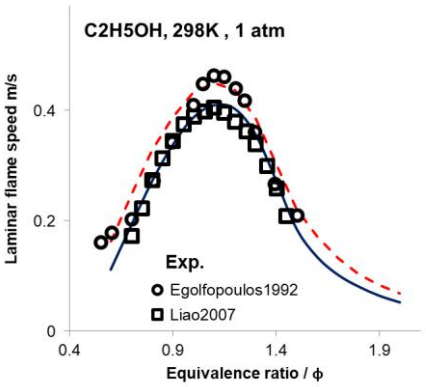
C2H5OH, 298K , 1 atm
Laminar flame speed m/s
0.4
0.2
0
0.4
0.9
1.4
1.9
Equivalence ratio / ϕ
Exp.
Egolfopoulos1992
Liao2007

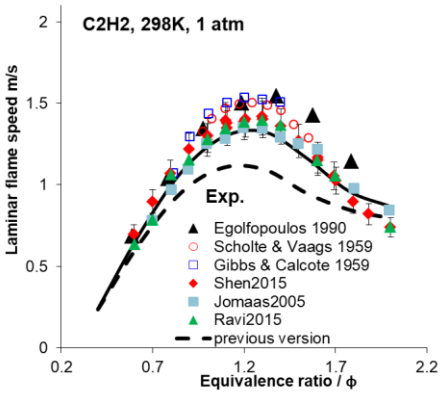
C2H2, 298K, 1 atm
Laminar flame speed m/s
2
1.5
1
0.5
0
0.2
0.7
1.2
1.7
2.2
Equivalence ratio / ϕ
Exp.
Egolfopoulos 1990
Scholte & Vaags 1959
Gibbs & Calcote 1959
Shen2015
Jomaas2005
Ravi2015
previous version

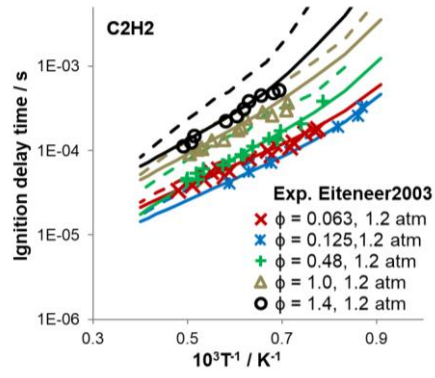
C2H2
Ignition delay time / s
1E-03
1E-04
1E-05
1E-06
0.3
0.5
0.7
0.9
10³T⁻¹ / K⁻¹
Exp. Eiteneer2003
ϕ = 0.063, 1.2 atm
ϕ = 0.125,1.2 atm
ϕ = 0.48, 1.2 atm
ϕ = 1.0, 1.2 atm
ϕ = 1.4, 1.2 atm

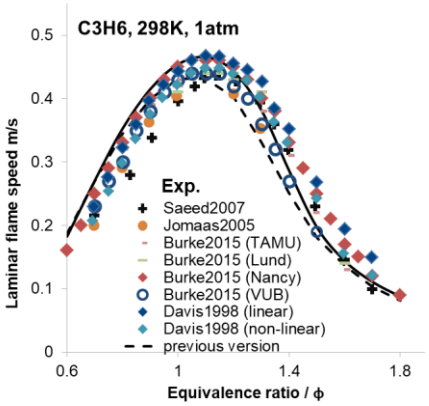
C3H6, 298K, 1atm
Laminar flame speed m/s
0.5
0.4
0.3
0.2
0.1
0
0.6
1
1.4
1.8
Equivalence ratio / ϕ
Exp.
Saeed2007
Jomaas2005
Burke2015 (TAMU)
Burke2015 (Lund)
Burke2015 (Nancy)
Burke2015 (VUB)
Davis1998 (linear)
Davis1998 (non-linear)
previous version

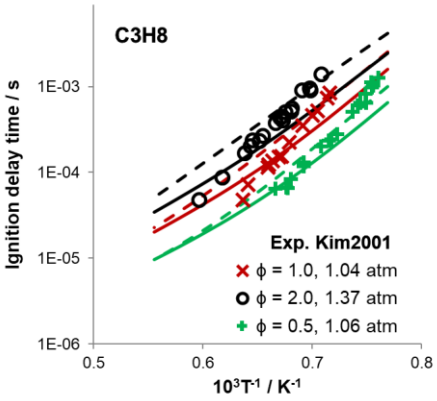
C3H8
Ignition delay time / s
1E-03
1E-04
1E-05
1E-06
0.5
0.6
0.7
0.8
10³T⁻¹ / K⁻¹
Exp. Kim2001
ϕ = 1.0, 1.04 atm
ϕ = 2.0, 1.37 atm
ϕ = 0.5, 1.06 atm

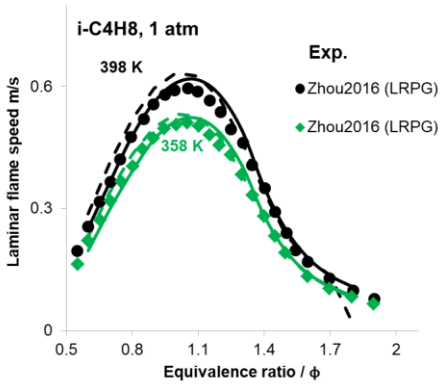
i-C4H8, 1 atm
Exp.
398 K
358 K
Zhou2016 (LRPG)
Zhou2016 (LRPG)
Laminar flame speed m/s
0.6
0.3
0
0.5
0.8
1.1
1.4
1.7
2
Equivalence ratio / ϕ

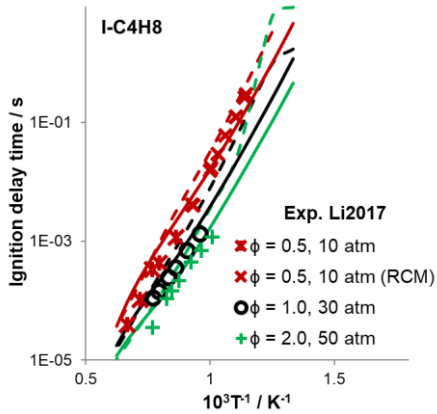
I-C4H8
Ignition delay time / s
1E-01
1E-03
1E-05
0.5
1
1.5
10³T⁻¹ / K⁻¹
Exp. Li2017
ϕ = 0.5, 10 atm
ϕ = 0.5, 10 atm (RCM)
ϕ = 1.0, 30 atm
ϕ = 2.0, 50 atm

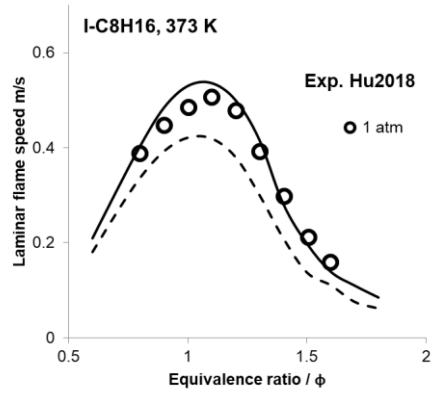
I-C8H16, 373 K
Exp. Hu2018
1 atm
Laminar flame speed m/s
0.6
0.4
0.2
0
0.5
1
1.5
2
Equivalence ratio / ϕ

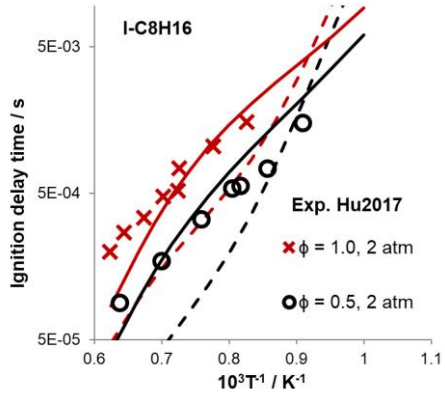
I-C8H16
Ignition delay time / s
5E-03
5E-04
5E-05
0.6
0.7
0.8
0.9
1
1.1
10³T⁻¹ / K⁻¹
Exp. Hu2017
ϕ = 1.0, 2 atm
ϕ = 0.5, 2 atm

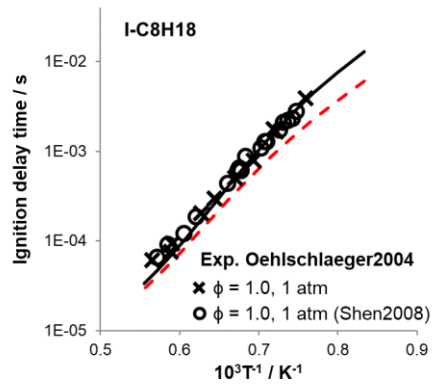
I-C8H18
Ignition delay time / s
1E-02
1E-03
1E-04
1E-05
0.5
0.6
0.7
0.8
0.9
10³T⁻¹ / K⁻¹
Exp. Oehlschlaeger2004
ϕ = 1.0, 1 atm
ϕ = 1.0, 1 atm (Shen2008)

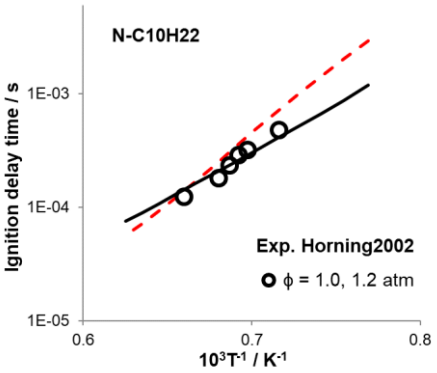
N-C10H22
Ignition delay time / s
1E-03
1E-04
1E-05
0.6
0.7
0.8
10³T⁻¹ / K⁻¹
Exp. Horning2002
ϕ = 1.0, 1.2 atm

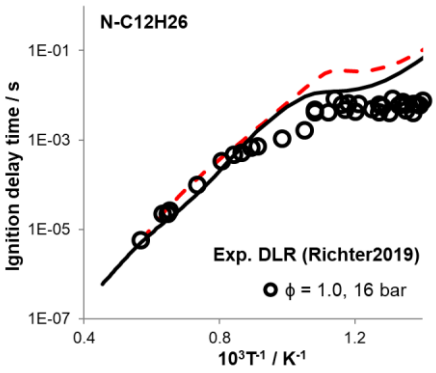
N-C12H26
Ignition delay time / s
1E-01
1E-03
1E-05
1E-07
0.4
0.8
1.2
10³T⁻¹ / K⁻¹
Exp. DLR (Richter2019)
ϕ = 1.0, 16 bar

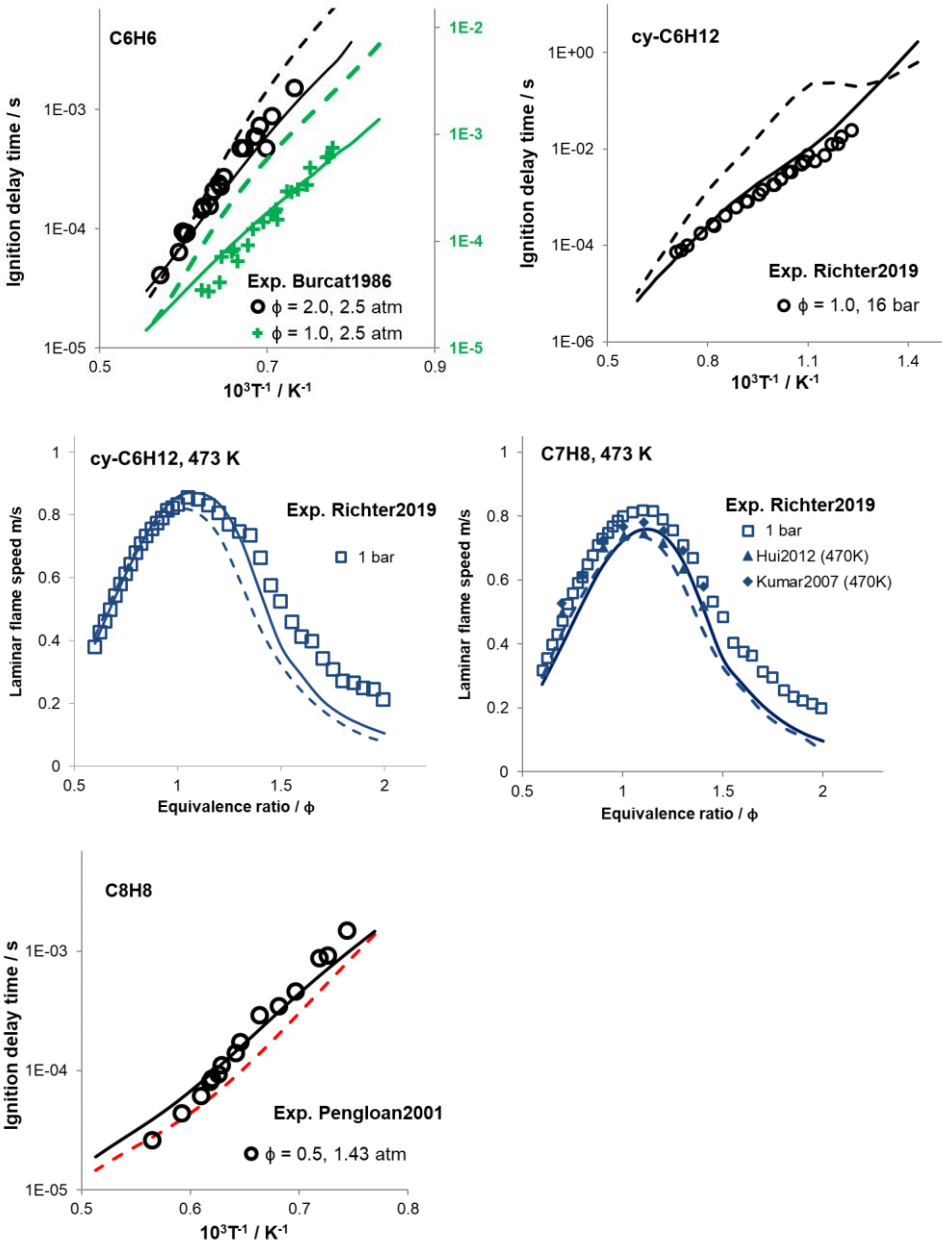

Fig. 23: Comparison of current mechanism prediction with previous version. Straight line: current mech; dash lines: previous mech.

3. Comparison of current model with literature mechanisms.

The comparison of our model prediction is presented with the well-known literature mechanisms POLIMI [18], LLNL [19], Jetsurf2.0 [20] and RWTH [21] that contains multiple hydrocarbon components. Not all fuel components are present in these mechanisms therefore, the comparison is limited. All the compared data shows the reaction model of present work and from the literature performs well for most conditions. Deviations among model prediction can be seen however no drastic deviations from the measurements are found in any case. Flame speed calculation with LLNL and to some extent POLIMI-mech requires extremely long computation time, the former due to its size and the latter for possibly containing stiff reactions.

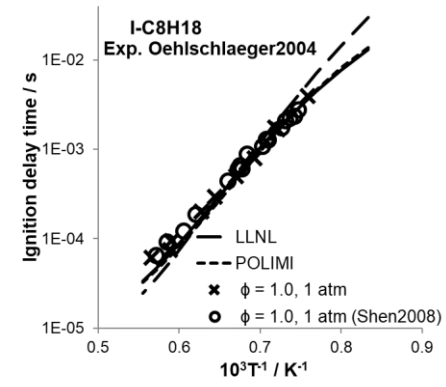
I-C8H18
Exp. Oehlschlaeger2004
Ignition delay time / s
1E-02
1E-03
1E-04
1E-05
0.5
0.6
0.7
0.8
0.9
10³T⁻¹ / K⁻¹
LLNL
POLIMI
ϕ = 1.0, 1 atm
ϕ = 1.0, 1 atm (Shen2008)

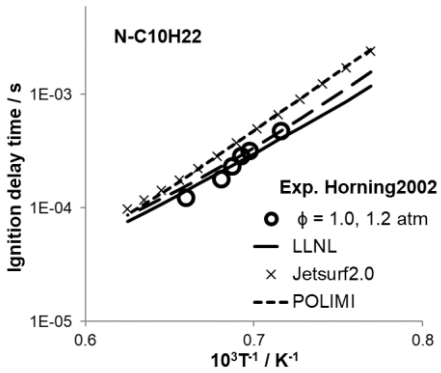
N-C10H22
Ignition delay time / s
1E-03
1E-04
1E-05
0.6
0.7
0.8
10³T⁻¹ / K⁻¹
Exp. Horning2002
ϕ = 1.0, 1.2 atm
LLNL
Jetsurf2.0
POLIMI

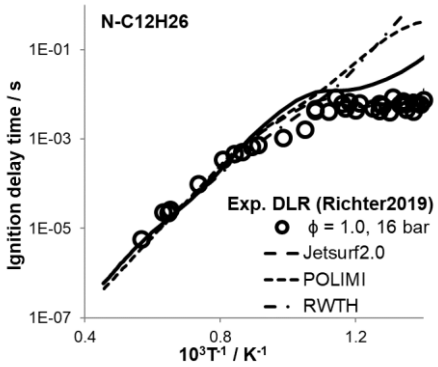
N-C12H26
Ignition delay time / s
1E-01
1E-03
1E-05
1E-07
0.4
0.8
1.2
10³T⁻¹ / K⁻¹
Exp. DLR (Richter2019)
ϕ = 1.0, 16 bar
Jetsurf2.0
POLIMI
RWTH

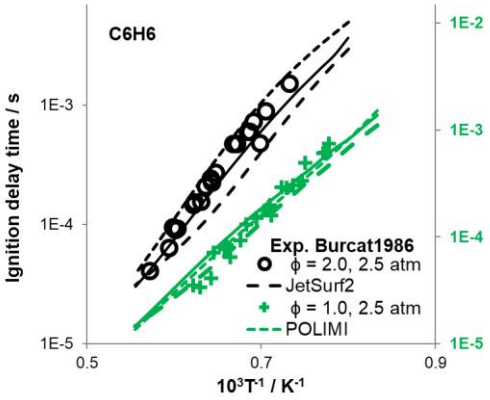
C6H6
Ignition delay time / s
1E-3
1E-4
1E-5
0.5
0.7
0.9
10³T⁻¹ / K⁻¹
1E-2
1E-3
1E-4
1E-5
Exp. Burcat1986
ϕ = 2.0, 2.5 atm
JetSurf2
ϕ = 1.0, 2.5 atm
POLIMI

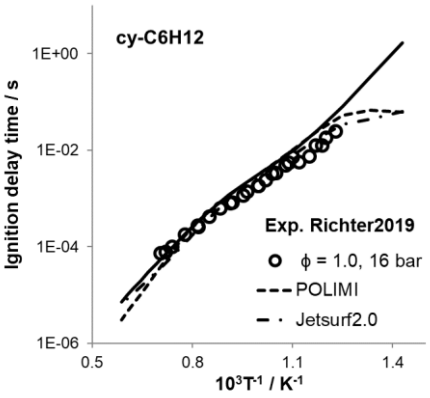
cy-C6H12
Ignition delay time / s
1E+00
1E-02
1E-04
1E-06
0.5
0.8
1.1
1.4
10³T⁻¹ / K⁻¹
Exp. Richter2019
ϕ = 1.0, 16 bar
POLIMI
Jetsurf2.0

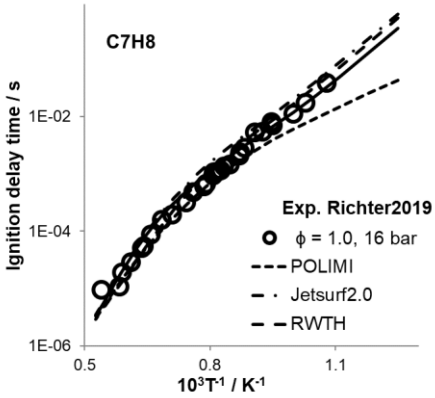
C7H8
Ignition delay time / s
1E-02
1E-04
1E-06
0.5
0.8
1.1
10³T⁻¹ / K⁻¹
Exp. Richter2019
ϕ = 1.0, 16 bar
POLIMI
Jetsurf2.0
RWTH

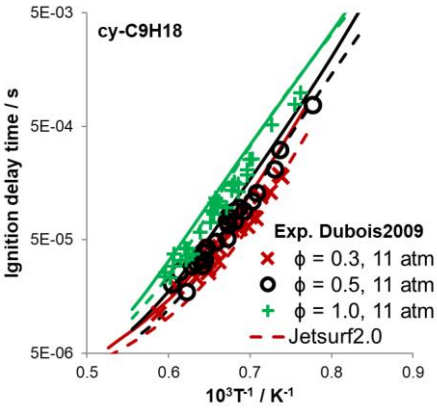
cy-C9H18
Ignition delay time / s
5E-03
5E-04
5E-05
5E-06
0.5
0.6
0.7
0.8
0.9
10³T⁻¹ / K⁻¹
Exp. Dubois2009
ϕ = 0.3, 11 atm
ϕ = 0.5, 11 atm
ϕ = 1.0, 11 atm
Jetsurf2.0

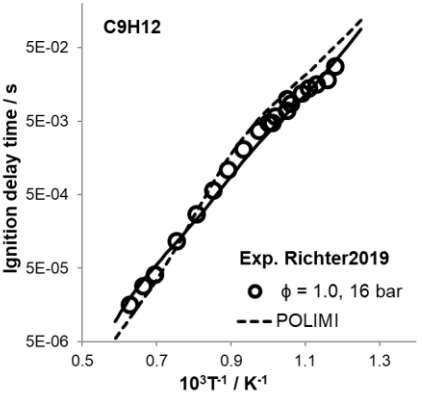
C9H12
Ignition delay time / s
5E-02
5E-03
5E-04
5E-05
5E-06
0.5
0.7
0.9
1.1
1.3
10³T⁻¹ / K⁻¹
Exp. Richter2019
ϕ = 1.0, 16 bar
POLIMI

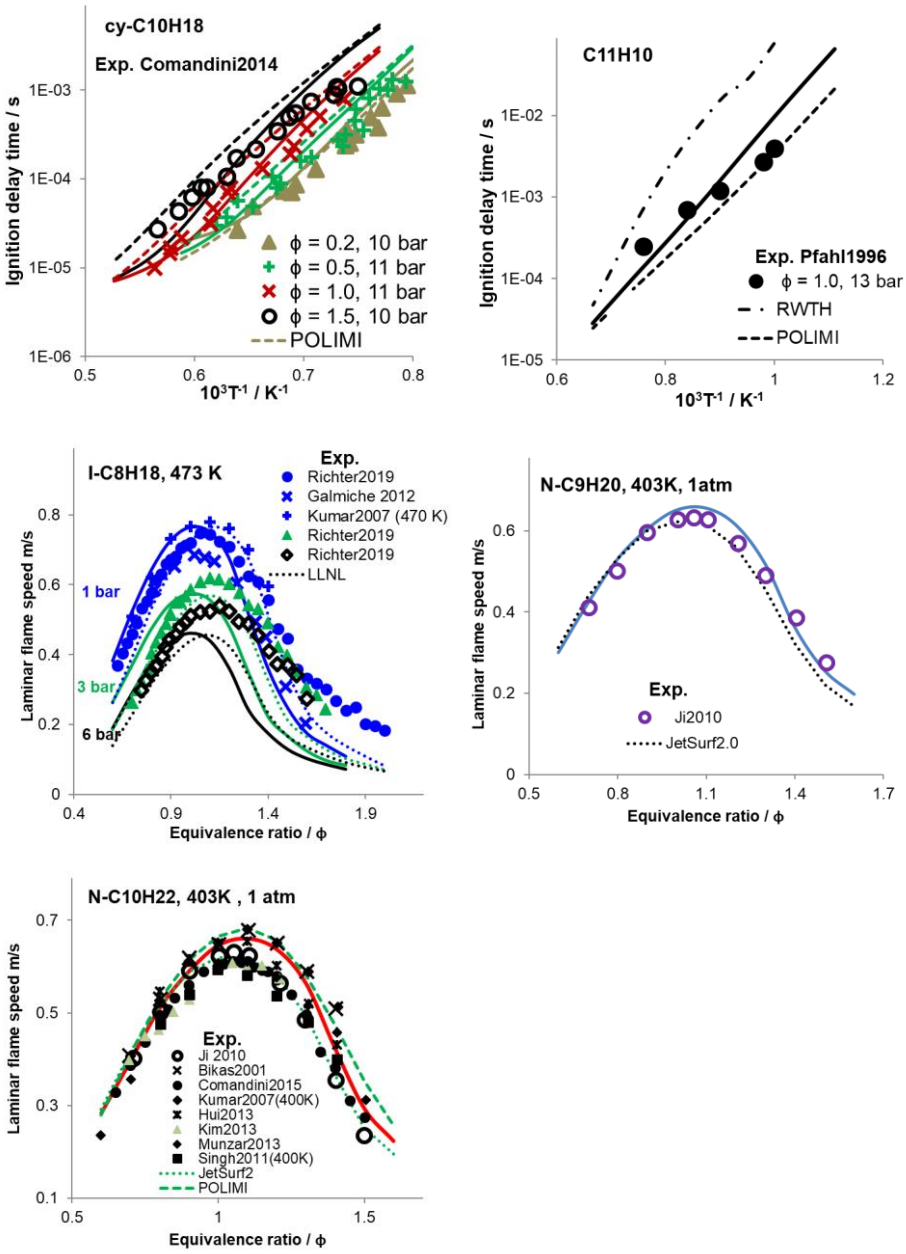

Fig. 24: Comparison of current mechanism prediction with the literature mechanisms.

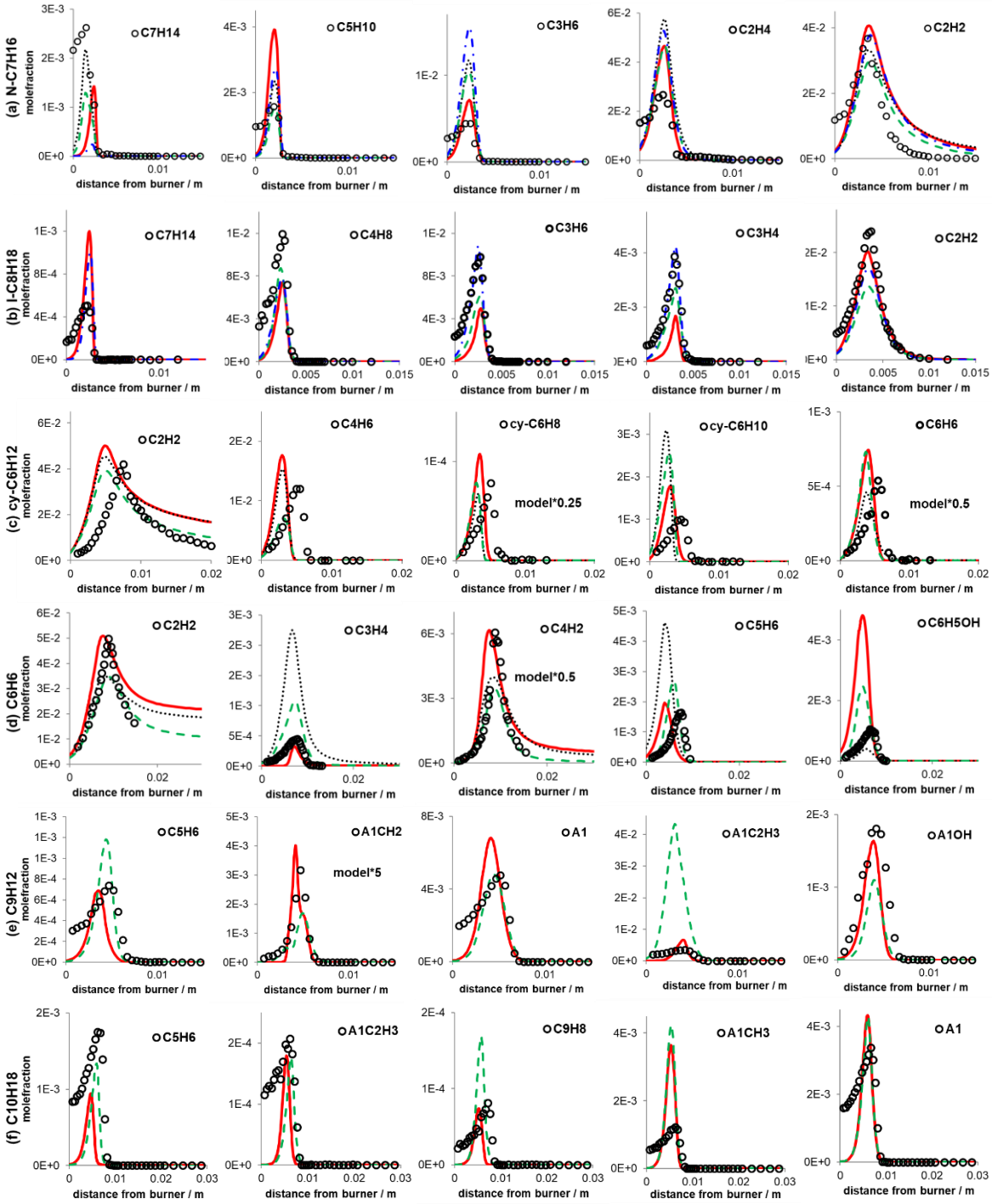

Fig. 25: Prediction of direct intermediate species formed from the fuel hydrocarbon in the stabilized flames presented in Fig 20. (a) n-C_7H_{16}, φ = 1.69, 40 mbar [Seidel2015], (b) i-C_8H_{18}, φ = 1.47, 40 mbar [Zeng2017a], (c) cy-C_6H_{12}, φ =2.0, 40 mbar [Li2011], (d) C_6H_6, φ =1.8, 26 mbar [Bittner1981], (e) C_9H_{12}, φ =1.79, 40 mbar [Wang2013z], (f) $C_{10}H_{18}$, φ =1.8, 40 mbar [Zeng2017]. Simulations: present work (——), Jetsurf2.0 (·····), POLIMI (– – –), RWTH (–·–·).

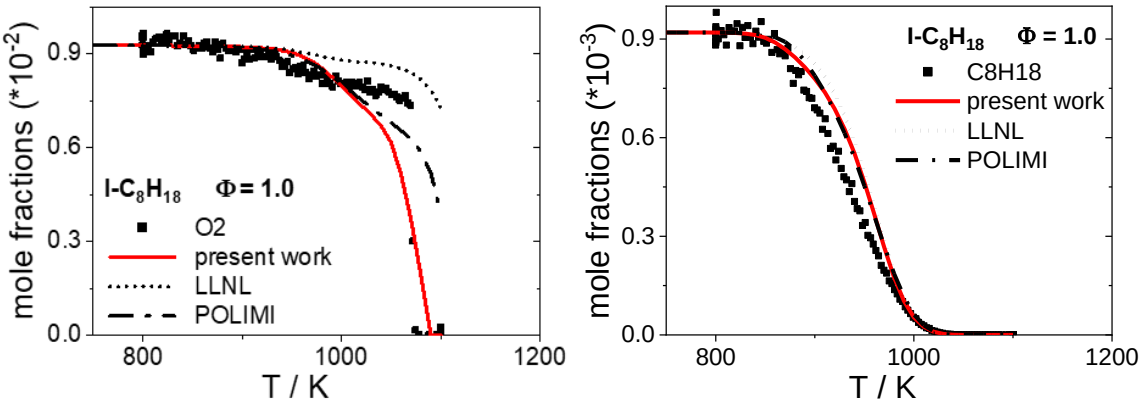

Fig. 26: Comparison of fuel and O_2 prediction by different models. Experiments obtained in DLR high temperature flow reactor for i-C8H18.

4. References

[**Keromnes2013**] Kéromnès A, Metcalfe WK, Heufer KA, Donohoe N, Das AK, Sung C, et al. An experimental and detailed chemical kinetic modeling study of hydrogen and syngas mixture oxidation at elevated pressures. Combust Flame 2013;160:995-1011.

[**Zhang2012**] Zhang Y, Huang Z, Wei L, Zhang J, Law CK. Experimental and modeling study on ignition delays of lean mixtures of methane, hydrogen, oxygen, and argon at elevated pressures. Combust Flame 2012;159:918–931.

[**Petersen1996**] Petersen EL, Rohrig M, Davidson DF, Hanson RK, Bowman CT. High-pressure methane oxidation behind reflected shock waves. Sym (Int) Combust 1996;26:799-806.

[**Eiteneer2003**] Eiteneer B, Frenklach M. Experimental and modeling study of shock-tube oxidation of acetylene. Int J Chem Kinet 2003;35:391–414.

[**Brown1999**] Brown CJ, Thomas GO. Experimental studies of shock-induced ignition and transition to detonation in ethylene and propane mixtures. Combust Flame 1999;117:861-870.

[**Curran1996**] Curran H, Simme JM, Dagaut P, Voisin D, Cathonnet M. The ignition and oxidation of allene and propyne: Experiments and kinetic modelling. Proc Combust Inst 1996;26:613–620.

[**Qin2001**] Qin Z, Yang H, Gardiner WC Jr. Measurement and modeling of shock-tube ignition delay for propene. Combust Flame 2001;124:246–254.

[**Kim2001**] Kim K, Shin KS. Shock tube and modelling study of the ignition of propane. Bull Korean Chem Soc 2001;22:303-307.

[**Fournet1999**] Fournet R, Bauge JC, Battin-Leclerc F. Experimental and modeling of oxidation of acetylene, propyne, allene, and 1,3-butadiene. Int J Chem Kinet 1999;31:361-379.

[**Li2017**] Li Y, Zhou C, Somers KP, Zhang K, Curran HJ. The oxidation of 2-butene: A high pressure ignition delay, kinetic modeling study and reactivity comparison with isobutene and 1-butene. Proc Combust Inst 2017;36:403-411.

[**Burcat1971**] Burcat A, Scheller K, Lifshitz A. Shock-tube investigation of comparative ignition delay times for C1-C5 alkanes. Combust Flame 1971;16:29–33.

[**Horning2002**] Horning DC, Davidson DF, Hanson RK. Study of the High-temperature autoignition of n-alkane/O2/Ar mixtures. J Propul Power 2002;18:363–371.

[**Healy2010**] Healy D, Donato NS, Aul CJ, Petersen EL, Zinner CM, Bourque G, Curran HJ. n-Butane: Ignition delay measurements at high pressure and detailed chemical kinetic simulations. Combust Flame 2010;157:1526–1539.

[**Cheng2016**] Cheng Y, Hu E, Deng F, Yang F, Zhang Y, Tang C, Huang Z. Experimental and kinetic comparative study on ignition characteristics of 1-pentene and n-pentane. Fuel 2016;172:263–272.
[**Westbrook2015**] Westbrook CK, Pitz WJ, Mehl M, Glaude P, Herbinet O, Bax S, et al. Experimental and kinetic modeling study of 2-methyl-2-butene: Allylic hydrocarbon kinetics. J Phys Chem A 2015;119:7462–7480.
[**McLean1994**] McLean IC, Smith DB, Taylor SC. The use of carbon monoxide/hydrogen burning velocities to examine the rate of the CO+OH reaction. Proc Combust Inst 1994;25:749-757.
[**Richter2016**] Richter S, Ermel J, Kick T, Braun-Unkhoff M, Naumann C, Riedel U. The influence of diluent gases on combustion properties of natural gas: A combined experimental and modeling study. J Eng Gas Turbines Power 2016;138:101503-101512.
[**Lowry2011**] Lowry W, de Vries J, Krejci M, Petersen EL, Serinyel Z, Metcalfe WK, et al. Laminar flame speed measurements and modeling of pure alkanes and alkane blends at elevated pressures. J Eng Gas Turbines Power 2011;133:091501.
[**Rozenchan2002**] Rozenchan G, Zhu DL, Law CK, Tse SD. Outward propagation, burning velocities, and chemical effects of methane flames up to 60 atm. Proc Combust Inst 2002;29:1461-1470.
[**Gu2000**] Gu XJ, Haq MZ, Lawes M, Woolley R. Laminar burning velocity and Markstein lengths of methane–air mixtures. Combust Flame 2000;121:41-58.
[**Davis1998**] Davis SG, Law CK. Determination of and fuel structure effects on laminar flame speeds of C1 to C8 hydrocarbons, Comb Sci Tech 1998;140:427-449.
[**Hassan1998**] Hassan MI, Aung KT, Faeth GM. Measured and predicted properties of laminar premixed methane/air flames at various pressures, Combust Flame 1998;115:539-550.
[**Vagelopoulos1998**] Vagelopoulos CM, Egolfopoulos FN, Direct experimental determination of laminar flame speeds, Sym (Int) Combust 1998;27:513-519.
[**Vagelopoulos1994**] Vagelopoulos CM, Egolfopoulos FN, Law CK. Further considerations on the determination of laminar flame speeds with the counterflow twin-flame technique. Sym (Int) Combust 1994;25:1341-1347.
[**Egolfopoulos1990**] Egolfopoulos FN, Zhu DL, Law CK. Experimental and numerical determination of laminar flame speeds: mixtures of C2-hydrocarbons with oxygen and nitrogen. Proc Combust Inst 1990;23:471-478.
[**Taylor1991**] Taylor SC. PhD Thesis. Burning velocity and the influence of flame stretch. University of Leeds 1991.
[**Hassan1994**] Hassan MI, Aung KT, Kwon KC, Faeth GM. Properties of laminar premixed hydrocarbon/air flames at various pressures. J. Propul Power 1994;14:479-488.
[**Scholte1959**] Scholte TG, Vaags PB. The burning velocity of hydrogen-air mixtures and mixtures of some hydrocarbons with air. Combust Flame 1959;3:495–501.
[**Gibbs1959**] Gibbs GJ, Calcote HF. Effect of molecular structure on burning velocity. J Chem Eng Data 1959;4:226–237.
[**Jomaas2005**] Jomaas G, Zheng XL, Zhu DL, Law CK. Experimental determination of counterflow ignition temperatures and laminar flame speeds of C2-C3 hydrocarbons at atmospheric and elevated pressures. Proc Combust Inst 2005;30:193-200.
[**Kochar2010**] Kochar Y, Vaden S, Lieuwen T, Seitzman J. Laminar flame speed of hydrocarbon fuels with preheat and low oxygen content. 2010, Paper No AIAA-2010-778.
[**Kochar2011**] Kochar Y, Seitzman J, Lieuwen T, Metcalfe WK, Burke SM, Curran HJ, et al. Laminar flame speed measurements and modeling of alkane blends at elevated pressures with various diluents. ASME Turbo Expo 2011; Paper No GT2011-45122.

[**Aung1995**] Aung KT, Tseng LK, Ismail MA, Faeth GM. Response to comment by SC Taylor and DB Smith on Laminar burning velocities and markstein numbers of hydrocarbon/air flames, Brief Communication, Combust Flame 1995;102:526–530.
[**Konnov2003**] Konnov AA, Dyakov IV, De Ruyck J. Measurement of adiabatic burning velocity in ethane-oxygen-nitrogen and in ethane-oxygen-argon mixtures, Exp Therm Fluid Sci 2003;27:379–384.
[**Bosschaart2004**] Bosschaart KJ, De Goey LPH, Burgers JM. The laminar burning velocity of flames propagating in mixtures of hydrocarbons and air measured with the heat flux method. Combust Flame 2004;136:261–269.
[**Dyakov2007**] Dyakov IV, De Ruyck J, Konnov AA. Probe sampling measurements and modeling of nitric oxide formation in ethane+air flames. Fuel 2007;86:98–105.
[**Saeed2007**] Saeed K, Stone R. Laminar burning velocities of propene–air mixtures at elevated temperatures and pressures. J Energy Inst 2007;80:73–82.
[**Burke2015**] Burke SM, Metcalfe W, Herbinet O, Battin-Leclerc F, Haasc FM, Santner J, et al. Combust Flame 2015;162:296–314.
[**Razus2010**] Razus D, Oancea D, Brinzea V, Mitu M, Movileanu C. Experimental and computed burning velocities of propane-air mixtures. Energy Convers Manag 2010;51:2979–2984.
[**Tang2010**] Tang C, Zheng J, Huang Z, Wang J. Study on nitrogen diluted propane–air premixed flames at elevated pressures and temperatures, Energy Convers Manag 2010;51:288–295.
[**Law2004**] Law CK, Kwon OC. Effects of hydrocarbon substitution on atmospheric hydrogen-air flame propagation. Int J Hydrog Energy 2010;29:867–879.
[**Zhao2004**] Zhao Z, Kazakov A, Li J, Dryer FL. The initial temperature and N2 dilution effect on the laminar flame speed of propane/air. Combust Sci Technol 2004;176:1705–1723.
[**Zhou1996**] Zhou M, Garner CP. Direct measurements of burning velocity of propane-air using particle image velocimetry. Combust Flame 1996;106:363–367.
[**VanMaaren1994**] van Maaren A, de Goey LPH. Stretch and the adiabatic burning velocity of methane-and propane-air flames. Combust Sci Technol 1994;102:309–314.
[**Tseng1993**] Tseng LK, Ismail MA, Faeth GM. Laminar burning velocities and Markstein numbers of hydrocarbon/air flames. Combust Flame 1993;95:410–426.
[**Metghalchi1980**] Metghalchi M, Keck JC. Laminar burning velocity of propane-air mixtures at high temperature and pressure. Combust Flame 1980;38:143–154.
[**Zhao2015**] Zhao P, Yuan W, Sun H, Li Y, Kelley AP, Zheng X, Law CK. Laminar flame speeds, counterflow ignition, and kinetic modeling of the butene isomers. Proc Combust Inst 2015;35: 309–316.
[**Zhou2016**] Zhou C, Li Y, O'Connor E, Somers KP, Thion S, Keesee C, et al. A comprehensive experimental and modeling study of isobutene oxidation. Combust Flame 2016;167:353-379.
[**Hirasawa2002**] Hirasawa T, Sung CJ, Joshi A, Yang Z, Wang H, Law CK. Determination of laminar flame speeds using digital particle image velocimetry: Binary Fuel blends of ethylene, n-Butane, and toluene. Proc Combust Inst 2002;29:1427–1434.
[**Cheng2017**] Cheng Y, Hu E, Lu X, Li X, Gong J, Li Q, Huang Z. Experimental and kinetic study of pentene isomers and n-pentane in laminar flames. Proc Combust Inst 2017;36:1279–1286.
[**Castaldi1995**] Castaldi MJ, Vincitore AM, Senkan SM, Microstructures of premixed hydrocarbon flames – methane. Comb Sci Technol 1995;107:1–19.
[**Bierkandt2015**] Bierkandt T, Kasper T, Akyildiz E, Lucassen A, Oßwald P, Koehler M, Hemberger P. Proc Combust Inst 2015;35:803–811.
[**Castaldi1996**] Castaldi MJ, Marinov NM, Melius CF, Huang J, Senkan SM, Pitz WJ, et al. Experimental and modeling investigation of aromatic and polycyclic aromatic hydrocarbon formation in a premixed ethylene flame. Sym (Int) Combust 1996;26:693-702.

[**Hansen2007**] Hansen N, Miller JA, Taatjes CA, Wang J, Cool TA, Law ME, et al. Photoionization mass spectrometric studies and modeling of fuel-rich allene and propyne flames. Proc Combust Inst 2007;31:1157–1164.
[**Atakan1998**] Atakan B, Hartlieb AT, Brand J, Kohse-Hoeinghaus K. An experimental investigation of premixed fuel-rich low-pressure propene/oxygen/argon flames by laser spectroscopy and molecular beam mass spectrometry. Sym (Int) Combust 1998;27:435–444.
[**Cool2005**] Cool TA, Nakajima K, Taatjes CA, McIlroy A, Westmoreland PR, Law ME, et al. Studies of a fuel-rich propane flame with photoionization mass spectrometry. Proc Combust Inst 2005;30:1681–1688.
[**Schenk2013**] Schenk M, Leon L, Moshammer K, Oßwald P, Zeuch T, Seidel L, et al. Detailed mass spectrometric and modeling study of isomeric butene flames. Combust Flame 2013;160:487–503
[**Marinov1998**] Marinov NM, Pitz WJ, Westbrook CK, Vincitore AM, Castaldi MJ, Senkan SM, et al. Aromatic and polycyclic aromatic hydrocarbon formation in a laminar premixed n-butane flame. Combust Flame 1998;114:192–213.
[**Ruwe2017**] Ruwe L, Moshammer K, Hansen N, Kohse-Hoeinghaus K. Consumption and hydrocarbon growth processes in a 2-methyl-2-butene flame. Combust Flame 2017;175:34–46.
[**Yahyaoui2006**] Yahyaoui M, Djebaïli-Chaumeix N, Dagaut P, Paillard CE, Gail S. Kinetics of 1-hexene oxidation in a JSR and a shock tube: experimental and modelling study. Combust Flame 2006;147:67–78.
[**Davidson2014**] Davidson DF, Hanson RK. Fundamental kinetics database, utilizing shock tube measurements volume 4: Ignition delay time measurements 2014.
[**Zhang2016**] Zhang K, Banyon C, Bugler J, Curran HJ, Rodriguez A, Herbinet O, et al. An updated experimental and kinetic modeling study of n-heptane oxidation. Combust Flame 2016;172:116–135.
[**He2016**] He J, Yong K, Zhang W, Li P, Zhang C, Li X. Shock tube study of ignition delay characteristics of n-nonane and n-undecane in argon. Energy Fuels 2016;30:8886−8895.
[**Richter2019**] Richter S, Braun-Unkhoff M, Kathrotia T, Naumann C, Kick T, Slavinskaya N, Riedel U. Methods and tools for the characterisation of a generic jet fuel. CEAS Aeronaut J 2019;10:925–935.
[**Assad2009**] Assad M, Leschevich VV, Penyazkov OG, Sevrouk KL, Tangirala VE, Joshi ND. Nonequilibrium phenomena: Plasma, combustion, atmosphere; Roy, G. D., Frolov, S. M., Starik, A. M., Eds.; Torus Press: Moscow 2009:210−220.
[**Fan2016**] Fan X, Wang G, Li Y, Wang Z, Yuan W, Zhao L. Experimental and kinetic modeling study of 1-hexene combustion at various pressures. Combust Flame 2016;173:151–160.
[**Kelley2010**] Kelley AP, Smallbone AJ, Zhu D, Law CK. Laminar flame speeds of C5 to C8 n-alkanes at elevated pressures and temperatures. AIAA Aerospace Sciences Meeting. 2010, Paper No 2010-774.
[**Ji2010**] Ji C, Dames E, Wang YL, Wang H, Egolfopoulos FN. Propagation and extinction of premixed C5–C12 n-alkane flames. Combust Flame 2010;157:277–287.
[**Comandini2015**] Comandini A, Dubois T, Chaumeix N. Laminar flame speeds of n-decane, n-butylbenzene, and n-propylcyclohexane mixtures. Proc Combust Inst 2015;35:671–678.
[**Kumar2007**] Kumar K, Freeh JE, Sung CJ, Huang Y. Laminar flame speeds of preheated iso-octane/O2/N2 and n-heptane/O2/N2 mixtures. J Propul Power 2007;23:428–436.
[**Hui2013**] Hui X, Sung CJ. Laminar flame speeds of transportation-relevant hydrocarbons and jet fuels at elevated temperatures and pressures. Fuel 2013;109:191–200.
[**Kim2013**] Kim HH, Won SH, Santner J, Chen Z, Ju Y. Measurements of the critical initiation radius and unsteady propagation of n-decane/air premixed flames. Proc Combust Inst 2013;34:929–936.

[**Munzar2013**] Munzar JD, Akih-Kumgeh B, Denman BM, Zia A, Bergthorson JM. An experimental and reduced modeling study of the laminar flame speed of jet fuel surrogate components. Fuel 2013;113:586–597.
[**Singh2011**] Singh D, Nishiie T, Qiao L. Experimental and kinetic modeling study of the combustion of n-decane, Jet-A, and S-8 in laminar premixed flames. Combust Sci Technol 2011;183:1002–1026.
[**Li2013**] Li B, Liu N, Zhao R, Zhang H, Egolfopoulos FN. Flame propagation of mixtures of air with high molecular weight neat hydrocarbons and practical jet and diesel fuels. Proc Combust Inst 2013;34:727–733.
[**Nawdiyal2015**] Nawdiyal A, Hansen N, Zeuch T, Seidel L, Mauss F. Experimental and modelling study of speciation and benzene formation pathways in premixed 1-hexene flames. Proc Combust Inst 2015;35:325–332.
[**Seidel2015**] Seidel L, Moshammer K, Wang X, Zeuch T, Kohse-Höinghaus K, Mauss F. Comprehensive kinetic modeling and experimental study of a fuel-rich, premixed n-heptane flame. Combust Flame 2015;162:2045–2058.
[**Doute1995**] Doute C, Delfau J, Akrich R, Vovelle C. Chemical structure of atmospheric pressure premixed n-decane and kerosene flames. Combust Sci Technol 1995;106:327-344.
[**Hu2017**] Hu E, Yin G, Gao Z, Liu Y, Ku J, Huang Z. Experimental and kinetic modeling study on 2,4,4-trimethyl-1-pentene ignition behind reflected. Fuel 2017;195:97–104.
[**Shen2008**] Shen HS, Vanderover J, Oehlschlaeger MA. A shock tube study of iso-octane ignition at elevated pressures: The influence of diluent gases. Combust Flame 2008;155:739–755.
[**Oehlschlaeger2004**] Oehlschlaeger MA, Davidson DF, Herbon JT, Hanson RK. Shock tube measurements of branched alkane ignition times and OH concentration time histories. Int J Chem Kinet 2004;36:67–78.
[**Slavinskaya2013**] Slavinskaya N, Saffaripour M, Saibov E, Herzler J, Naumann C, Thomas L, Riedel U. Reaction models for i-C10H22 and i-C11H24 oxidation. 6th European Combustion Meeting 2013; Paper No P2-14.
[**Richter2018**] Richter S, Kathrotia T, Naumann C, Kick T, Slavinskaya N, Braun-Unkhoff M, Riedel U. Experimental and modeling study of farnesane. Fuel 2018;215:22-29.
[**Hu2018**] Hu E, Yin G, Ku J, Gao Z, Huang Z. Experimental and kinetic study of 2,4,4-trimethyl-1-pentene and iso-octane in laminar flames. Proc Combust Inst 2018;37:1709–1716.
[**Galmiche2012**] Galmiche B, Halter F, Foucher F. Effects of high pressure, high temperature and dilution on laminar burning velocities and Markstein length of iso-octane/air mixtures. Combust Flame 2012;159:3286–3299.
[**Richter2019a**] Richter S, Naumann C, Kathrotia T, Braun-Unkhoff M, Riedel U. Synthesized alternative kerosenes – Characterization through experiments and modeling, Proc 9th European Combustion Meeting 2019; Paper No S5_All_20.
[**Richter2019b**] Richter S, Braun-Unkhoff M, Herzler J, Methling T, Naumann C, Riedel U. An investigation of combustion properties of a gasoline primary reference fuel surrogate blended with butanol. ASME Turbo Expo 2019; Paper No GT2019-90911.
[**Zeng2017a**] Zeng M, Wullenkord J, Graf I, Kohse-Höinghaus K. Influence of dimethyl ether and diethyl ether addition on the flame structure and pollutant formation in premixed iso-octane flames. Combust Flame 2017;184:41–54.
[Osswald2014] Osswald P. (2014) Unpublished data.
[**Dubois2009**] Dubois T, Chaumeix N, Paillard C. Experimental and modeling study of n-propylcyclohexane oxidation under engine-relevant conditions. Energy Fuels 2009;23:2453–2466.
[**Comandini2014**] Comandini A, Dubois T, Abid S, Chaumeix N. Comparative study on cyclohexane and decalin oxidation. Energy Fuels 2014;28:714−724.

[**Li2011**] Li W, Law ME, Westmoreland PR, Kasper T, Hansen N, Kohse-Höinghaus K. Multiple benzene-formation paths in a fuel-rich cyclohexane flame. Combust Flame 2011;158:2077–2089.
[**Pousse2010**] Pousse E, Porter R, Biet J, Warth V, Glaude PA, Fournet R, Battin-Leclerc F. Lean methane premixed laminar flames doped by components of diesel fuel II: n-Propylcyclohexane. Combust Flame 2010;157:75–90.
[**Zeng2017**] Zeng M, Li Y, Yuan W, Li T, Wang Y, Zhou Z, et al. Experimental and kinetic modeling study of laminar premixed decalin flames. Proc Combust Inst 2017;36:1193–1202.
[**Burcat1986**] Burcat A, Snyder C, Brabbs T. Ignition delay times of benzene and toluene with oxygen in argon mixtures, 1986;NASA Technical Memorandum 87312.
[**Pengloan2001**] Pengloan G, Dagaut P, Djebaili-Chaumeix N, Paillard CE, Cathonnet M, Combust Inst, French Section, Orléans, 2001.
[**Wang2013**] Wang H, Gerken WJ, Wang W, Oehlschlaeger MA, Experimental study of the high-temperature autoignition of tetralin. Energy Fuels 2013;27:5483-5487.
[**Pfahl1996**] Pfahl U, Fieweger K, Adomeit G, Self-ignition of diesel relevant hydrocarbon-air mixtures under engine conditions. Proc Combust Inst 1996;26:781–789.
[**Heimel1957**] Heimel S, Weast RC. Effect of initial mixture temperature on the burning velocity of benzene-air, n-heptane-air, and isooctane-air mixtures. Sym (Int) Combust 1957;6:296-302.
[**Hui2012**] Hui X, Das AK, Kumar K, Sung CJ, Dooley S, Dryer FL. Laminar flame speeds and extinction stretch rates of selected aromatic hydrocarbons. Fuel 2012;97:695–702.
[**Bittner1981**] Bittner JD, Howard JB. Composition profiles and reaction mechanisms in a near-sooting premixed benzene/oxygen/argon flame. Proc Combust Sym 1981:18:1105-1116.
[**Detilleux2009**] Detilleux V, Vandooren J. Experimental and kinetic modeling evidences of a c7h6 pathway in a rich toluene flame. J Phys Chem A 2009;113:10913–10922.
[**Yuan2015**] Yuan W, Li Y, Dagaut P, Yang J, Qi F. Experimental and kinetic modeling study of styrene combustion. Combust Flame 2015;162:1868–1883.
[**Pousse2010a**] Pousse E, Tian ZY, Glaude PA, Fournet R, Battin-Leclerc F. A lean methane premixed laminar flame doped with components of diesel fuel part III: Indane and comparison between n-butylbenzene, n-propylcyclohexane and indane. Combust Flame 2010;157:1236–1260.
[**Wang2013z**] Wang Z, Li Y, Zhang F, Zhang L, Yuan W, Wang Y, Qi F. An experimental and kinetic modeling investigation on a rich premixed n-propylbenzene flame at low pressure. Proc Combust Inst 2013;34:1785–1793.
[**Noorani2010**] Noorani K, Akih-Kumgeh B, Bergthorson JM, Comparative high temperature shock tube ignition of C1−C4 primary alcohols, Energy Fuels 2010;24:5834–5843.
[**Burke2016**] Burke U, Metcalfe WK, Burke SM, Heufer KA, Dagaut P, Curran HJ. A detailed chemical kinetic modeling, ignition delay time and jet-stirred reactor study of methanol oxidation. Combust Flame 2016;165:125-136.
[**Yasunaga2008**] Yasunaga K, Kubo S, Hoshikawa H, Kamesawa T, Hidaka Y. Shock-tube and modeling study of acetaldehyde pyrolysis and oxidation. Int J Chem Kinet 2008;40:73-102.
[**Natarajan1981**] Natarajan K, Bhaskaran KA. An experimental and analytical investigation of high temperature ignition of ethanol. Int Sym Shock Waves 1981;13:834-842.
[**Davidson2010**] Davidson DF, Ranganath SC, Lam KY, Liaw M, Hong Z, Hanson RK. Ignition delay time measurements of normal alkanes and simple oxygenates. J Propul Power 2010;26:280–287.
[**Black2010**] Black G, Curran HJ, Pichon S, Simmie JM, Zhukov V, Bio-butanol: Combustion properties and detailed chemical kinetic model. Combust Flame 2010;157:363–373.
[**Ngugi2020**] Ngugi J, Richter S, Braun-Unkhoff M, Naumann C, Riedel U. ASME Turbo Expo 2020; Paper No GT2020-14702.

[**Christensen2015**] Christensen M, Abebe MT, Nilsson EJK, Konnov AA. Kinetics of premixed acetaldehyde + air flames. Proc Combust Inst 2015;35:499–506.
[**Veloo2013**] Veloo P, Dagaut P, Togbe C, Dayma G, Sarathy SM, Westbrook CK, Egolfopoulos FN. Experimental and modeling study of the oxidation of n- and iso-butanal. Combust Flame 2013;160:1609–1626.
[**Vancoillie2012**] Vancoillie J, Christensen M, Nilsson EJK, Verhelst S, Konnov AA. Temperature dependence of the laminar burning velocity of methanol flames. Energy Fuels 2012;26:1557−1564.
[**Egolfopoulos1992**] Egolfopoulos FN, Du DX, Law CK. A comprehensive study of methanol kinetics in freely-propagating and burner-stabilized flames, flow and static reactors, and shock tubes. Combust Sci Technol 1992;83:33−75.
[**Veloo2010**] Veloo PS, Wang YL, Egolfopoulos FN, Westbrook CK. A comparative experimental and computational study of methanol, ethanol, and n-butanol flames. Combust Flame 2010;157:1989−2004.
[**Egolfopoulos1992a**] Egolfopoulos FN, Du DX, Law CK. A study on ethanol oxidation kinetics in laminar premixed flames, flow reactors, and shock tubes. Proc Comb Inst 1992;24:833–841.
[**Liao2007**] Liao SY, Jiang DM, Huang ZH, Zeng K, Cheng Q. Determination of the laminar burning velocities for mixtures of ethanol and air at elevated temperatures. Appl Therm Eng 2007;27:374–380.
[**Vries2011**] de Vries J, Lowry WB, Serinyel Z, Curran HJ, Petersen EL. Laminar flame speed measurements of dimethyl ether in air at pressures up to 10 atm. Fuel 2011;90:331-338.
[**Daly2001**] Daly CA, Simmie JM, Wuermel J, DjebaIli N, Paillard C. Burning velocities of dimethyl ether and air. Combust Flame 2001;125:1329-1340.
[**Qin2005**] Qin X, Ju Y. Measurements of burning velocities of dimethyl ether and air premixed flames at elevated pressures. Proc Combust Inst, 2005;30:233-240.
[**Wang2009**] Wang YL, Holley AT, Ji C, Egolfopoulos FN, Tsotsis TT, Curran HJ. Propagation and Extinction of Premixed Dimethyl-Ether/Air Flames. Proc Combust Inst 2009;32:1035-1042.
[**Sun2017**] Sun W, Wang G, Li S, Zhang R, Yang B, Yang J, et al. Speciation and the laminar burning velocities of poly(oxymethylene) dimethyl ether 3 (POMDME3) flames: An experimental and modeling study. Proc Combust Inst 2017;36:1269–1278.
[**Leplat2010**] Leplat N, Vandooren J. Experimental investigation and numerical simulation of the structure of CH3CHO/O2/Ar flames at different equivalence ratios. Combust Sci Technol 2010;182:436–448.
[**Cool2007**] Cool TA, Wang J, Hansen N, Westmoreland PR, Dryer FL, Zhao Z, et al. Photoionization mass spectrometry and modeling studies of the chemistry of fuel-rich dimethyl ether flame. Proc Combust Inst 2007;31:285–293.
[**Leplat2011**] Leplat N, Dagaut P, Togbe C, Vandooren J. Numerical and experimental study of ethanol combustion and oxidation in laminar premixed flames and in jet-stirred reactor. Combust Flame 2011;158:705–725.
[**Dagaut1998**] Dagaut P, Daly C, Simmie JM, Cathonnet M. The oxidation and ignition of dimethylether from low to high temperature (500–1600 K): Experiments and kinetic modelling. Sym (Int) Combust 1998;27:361–369.
[**Sun2018**] Sun W, Tao T, Lailliau M, Hansen N, Yang B, Dagaut P. Exploration of the oxidation chemistry of dimethoxymethane: Jet-stirred reactor experiments and kinetic modelling. Combust Flame 2018;193:491–501.
[**Tan1994**] Tan Y, Dagaut P, Cathonnet M, Boettner J. Acetylene oxidation in a JSR from 1 to 10 atm and comprehensive kinetic modeling, Combust Sci Technol 1994;102:21-55.

[**LeCong2009**] Le Cong T, P. Dagaut P. Oxidation of H2/CO2 mixtures and effect of hydrogen initial concentration on the combustion of CH4 and CH4/CO2 mixtures: Experiments and modelling. Proc Combust Inst 2009;32:427–435.
[**Dagaut2002**] Dagaut P. On the kinetics of hydrocarbons oxidation from natural gas to kerosene and diesel fuel. Phys Chem Chem Phys 2002;4:2079–2094.
[**Herbinet2012**] Herbinet O, Husson B, Serinyel Z, Cord M, Warth V, Fournet R, et al. Experimental and modeling investigation of the low-temperature oxidation of n-heptane, Combust Flame 2012;159:3455–3471.
[**Rotavera2011**] Rotavera B, Dievart P, Togbe C, Dagaut P, Petersen EL. Oxidation kinetics of n-nonane: Measurements and modeling of ignition delay times and product concentrations. Proc Combust Inst 2011;33:175–183.
[**Moreac2006**] Moréac G, Dagaut P, Roesler JF, Cathonnet M. Nitric oxide interactions with hydrocarbon oxidation in a jet-stirred reactor at 10 atm. Combust Flame 2006;145:512–520.
[**Dagaut2013**] Dagaut P, Ristori A, Frassoldati A, Faravelli T, Dayma G, Ranzi E. Experimental study of tetralin oxidation and kinetic modeling of its pyrolysis and oxidation. Energy Fuels 2013;27:1576−1585.
[**Mati2007**] Mati K, Ristori A, Pengloan G, Dagaut P. Oxidation of 1-methylnaphthalene at 1–13 atm: Experimental study in a JSR and detailed chemical kinetic modeling, Combust Sci Technol 2007;179:1261-1285.
[**Bikas2001**] Bikas G, Peters N. Kinetic modelling of n-decane combustion and autoignition: Modeling combustion of n-decanem. Combust Flame 2001;126:1456–1475.
[**Dugger1952**] Dugger GL. Effect of initial mixture temperature on flame speed of methane-air, propane-air, and ethylene-air mixtures. NACA-Report-1061, 1952.
[**Shen2015**] Shen X, Yang X, Santner J, Sun J, Ju Y. Experimental and kinetic studies of acetylene flames at elevated pressures. Proc Combust Inst 2015;35:721–728.
[**Ravi2015**] Ravi S, Sikes TG, Morones A, Keesee CL, Petersen EL. Comparative study on the laminar flame speed enhancement of methane with ethane and ethylene addition. Proc Combust Inst 2015;35:679–686.